

**VOLTAMMETRIC AND OPTICAL SENSORS FOR INDIVIDUAL,
DUAL AND SIMULTANEOUS DETERMINATION OF
SOME ANTIOXIDANTS AND BIOMARKERS**

Thesis submitted to
Cochin University of Science and Technology
in partial fulfilment of the requirements
for the award of the degree of
Doctor of Philosophy
in
Chemistry
by

Ambily Thomas
(Reg. No. 5207)



Department of Applied Chemistry
Cochin University of Science and Technology
Kochi - 22

March 2019

Voltammetric and optical sensors for individual, dual and simultaneous determination of some antioxidants and biomarkers

Ph. D. Thesis under the Faculty of Sciences

By

Ambily Thomas

Research Fellow

Department of Applied Chemistry

Cochin University of Science and Technology

Kochi, India - 682022

Email: ambilyasb@gmail.com

Supervising Guide

Dr. K. Girish Kumar

Professor & Head

Department of Applied Chemistry

Cochin University of Science and Technology

Kochi, India - 682022

Email: giri@cusat.ac.in

Department of Applied Chemistry

Cochin University of Science and Technology

Kochi, India 682022

March 2019

DEPARTMENT OF APPLIED CHEMISTRY
COCHIN UNIVERSITY OF SCIENCE AND TECHNOLOGY
KOCHI - 682022, INDIA



Dr. K. Girish Kumar
Professor & Head

Tel: 0484 - 2575804
E-mail: chem.@cusat.ac.in

Date: 27 March 2018

Certificate

Certified that the work entitled “**Voltammetric and optical sensors for individual, dual and simultaneous determination of some antioxidants and biomarkers**”, submitted by Ms. Ambily Thomas, in partial fulfilment of the requirements for the degree of Doctor of Philosophy in Chemistry to Cochin University of Science and Technology, is an authentic and bonafide record of the original research work carried out by her under my supervision at the Department of Applied Chemistry. Further, the results embodied in this thesis, in full or in part, have not been submitted previously for the award of any other degree. All the relevant corrections and modifications suggested by the audience during the pre-synopsis seminar and recommended by the Doctoral committee have been incorporated in the thesis.

K. Girish Kumar
(Supervising Guide)

Declaration

I hereby declare that the work presented in this thesis entitled “**Voltammetric and optical sensors for individual, dual and simultaneous determination of some antioxidants and biomarkers**” is based on the original work carried out by me under the guidance of Dr. K. Girish Kumar, Professor & Head, Department of Applied Chemistry, Cochin University of Science and Technology and has not been included in any other thesis submitted previously for the award of any degree.

Kochi-22
27/03/2019

Ambily Thomas

Dedicated to
My Angels...

Acknowledgement

'A dream has come true'

I am grateful to 'the plan of God' that has given me a chance to ride through the wonderful path of scientific research. Undoubtedly, this journey would not have reached this juncture without the flawless support of many people.

I am indebted to my supervising guide Dr. K. Girish Kumar, Professor and Head, Dept. of Applied Chemistry, CUSAT. He is the one, who gave me an opportunity to do research under his guidance. An opportunity through which I was able to see light, even in the darkest moment of my life. He always tried to pose many challenges in front of the researcher in me. It was the questions posed by him that provoked my idle intellectual mind to fight against various problems to arrive at a solution. Again, a solution for a problem may be achieved through different ways and means. In research, hardwork meets glorious victory only when the path followed is systematic. I am honoured to be a researcher under the guidance of Dr. K. G. K, who is a role model as a highly systematic human. He always demands from his students, not only to be a researcher but also to be a responsible social being. He tried to give us a large number of opportunities in and outside the university where we can develop and flourish our aesthetic skills. He has been very affectionate and was always ready to help us, even in the midst of his busy schedule. I am extremely lucky and blessed to have Dr. K. Girish Kumar as my research guide. At this point, special mention about the better half our mentor, Dr. Anitha I, Principal, Kunjikuttan Thampuran College, Kodungalloor, for her love and support.

I am privileged to have Dr. K. Sreekumar, Professor, Department of Applied Chemistry, Cochin University of Science and Technology, Kochi, as my Doctoral

Committee Member. I remember his guidance, constructive criticism, appreciation and continuous help that he has offered during the course of this study.

I am thankful to all faculty members of Department of Applied Chemistry, CUSAT for their inspiration and timely help. I also acknowledge the help of various non – teaching staff members who rendered me a lot of support.

I am grateful to the members of Travancore Titanium Products Limited, Thiruvananthapuram for all the support offered. I acknowledge the encouragement and kindness shown by my superiors Dr. K. Johnson, Ms. Shilaja Devi, Dr. Timy Jose, Mr. D. Sreedas, Deputy Managers and my colleagues.

Research meets success when the path chosen is appropriate. It was from my lab mates I got inspired to choose the best from a large number of possibilities. I can never forget the support offered by Dr. Divya and Dr. Anuja who introduced to me 'the world of sensors'. Beautiful tips from my seniors Dr. Theresa, Dr. Jesny, Dr. Jintha, Dr. Monica, Dr. Swathy, Dr. Soumya, Dr. Ammu, Dr. Unni, Zafna, Shalini have strengthened me to meet the hurdles in between my research tenure. My dear lab mates Sanu, Manna, Devika, Soniya, Swathy, Golda and Dr. Sheela have all extended their support in a very special way and I gained a lot from them, through various personal and academic interactions.

I am happy to remember the fruitful discussions that happened between me and those students who came to do projects in our lab. I remember the nice time spent with Lakshmi, Aparna, Meera, Jilcy, Nihal, Radhika, Kavya, Arun, Shilpa and Bhagyalakshmi.

I thank Council of Scientific and Industrial Research (CSIR), New Delhi For the financial services rendered in the form of fellowship and Kerala State Council for

Science, Technology and Environment (KSCSTE), Kerala and Department of Science and Technology (DST), New Delhi for the funding assistance in the form of projects.

I am happily acknowledging, the help extended by scientists at STIC, CUSAT, Department of Photonics, CUSAT and Department of Physics, CUSAT for various analysis accomplished.

I owe a lot to my parents, who encouraged and helped me at every stage of my personal and academic life and longed to see this moment come true. Words cannot express how much I am grateful to my father, mother, sister and brother and in-laws for all the sacrifices that they have made on my behalf. I am very much indebted to my parents and in-laws who supported me in every possible way to see the completion of this work, I can never forget the support and help drawn from Lincy, my lovely friend who motivated me a lot through her words and deeds.

I fondly recall with love, the emotional support and consistent encouragement exhibited by my husband and my little angels. I can never forget the way in which they have adjusted to keep me comfortable and free. It is their love and prayers, that made me strong enough to complete my research tenure successfully.

I thank the almighty God for all his blessings throughout my life.

Ambily Thomas

||| Preface |||

Sensors are self contained devices which provide real-time analytical specifics of a test sample. The analytical utility of the sensor includes the detection of a particular species (the analyte) in the observed matrix along with its quantification. In some cases, a sensor offers the detection and/or determination of more than one analyte individually or even simultaneously. Individual or simultaneous determination of various species present in physiological fluids and food is of great demand in the modern world.

The chemical information regarding the determinand is converted to a readable output through mainly two processes - sensing (recognition) and transduction. The *recognition element* of the sensor interacts more or less selectively with the analyte/analytes in such a way that the resultant output will be directly proportional to the concentration of the species. In some instances the interaction between the analyte and the recognition element can produce changes in the properties of the recognition element which could be used for specific detection purposes. Various nanomaterials, electro-polymers, quantum dots etc. are widely used as label free recognition elements.

The resultant interaction between the analyte and the recognition element will be transferred or translated to a readable output with the help of a *transducer*. A number of transduction techniques are used for the read out including various electrochemical and optical methods. Among them the most widely accepted and used are voltammetry, colorimetry and fluorescence owing to their inherent superlative features such as simplicity,

very fast responses, detection and determination of very lower concentrations of the analyte etc.

Voltammetric sensors rely upon the principle that the species undergo oxidation or reduction at a potential which is characteristic to them. Here the analytical signal will be a voltammogram which measures the current as a function of applied potential and the responsive current will be plotted against the concentration to get the calibration graph. Among the working, reference and auxiliary electrodes, working electrode will be acting as the recognition element. In order to increase the efficiency of the working electrode, it will be chemically modified with various materials such as nanomaterials, electropolymers etc. Such chemically modified electrodes can enable the determination of one or more analytes individually or simultaneously.

Colorimetric sensors are developed on basis of Beer-Lambert's law and a colour producing agent acts as the recognition elements. Nowadays metal nanoparticles are introduced in colorimetric systems to increase the sensitivity of the method. In such cases, aggregation or anti – aggregation of metal nanoparticles (the probe) induced by analytes causes colour changes enabling colorimetric analysis of that analyte. The absorbance of the probe in the absence and/or presence of the analyte provide the analytical signal. The ratio or difference of the absorbance is directly related to the concentration of the species to get the calibration graph. In rare cases different analytes can impart different colours to a single probe which can be used for their detection.

Fluorescence sensors rely upon the interaction between the analyte and probe which cause fluorescence quenching/enhancement enabling fluorimetric analysis of that analyte. Here the recognition element will be a fluorophore and cadmium based quantum dots have been used in sensors recently owing to their high quantum yield, surface functionalisation possibilities etc. Ratio of fluorescence intensity of the probe in the absence and presence of the analyte is directly related to the concentration of the species to obtain the calibration curve.

The thesis titled “*Voltammetric and optical sensors for individual, dual and simultaneous determination of some antioxidants and biomarkers*” has been divided into eight chapters. The content of the chapters are briefly presented as follows.

Chapter 1 brings together a brief idea about the various techniques which has been used for the development of chemical sensors. Nanoparticle and/or polymer modified electrodes based voltammetric and nanoparticle or semiconductor nano crystals based optical sensing approaches is detailed in this chapter. The second half of this chapter gives a detailed review on the successful efforts that have been already reported in the field of aforementioned sensing approaches.

Chapter 2 details the materials, instruments and methodologies used for the development of various sensors described in the thesis. Procedures for the preparation of buffer solutions, preparation of standard and test samples, various methods used for sensor development, comparison of sensor performance with classic methods and thereby validation of the newly developed sensors etc. are also included in this chapter.

Chapter 3 describes the development of a voltammetric sensor for *dopamine* based on poly(4-amino-3-hydroxy naphthalene sulphonic acid)/Co nanoparticle/GCE (pAHNSA/CoNP/GCE). Optimal conditions such as supporting electrolyte, pH of the supporting electrolyte, number of cycles of polymerisation of pAHNSA, number cycles of electro deposition of CoNP required for the sensitive determination of dopamine using the modified electrode have been identified and the results are given this chapter. The chapter discusses the sensor performance in terms of tolerance of the sensor towards the structurally similar as well as coexistent matrix, linear range and limit of detection. The chapter also describes the application of the sensor for the determination of dopamine in artificial physiological samples having similar constitution with blood serum, urine and cerebrospinal fluid and the validation of the sensor by comparing it with the results obtained from HPLC method.

Chapter 4 explains the development of tyrosine capped silver nanoparticles based colorimetric sensor for the determination of the biothiols- *glutathione and cysteamine*. Various parameters such as, the medium of study, pH of the medium, and effect of time, that can influence the determination of the biothiols have been optimised and the results are included in this chapter. Furthermore, the mechanism underlying the sensing process is also discussed in detail. The efficacy of the sensor in the detection as well as determination of the analytes has been described in terms of selectivity, effect of foreign species, linear working range and limit of detection of the sensor. Application study conducted in artificial blood serum and the comparison study with classic methods are also dealt in this chapter.

Chapter 5 discusses the development of square wave voltammetric sensor for the simultaneous determination of two antioxidants used in food - *tert-butyl hydroquinone* and *propyl gallate* using acetylene black modified gold electrode. Most suitable conditions for the simultaneous determination are discussed. Electrochemical oxidation of both of these antioxidants follow diffusion controlled mechanism and the diffusion coefficients obtained with the help of chronoamperometric measurements are included in this chapter. Calibration graphs for individual and simultaneous determination are presented and discussed. Effect of increment in the concentration of one antioxidant on the determination of the other is given. Effect of various species including other antioxidants, coexistent matrix etc. is also detailed. Applicability of the sensor was established by determining the concentrations in the spiked oil and butter samples and the results are incorporated in the chapter.

Chapter 6 deals with the development of voltammetric sensor based on acetylene black-chitosan modified gold electrode for the simultaneous determination of the biomolecules- *serotonin* and *melatonin*. Synergised catalytic activity of the modifiers towards the biomolecules is confirmed with the help of square wave voltammetry and electrochemical impedance spectroscopy. Optimisation of different experimental parameters is done. Diffusion coefficients and heterogeneous rate constants are calculated. The chapter also details the performance of the sensor in terms of dynamic range, detection limit, selectivity etc. Applicability of the sensor in spiked samples of artificial blood serum was evaluated and the results are described in the chapter.

Chapter 7 focuses on the development of fluorescence sensor for the determination of biomolecules- *serotonin* and its metabolite *5-hydroxy indole acetic acid* based on the quenching of fluorescence of mercaptopropionic acid capped CdTe quantum dots. Mechanisms behind the sensing of the biomolecules were recognised with the help of various techniques mainly from fluorescence decay traces. Optimal conditions for the determination of the biomolecules were recognised and are and are detailed in the chapter. Applicability of the developed assay is also discussed.

Chapter 8 outlines the summary and future outlook of the research work.

The list of cited references is compiled and given at the end of the thesis as a separate section.

Contents

Chapter 1

| | |
|--|-------------|
| INTRODUCTION..... | 1-56 |
| 1.1 Sensors..... | 2 |
| 1.2 Constitution of a sensor | 2 |
| 1.3 Electrochemical sensors | 3 |
| 1.3.1 Electrochemical techniques and voltammetry | 3 |
| 1.3.2 Voltammetry- The transduction technique | 4 |
| 1.3.3 Various processes occurring in the system on application of potential | 6 |
| 1.3.4 Measurement of current | 7 |
| 1.3.5 Chemically modified electrodes – The recognition element | 9 |
| 1.3.5.1 Nano materials and/or polymers modified electrodes | 10 |
| 1.4 Optical sensors..... | 11 |
| 1.5 Colorimetric sensors | 11 |
| 1.5.1 Colorimetry/Spectrophotometry – The transduction technique | 11 |
| 1.5.2 Processes leading to sensing | 12 |
| 1.5.3 Silver nanoparticles- The recognition element | 14 |
| 1.5.3.1 Synthesis and functionalization of nanoparticles | 14 |
| 1.6 Fluorescence sensors | 15 |
| 1.6.1 Fluorescence- the transduction technique | 15 |
| 1.6.2 Irradiation of light- The input | 16 |
| 1.6.3 Processes leading to sensing | 17 |
| 1.6.4 Contact or static quenching..... | 17 |
| 1.6.5 Collisional or dynamic quenching | 18 |
| 1.6.6 Combination of both static and dynamic quenching..... | 19 |
| 1.6.7 Fluorophores - the recognition element | 19 |
| 1.6.8 Quantum dots | 20 |
| 1.6.9 Surface functionalised QDs | 22 |

| | |
|---|----|
| 1.7 Objectives of the present investigations | 22 |
| 1.8 Literature review of different voltammetric sensors | 23 |
| 1.8.1 Acetylene black nanoparticles as modifiers | 23 |
| 1.8.2 pAHNSA as modifiers | 34 |
| 1.9 Literature review of various colorimetric sensors | 37 |
| 1.10 Literature review of various fluorescence sensors | 51 |

Chapter 2

| | |
|--|--------------|
| MATERIALS AND METHODS..... | 57-70 |
| 2.1 Reagents | 58 |
| 2.2 Instruments | 59 |
| 2.3 Preparation of sensing element..... | 60 |
| 2.3.1 Cleaning of electrodes..... | 60 |
| 2.3.2 Fabrication of CoNP/GCE | 61 |
| 2.3.3 Fabrication of pAHNSA/CoNP/GCE | 61 |
| 2.3.4 Fabrication of acetylene black modified gold electrode | |
| (AB/GE) | 61 |
| 2.3.5 Fabrication of AB-C modified gold electrode (AB-C/GE).. | 62 |
| 2.3.6 Synthesis of tyrosine capped silver nanoparticles | |
| (AgNP - Tyr)..... | 62 |
| 2.3.7 Synthesis of MPA capped CdTe quantum dots | 62 |
| 2.4 Preparation of stock solutions | 63 |
| 2.5 Preparation of buffer solutions | 63 |
| 2.6 Analytical procedure | 65 |
| 2.6.1 Voltammetric measurements..... | 66 |
| 2.6.2 Colorimetric measurements | 66 |
| 2.6.3 Fluorescence measurements..... | 66 |
| 2.7 Preparation of real/artificial samples..... | 66 |
| 2.7.1 Preparation of artificial urine | 67 |
| 2.7.2 Preparation of artificial blood serum | 67 |
| 2.7.3 Preparation of artificial cerebrospinal fluid | 67 |
| 2.7.4 Treatment of coconut oil/butter sample | 67 |
| 2.8 Reference methods used for validation of methods | 68 |

| | |
|---|----|
| 2.8.1 Spectrophotometric determination of glutathione and Cysteamine..... | 68 |
| 2.8.2 HPLC-UV determination of dopamine | 68 |
| 2.8.3 Spectrophotometric determination of propyl gallate | 68 |
| 2.8.4 HPLC-UV determination of tert-butyl hydroquinone | 69 |
| 2.8.5 Spectrophotometric determination of serotonin and melatonin | 69 |
| 2.8.6 HPLC-UV determination of 5-hydroxyindoleacetic acid .. | 70 |

Chapter 3

| | |
|---|--------------|
| VOLTAMMETRIC SENSOR FOR THE DETERMINATION OF DOPAMINE..... | 71-90 |
| 3.1 Introduction | 72 |
| 3.2 Experimental..... | 74 |
| 3.2.1 Electrochemical measurements..... | 74 |
| 3.3 Results and Discussion | 74 |
| 3.3.1 Electrocatalytic action of pAHNSA/CoNP/GCE | 74 |
| 3.3.2 Performance characteristics of the sensor..... | 77 |
| 3.3.2.1 Supporting electrolyte | 77 |
| 3.3.2.2 pH of supporting electrolyte..... | 77 |
| 3.3.2.3 Thickness of film | 78 |
| 3.3.2.4. Characterisation of the electrode..... | 80 |
| 3.3.3 Kinetic and mechanistic aspects of electrooxidation | 83 |
| 3.3.3.1 Diffusion controlled electro-oxidation of DA..... | 83 |
| 3.3.4 Concentration Study..... | 85 |
| 3.3.5 Effect of coexisting species..... | 88 |
| 3.3.6 Application study | 88 |
| 3.4 Conclusions | 89 |

Chapter 4

| | |
|---|---------------|
| COLORIMETRIC SENSOR FOR THE DETERMINATION OF BIOTHIOLS - GLUTATHIONE AND CYSTEAMINE..... | 91-110 |
| 4.1 Introduction | 92 |

| | | |
|---------|--|-----|
| 4.2 | Experimental..... | 94 |
| 4.2.1 | Colorimetric detection and determination of Cyste and GSH..... | 95 |
| 4.2.2 | Electrochemical measurements of GSH | 95 |
| 4.2.3 | Application study | 96 |
| 4.3 | Results and discussion..... | 96 |
| 4.3.1 | UV-visible study of AgNPs | 96 |
| 4.3.2 | Sensing mechanism of Cyste | 98 |
| 4.3.3 | Sensing mechanism of GSH | 100 |
| 4.3.4 | Analytical performance of the sensor | 103 |
| 4.3.4.1 | Effect of reaction medium and pH | 103 |
| 4.3.4.2 | Concentration study..... | 103 |
| 4.3.4.3 | Selectivity and interference | 105 |
| 4.3.4.4 | Analytical application | 108 |
| 4.4. | Conclusions | 109 |

Chapter 5

VOLTAMMETRIC SENSOR FOR SIMULTANEOUS DETERMINATION OF ANTIOXIDANTS – TERT - BUTYL HYDROQUINONE AND PROPYL GALLATE.....111-136

| | | |
|---------|--|-----|
| 5.1 | Introduction | 112 |
| 5.2 | Experimental..... | 113 |
| 5.2.1 | Analytical procedure | 113 |
| 5.3.2 | Performance Characteristics of the Developed Sensor | 115 |
| 5.3.2.1 | Choice of the supporting electrolyte..... | 115 |
| 5.3.2.2 | Effect of pH..... | 115 |
| 5.3.2.3 | Effect of AB- Nafion film thickness | 117 |
| 5.3.3 | Mechanistic and kinetic aspects of electro-oxidation | 122 |
| 5.3.3.1 | Variation of peak current with scan rate..... | 122 |
| 5.3.3.2 | Calculation of diffusion coefficient | 124 |
| 5.3.3.3 | Calculation of number of electrons and protons... .. | 125 |
| 5.3.4 | Square wave voltammetric responses of TBHQ and PG ... | 126 |
| 5.3.4.1 | Comparison of developed method with reported | 129 |
| 5.3.5 | Selectivity and Interference | 130 |

| | |
|------------------------------------|-----|
| 5.3.6 Analytical Application | 133 |
| 5.4 Conclusions | 134 |

Chapter 6

VOLTAMMETRIC SENSOR FOR SIMULTANEOUS DETERMINATION OF TRYPTAMINES – SEROTONIN AND MELATONIN.....137-160

| | |
|---|-----|
| 6.1 Introduction | 138 |
| 6.2 Experimental..... | 140 |
| 6.3 Results and discussion..... | 140 |
| 6.3.1 Electro-catalysis by AB-C | 140 |
| 6.3.2 Performance characteristics of the sensor | 142 |
| 6.3.2.1 Influence of various supporting electrolytes | 142 |
| 6.3.2.2 Effect of volume of AB-C suspension..... | 143 |
| 6.3.2.3 Effect of pre-concentration of ST and MT..... | 147 |
| 6.3.3 Mechanistic and kinetic aspects | 147 |
| 6.3.3.1 Diffusion controlled electro-oxidation..... | 147 |
| 6.3.3.2 Calculation of diffusion coefficient | 149 |
| 6.3.3.3 Calculation of number of electrons | 150 |
| 6.3.3.4 Variation of overpotential with scan rate | 151 |
| 6.3.4 Variation of peak current with concentration of ST/MT ... | 152 |
| 6.3.4.1 Comparison of developed sensor with reported . | 154 |
| 6.3.5 Selectivity and effect of possibly co-existing species..... | 156 |
| 6.3.6 Application of developed sensor in synthetic blood serum..... | 159 |
| 6.4 Conclusions | 159 |

Chapter 7

FLUORIMETRIC SENSOR FOR THE DETERMINATION OF SEROTONIN AND ITS METABOLITE 5-HYDROXY INDOLE ACETIC ACID.....161-178

| | |
|----------------------------------|-----|
| 7.1 Introduction | 162 |
| 7.2 Experimental..... | 164 |
| 7.2.1 Analytical procedure | 164 |

| | |
|---|-----|
| 7.2.2 HPLC-UV determination of HIAA..... | 165 |
| 7.3 Results and Discussion..... | 165 |
| 7.3.1 Characterisation and fluorescence behavior of CdTe QDs in the absence of ST or HIAA | 165 |
| 7.3.2 Fluorescence behavior of CdTe-MPA QDs in the presence of ST and mechanism behind its sensing..... | 167 |
| 7.3.3 Fluorescence behavior of CdTe-MPA QDs in the presence of HIAA and mechanism behind its sensing..... | 169 |
| 7.3.4 Optimisation of experimental conditions..... | 171 |
| 7.3.4.1 Effect of time..... | 171 |
| 7.3.4.2 Calibration graphs | 172 |
| 7.3.4.3 Selectivity..... | 174 |
| 7.3.4.4 Effect of foreign species..... | 175 |
| 7.3.4.5 Application study..... | 177 |
| 7.4 Conclusions | 178 |

Chapter 8

| | |
|-----------------------------|----------------|
| SUMMARY..... | 179-182 |
| 8.1 Developed sensors | 180 |
| 8.2 Future outlook | 182 |

| | |
|------------------------|----------------|
| REFERENCES..... | 183-210 |
|------------------------|----------------|

| | |
|----------------------------------|----------------|
| LIST OF PUBLICATIONS..... | 211-213 |
|----------------------------------|----------------|

List of Tables

| | | |
|------------|--|-----|
| Table 3.1: | Comparison of the linear range and LOD of the existing DA sensors based on chemical modification of GCE..... | 87 |
| Table 3.2: | Determination of DA in artificial biological samples..... | 89 |
| Table 4.1: | Determination of Cyste and GSH in artificial blood serum..... | 109 |
| Table 4.2: | Determination of Cyste and GSH in artificial blood serum using reference method | 109 |
| Table 5.1: | Fitted impedance values for AB modified electrodes with different thickness (experiments were carried out in 0.1 M PBS (pH 2) containing 5.0×10^{-5} M PG)..... | 122 |
| Table 5.2: | Comparison of detection limit and linear range of TBHQ..... | 128 |
| Table 5.3: | Comparison of detection limit and linear range of PG | 129 |
| Table 5.4: | Effect of various foreign species on the determination of 5.0×10^{-5} M TBHQ and 5.0×10^{-5} M PG | 132 |
| Table 5.5: | Application of the developed method for the determination of TBHQ in coconut oil and butter samples and comparison with HPLC-UV..... | 133 |
| Table 5.6: | Application of the developed method for the determination of PG in coconut oil and butter samples and comparison with spectrophotometric method | 134 |
| Table 6.1: | Comparison of results obtained for individual as well as simultaneous determination of ST and MT..... | 154 |
| Table 6.2: | Comparison of the proposed sensor with latest reported sensors for serotonin | 155 |
| Table 6.3: | Comparison of the proposed sensor with latest reported sensors for melatonin | 156 |
| Table 6.4: | Effect of foreign species | 158 |
| Table 6.5: | Application of the sensor in artificial blood serum..... | 159 |
| Table 7.1: | Effect of foreign species | 176 |
| Table 7.2: | Application of the sensor in artificial blood serum..... | 177 |

List of Figures

| | | |
|-------------|--|----|
| Figure 3.1: | Overlay of cyclic voltammogram of 1.0×10^{-4} M DA at (a) bare GCE (b) CoNP/GCE and (c) pAHNSA/CoNP/GCE. | 75 |
| Figure 3.2: | Overlay of square wave voltammogram of 1.0×10^{-4} M DA at (a) bare GCE (b) CoNP/GCE (c) pAHNSA/GCE and (d) pAHNSA/CoNP/GCE. | 76 |
| Figure 3.3: | (a) Plot of peak potential with pH of the supporting electrolyte. (b) Plot of anodic peak current 1.0×10^{-4} M DA with varying number of cycles for the electro deposition of CoNP. (c) Plot of anodic peak current 1.0×10^{-4} M DA with varying number of cycles for the electro-polymerisation of pAHNSA. | 78 |
| Figure 3.4: | SEM images of (a) bare GCE (b) CoNP/GCE and (c) pAHNSA/CoNP/GCE. | 80 |
| Figure 3.5: | Overlay of cyclic voltammograms of 2.0×10^{-3} M $K_3[Fe(CN)_6]$ on bare GCE at various scan rates. | 81 |
| Figure 3.6: | A. EIS spectra of 0.1 M KCl containing 5 mM $[Fe(CN)_6]^{3-/4-}$ at (a) bare GCE and pAHNSA/CoNP/GCE. B. Nyquist plots of 0.1 M PBS (pH 7) containing 1.0×10^{-5} M DA at (a) bare GCE and pAHNSA/CoNP/GCE. | 82 |
| Figure 3.7: | Cyclic voltammograms of 5.0×10^{-6} M DA at various scan rates, inset: Plot of $\log I_p$ vs. $\log v$ | 83 |
| Figure 3.8: | Chronoamperograms of various concentrations of DA, inset (a) plot of I_{pa} for DA vs. $t^{1/2}$ (b) plot of slope of (I_{pa} vs. $t^{1/2}$) vs. concentration of DA. | 84 |
| Figure 3.9: | Overlay of square wave voltammograms of DA at varying concentration from 1.0×10^{-4} M to 2.0×10^{-7} M. Inset: calibration plot of DA in the range 5.0×10^{-5} M to 5.0×10^{-7} M. | 86 |
| Figure 4.1: | Absorption spectra of (a) AgNP-Tyr (b) AgNPs in presence of 3.0×10^{-6} M Cyste and (c) AgNPs in presence of 1.0×10^{-4} M GSH; inset: photographs of solutions of (a) AgNP-Tyr (b) AgNPs with Cyste and (c) AgNPs with GSH. | 97 |

| | | |
|---------------|---|-----|
| Figure 4.2: | TEM images of (a) AgNP-Tyr (b) AgNPs in presence of Cyste and (c) AgNPs after reaction with GSH | 97 |
| Figure 4.3: | FTIR spectra of (a) Cyste alone and (b) Cyste after reaction with AgNPs | 98 |
| Figure 4.4: | Zeta potential analysis of AgNPs in the (a) absence and (b) presence of Cyste and DLS spectrum of AgNPs in the (c) absence and (d) presence of Cyste..... | 99 |
| Figure. 4.5: | Variation in the absorption ratios of AgNPs in presence of (a) 1.0×10^{-6} M (b) 2.0×10^{-6} M and (c) 3.0×10^{-6} M Cyste with time | 100 |
| Figure. 4.6: | Overlay of voltammograms of (a) AgNO_3 (b) AgNP-Tyr and (c) AgNP-Tyr in presence of GSH on GCE..... | 101 |
| Figure. 4.7: | Variation in $(A-A_0)$ of AgNPs in presence of (a) 1.0×10^{-5} M and (b) 5.0×10^{-5} M GSH with time | 102 |
| Figure. 4.8: | (a) Absorption spectra of AgNPs in presence of various concentrations of Cyste from 3.0×10^{-6} M to 5.0×10^{-8} M; inset: A plot of absorption ratio (A/A_0) with concentration of Cyste. (b) Calibration graph of Cyste in the range 1.1×10^{-6} M to 5.0×10^{-8} M; inset: photographs showing colour change of AgNPs in presence of Cyste | 104 |
| Figure. 4.9: | Absorption spectra of AgNPs in presence of GSH in the range 1.0×10^{-5} M to 5.0×10^{-7} M; inset(a) Calibration graph of GSH and inset(b) photographs showing colour change of AgNPs in presence of GSH..... | 105 |
| Figure. 4.10: | Selectivity of AgNP-Tyr towards different species. (Concentration of each species = 1.0×10^{-4} M other than 3.0×10^{-6} M Cyste) | 106 |
| Figure. 4.11: | Absorption spectra of AgNP-Cyste along with different species; Inset: Bar diagram representing the change in (A/A_0) of AgNP- Cyste, produced by each species | 107 |
| Figure. 4.12: | Absorption spectra of AgNPs in presence of GSH and different coexisting species; inset: Bar diagram representing the change in (A_0-A) produced by each species | 107 |
| Figure 5.1: | SWV of TBHQ and PG (1.0×10^{-6} M each) at bare GE and AB/GE..... | 114 |

| | | |
|-------------|---|-----|
| Figure 5.2: | Variation of over potential for the electro-oxidation of TBHQ and PG with pH..... | 116 |
| Figure 5.3: | Responses of TBHQ and PG in 0.1 M PBS of (a) pH 7 and (b) pH2 | 117 |
| Figure 5.4: | SEM images of (a) bare GE (b) AB/GE and (c) AB/GE (zoomed image), FESEM images of (d) bare GE (e) AB/GE and (f) AB/GE (zoomed image)..... | 118 |
| Figure 5.5: | Cyclic voltammetric response of 2.0×10^{-3} M $K_3[Fe(CN)_6]$ at different scan rates at gold electrode modified with various amounts of 1.25 gL^{-1} suspension of AB-Nafion; (a) bare GE (b) $1 \mu\text{L}$ (c) $2 \mu\text{L}$ and (d) $3 \mu\text{L}$ of suspension..... | 119 |
| Figure 5.6: | Electrochemical impedance spectrum of (a) bare GE and GE modified with (b) $1 \mu\text{L}$ (c) $2 \mu\text{L}$ (d) $3 \mu\text{L}$ (e) $4 \mu\text{L}$ and (f) $5 \mu\text{L}$ of AB suspension, inset: equivalent circuit..... | 121 |
| Figure 5.7: | LSV response of (a) 1.0×10^{-5} M TBHQ with varying scan rates from 0.02 Vs^{-1} to 0.1 Vs^{-1} , inset : a plot of $\log I$ vs. $\log v$ (b) 1.0×10^{-5} M PG with varying scan rates from 0.04 Vs^{-1} to 0.4 Vs^{-1} , inset : a plot of $\log I$ vs. $\log v$ | 123 |
| Figure 5.8: | Overlay of chronoamperograms for various concentrations of (a) TBHQ and (b) PG, inset (i) plot of current for TBHQ vs. $t^{1/2}$ (ii) plot of slope of (I vs. $t^{1/2}$) vs. concentration of TBHQ (iii) plot of current for PG vs. $t^{1/2}$ (iv) plot of slope of (I vs. $t^{1/2}$) vs. concentration of PG..... | 124 |
| Figure 5.9: | SWV response of (a) various concentrations of TBHQ in the range 1.0×10^{-4} M to 3.0×10^{-7} M, inset: plot of anodic peak current vs. concentration (1.0×10^{-6} M to 3.0×10^{-7} M) (b) various concentrations of PG in the range 1.0×10^{-4} M to 7.0×10^{-8} M, inset: plot of anodic peak current vs. concentration (1.0×10^{-4} M to 7.0×10^{-8} M) (c) simultaneous oxidation of TBHQ and PG in an equimolar mixture with concentration of each antioxidant ranging from 1.4×10^{-6} M to 1.0×10^{-7} M, inset: Plot of anodic peak current for simultaneous oxidation of TBHQ and PG vs. concentration (1.4×10^{-6} M to 1.0×10^{-7} M)..... | 127 |

| | | |
|-------------|--|-----|
| Figure 5.10 | Overlay of SWV of (a) TBHQ in the range 1.0×10^{-4} M to 4.0×10^{-7} M in presence of 1.0×10^{-6} M PG, inset: plot of anodic peak current vs. concentration of TBHQ (b) PG in the range 1.0×10^{-4} M to 1.0×10^{-7} M in presence of 5.0×10^{-5} M TBHQ, inset: plot of anodic peak current vs. concentration of PG | 131 |
| Figure 6.1: | SWV of ST and MT (1.0×10^{-4} M each) at (a) bare GE (b) GE modified with AB | 141 |
| Figure 6.2: | Plot of E_p vs pH for (a) 1.0×10^{-5} M ST and (b) 1.0×10^{-4} M MT, inset: voltammograms at various pH..... | 143 |
| Figure 6.3: | SEM images of (a) bare GE (b) GE modified with 4 μ L of 1 mg/mL AB suspension and (c) GE modified with 4 μ L of 1 mg/mL AB-Chitosan suspension | 144 |
| Figure 6.4: | Plots of current obtained for 2mM $K_3[Fe(CN)_6]$ vs. square root of scan rate at (a) bare GE (b) GE modified with 4 μ L of 1mg/mL AB suspension and (c) GE modified with 4 μ L of 1mg/mL AB-Chitosan suspension, inset: voltammograms obtained at various potential scan rate..... | 144 |
| Figure 6.5: | Electrochemical impedance spectrum obtained in 0.1 M KCl containing 5 mM $[Fe(CN)_6]^{3-/4-}$ at (a) bare GE (b) GE modified with 4 μ L of 1mg/mL AB suspension (c) GE modified with 4 μ L of 1mg/mL AB-Chitosan suspension and (inset) zoomed image of (c)..... | 145 |
| Figure 6.6: | Electrochemical impedance spectrum obtained in 0.1 M PBS containing (A) 1.0×10^{-4} M ST and (B) 1.0×10^{-4} M MT at (a) bare GE and (b) GE modified with 4 μ L of 1mg/mL AB-Chitosan suspension | 146 |
| Figure 6.7: | LSV response of (a) 1.0×10^{-4} M ST with varying scan rates from 0.03 Vs^{-1} to Vs^{-1} , inset i : a plot of $\log I_p$ vs. $\log v$, inset ii: a plot of E_p vs. $\ln v$ (b) 1.0×10^{-4} M MT with varying scan rates from 0.02 Vs^{-1} to 0.20 Vs^{-1} , inset iii: a plot of $\log I_p$ vs. $\log v$, inset iv: a plot of E_p vs. $\ln v$ | 148 |
| Figure 6.8: | Overlay of chronoamperograms for various concentrations of (a) ST and (b) MT, inset (i) plot of current for ST vs. $t^{1/2}$ (ii) plot of slope of (I_p vs. $t^{1/2}$) vs. | |

| | | |
|--------------|--|-----|
| | concentration of ST (iii) plot of current for MT vs. $t^{1/2}$ (iv) plot of slope of (I_p vs. $t^{1/2}$) vs. concentration of MT..... | 149 |
| Figure 6.9: | SWV response of (a.i) various concentrations of ST in the range 1.0×10^{-4} M to 5.0×10^{-7} M, (a.ii) plot of anodic peak current vs. concentration (1.0×10^{-4} M to 5.0×10^{-7} M) (b.i) various concentrations of MT in the range 4.5×10^{-4} M to 2.0×10^{-5} M, (b.ii) plot of anodic peak current vs. concentration (4.5×10^{-4} M to 2.0×10^{-5} M) (c.i) simultaneous oxidation of ST and MT in an equimolar mixture with concentration of each antioxidant ranging 2.0×10^{-4} M to 1.0×10^{-5} M, (c.ii) plot of anodic peak current for simultaneous oxidation of ST and MT vs. concentration (2.0×10^{-4} M to 1.0×10^{-5} M)..... | 152 |
| Figure 6.10: | Overlay of SWV of (a.i) ST in the range 1.0×10^{-4} M to 5.0×10^{-6} M in presence of 1.0×10^{-4} M MT (a.ii) plot of anodic peak current vs. concentration of ST (b.i) MT in the range 5.0×10^{-4} M and 5.0×10^{-5} M in presence of 5.0×10^{-5} M ST (b.ii) plot of anodic peak current vs. concentration of MT..... | 157 |
| Figure 7.1: | A contour map describing fluorescence intensity of QDs in a range of excitation wavelength | 164 |
| Figure 7.2: | a) Absorption spectrum, b) TEM image and c) DLS spectrum of CdTe QDs | 166 |
| Figure 7.3: | TEM image of QDs in the i) absence and ii, iii) presence of ST..... | 168 |
| Figure 7.4: | a) 5.0×10^{-5} M ST, b) 1.0×10^{-4} M ST, c) CdTe QDs, d) 5.0×10^{-5} M ST added to QDs, e) 1.0×10^{-4} M ST added to QDs.. | 169 |
| Figure 7.5: | Change in fluorescence intensity of a) QDs b) 1.0×10^{-6} M ST and c) 5.0×10^{-6} M ST with time..... | 171 |
| Figure 7.6: | a) Fluorescence spectra of QDs in presence of varying concentration of ST and b) linear plot of $\frac{I_0}{I}$ with concentration of ST..... | 172 |
| Figure 7.7: | a) Fluorescence spectra of QDs in presence of various concentrations of HIAA b) plot of $\frac{I_0}{I}$ vs. concentration of HIAA and c) plot of $\log\left(\frac{I_0}{I}\right)$ vs. concentration of HIAA. | 173 |

| | | |
|-------------|--|-----|
| Figure 7.8: | a) Plot of $\left[\frac{I_0}{I} - 1 \right] \frac{1}{[Q]}$ vs concentration of HIAA b) plot of $\frac{\tau_0}{\tau}$ vs concentration of HIAA. | 174 |
| Figure 7.9: | Fluorescence spectra of QDs in presence of various species at 1.0×10^{-3} M concentration..... | 175 |

||| List of Schemes |||

| | | |
|------------|---|-----|
| Scheme 3.1 | Mechanism of electro-oxidation of DA | 85 |
| Scheme 3.2 | Schematic representation of voltammetric sensor for dopamine..... | 90 |
| Scheme 4.1 | Structures of GSH, Lcys and Cyste | 92 |
| Scheme 4.2 | Schematic representation of colorimetric sensor for the determination of biothiols - glutathione and cysteamine..... | 110 |
| Scheme 5.1 | Mechanism of electro-oxidation of (a) TBHQ and (b) PG | 126 |
| Scheme 5.2 | Voltammetric sensor for simultaneous determination of the antioxidants – tert - butyl hydroquinone and propyl gallate | 135 |
| Scheme 6.1 | Voltammetric sensor for simultaneous determination of the tryptamines – serotonin and melatonin | 160 |

Chapter 1

Introduction

| | |
|------------------------|---|
| <i>C o n t e n t s</i> | 1.1 <i>Sensors</i> |
| | 1.2 <i>Constitution of a sensor</i> |
| | 1.3 <i>Electrochemical sensors</i> |
| | 1.4 <i>Optical sensors</i> |
| | 1.5 <i>Colorimetric sensors</i> |
| | 1.6 <i>Fluorescence sensors</i> |
| | 1.7 <i>Objectives</i> |
| | 1.8 <i>Literature review of voltammetric sensors</i> |
| | 1.9 <i>Literature review of colorimetric sensors</i> |
| | 1.10 <i>Literature review of fluorescence sensors</i> |

Sensors are self contained devices which provide real-time analytical specifics of a test sample.¹ It can deliver immediate information about specific compounds or ions in a complex matrix. They are used to identify the presence, followed by quantification of a particular species (the analyte) present in the matrix under observation.

1.1 Sensors

Sensors are self contained devices which provide real-time analytical specifics of a test sample.¹ They are used for identification, followed by quantification of a particular species (the analyte) present in the matrix under observation. In the present scenario, a sensor is primarily used as a diagnostic tool in various fields like clinical analysis, quality control, chemical monitoring etc. In clinical analysis, a chemical sensor may be used to identify diseases such as carcinoid tumors, neurodegenerative disorder, cardiovascular disorders, rheumatoid arthritis, diabetes etc. at the early stages. This is accomplished by the quantification of traces of various chemicals produced in the physiological fluids by the onset of these diseases. These chemicals which are generated in the body fluids especially at disease conditions are called the biomarkers.

In exceptional cases, the quantification of more than one biomarker or their ratio can unwrap more information about the state of a disease. Thus individual or simultaneous determination of these biomarkers present in physiological fluids is of great demand. This is the same in the case of food quality analysis. A chemical sensor offers the detection and/or determination of more than one analyte individually or even simultaneously.

1.2 Constitution of a sensor

The chemical information regarding the analyte is converted to a comprehensible output through mainly two processes - sensing (recognition) and transduction². The **recognition element** of the sensor interacts more or less selectively with the analyte/analytes in such a way that the resulting interaction will be directly proportional to the concentration of the species.

In some instances the interaction between the analyte and the recognition element can produce changes in the properties of the recognition element which could be used for specific detection purposes. Various nanomaterials, electro-polymers, quantum dots etc. are widely used as label free recognition elements.

The resultant interaction between the analyte and the recognition element will be transferred or translated to a readable output with the help of a *transducer*². A number of transduction techniques are used for the read out including various electrochemical and optical methods. Among them the most widely accepted and adopted ones are voltammetry, colorimetry and fluorimetry owing to their inherent superlative features such as simplicity, very fast responses, detection and determination of very lower concentrations of the analyte etc.

1.3 Electrochemical sensors

1.3.1 Electrochemical techniques and voltammetry

Test samples of aqueous matrix are usually analysed with the help of electrochemical transduction means. Electrochemical methods rely upon the charge distribution and charge transfer reactions, chiefly electron transfer reactions, occurring at the interface of solution and electrode. In some electrochemical methods, electro-chemical reactions at equilibrium are studied. In such methods, the electromotive force produced in the cell is a variable. In *potentiometric sensors*, the potential difference developed on either side of a membrane (the recognition element) due to ion exchange is correlated to the concentration of the species. In some other cases, electro-chemical reactions at non-equilibrium conditions are studied where the

reaction will proceed with a specific trend to any one end, to oxidation or reduction³. The reaction will induce flow of current in the system. The current produced at a certain potential will be directly related to the concentration of the reacting species in *amperometric sensors*³. Some methods depend on the current developed in the system upon application of a range of potential. Since a species undergo oxidation or reduction at a potential which is characteristic to it, the current produced at a given potential may be correlated to the concentration of the species. Current – potential curves are obtained with analytical intention in *voltammetric sensors*³.

1.3.2 Voltammetry- The transduction technique

Voltammetry is a highly sensitive electrochemical method resonating between evaluation of current and potential. There are various voltammetric techniques, the uniqueness of which rely on the mode of application of potential to the system and measurement of current. These variations can bring out different information regarding physical, chemical and electrochemical nature of the reaction. They include highly sensitive quantification, number of electrons involved in the electrochemical reactions, diffusion coefficients and rate constants. Various forms of voltammetric techniques used for development and optimization of a sensor are detailed below.

Cyclic Voltammetry is based on the application of varying potential at a specific scan rate in both forward and reverse directions, monitoring the current. If the potential scanning is done only in one direction then the technique is termed as *linear sweep voltammetry*. Though cyclic

voltammetry is not frequently used to determine an analyte quantitatively, it is widely used to ascertain the redox nature of a reaction, to understand reaction intermediates and to obtain stability of reaction products. The important parameters of a cyclic voltammogram are the peak potentials (E_{pa} , E_{pc}) and peak currents (i_{pa} , i_{pc}) of the anodic and cathodic peaks, respectively. The separation between anodic and cathodic peaks points to the reversibility of the reaction.⁴

$$\Delta E_p = E_{pa} - E_{pc} = 2.303 RT/nF$$

A reversible redox reaction with n electrons shows ΔE_p value equal to $\frac{0.059}{n}$ V at 25 °C. The reversible nature of the reaction is a characteristic of quick electron transfer process compared to diffusion of analyte from bulk solution to the interface. Irreversibility due to a dawdling electron transfer rate results in larger ΔE_p value than $\frac{0.059}{n}$ V, gives a quasi reversible or irreversible system. For a reversible reaction, the concentration is related to peak current by the Randles - Sevcik expression (at 25 °C)⁵

$$i_p = (2.687 \times 10^5) n^{3/2} \nu^{1/2} D^{1/2} A C$$

where i_p is the peak current (A), A is the electrode area (cm²), D is the diffusion coefficient (cm² s⁻¹), C is the concentration in mol cm⁻³, and ν is the scan rate in V s⁻¹.

Square wave voltammetry (SWV) is a prominent electrochemical technique appropriate for analytical application, mechanistic study and electro kinetic measurements of electrode processes⁶. SWV is one the most commonly used pulse technique owing to its superior properties including

fast response, low background currents and high signal to noise ratio. It unifies the advantages of pulse techniques (enhanced sensitivity), cyclic voltammetry (insight into the electrode mechanism) and impedance techniques (kinetic information of very fast electrode processes).

The modern SWV, incorporated in digital electrochemical instruments utilizes a typical potential modulation consisting of a staircase potential ramp modified with square shaped potential pulses. At each step of the staircase ramp, two equal in height and oppositely directed potential pulses are imposed which complete a single potential cycle in SWV. The net current, i_{net} , is obtained by taking the difference between the forward and reverse currents ($i_{\text{for}} - i_{\text{rev}}$) and is centered on the redox potential. The peak height is directly proportional to the concentration of the electro-active species and extremely low detection limits are possible.

1.3.3 Various processes occurring in the system on application of potential

Application of potential to the electrode in contact with an electrolytic solution; will rearrange the randomly distributed dipoles in the solution to form an electrical double layer. i.e. the distribution of charges opposite to that of the electrode at the immediate zone at the interface next to the electrode surface. Such double layer formation has been well researched by Helmholtz in 1870s and theories regarding them were formulated and suitably modified till date.⁷

During the electrode process the analyte travels from the bulk of the solution to the diffusion layer, then to the electrical double layer and to the electrode surface where it gets converted to the product. Thus, the rate of the

electrode process depends on the rate at which the electron transfer processes (oxidation or reduction) occur at the interface (*electrode kinetics*) as well as the rate at which the analyte reaches the electrode surface (*mass transport*)⁸. The mass transport may occur in three different ways—*convection, migration and/ or diffusion*. In voltammetry the the first two means of mass transport is usually suppressed by keeping the solution stationary and by the introduction of highly concentrated supporting electrolyte. Thus the electrode processes in voltammetry are controlled by diffusion of the analyte. The current registered at the electrode will be dependent variable of the diffusion as well as the electrode kinetics⁹.

1.3.4 Measurement of current

In a typical electrochemical cell, the electrolysis entails oxidation or reduction of species at anode or cathode respectively. Different compounds may undergo these reactions simultaneously. In order to avoid this and to get reliable analytical information, the electro-chemical cell is operated in such a way that the reaction under focus occurs only at any one of these electrodes termed as *working electrode or indicator electrode* (WE). The current produced in a system is a variable, dependent of the applied potential. Potent attempts are needed to maintain the potential of WE constant, so as to study the electrochemical reaction quantitatively. Two approaches are widely used to control the potential of the WE namely two electrodes system or three electrodes system¹⁰.

In a two electrode system, in the absence of external potential the system remains at equilibrium. When an external voltage is applied, the potential of the WE modify without altering that of the other electrode

termed as *reference electrode* (RE). RE possess well defined, stable equilibrium potential and is non-polarisable. In an electrochemical cell, the potential of an electrode is adjusted with respect to RE. The best known example of RE is standard hydrogen electrode. Due to the difficulty in its practical use, many other electrodes such as Hg/Hg₂Cl₂ electrode or Ag/AgCl electrode are used¹⁰.

At a given potential, current flow begins which in turn develops a potential difference across the electrolyte. The potential drop in accordance with the Faraday's law, given by $R_s i$ is commonly called the ohmic drop. If current produced is in the order of microamperes or less than that, the ohmic drop produced will be negligible which allows the quantitative assessment of the electro-chemical reaction. However the voltage drop becomes a critical problem when the current – potential curve is to be obtained⁷.

More meticulous control of potential is accomplished with the help of a three electrode cell. Here a new electrode, the *auxiliary electrode or counter electrode* (AE) is introduced, between which and WE the current is measured. Since no current is allowed to flow through the reference electrode, its equilibrium will be maintained. Thus, the potential of the WE can be adjusted without suffering any interference from the ohmic drop in comparison to a two-electrode cell.¹⁰

In order to maintain the proper functioning of the three electrode system, AE having larger surface area than that of the WE is preferred. The larger surface area helps to lower the current density produced by any reactions that may occur at AE. Thereby it avoids the interventions which

may be produced by reactions in the solution or at AE. A platinum coil or wire is widely preferred as AE.

WE is the electrode at which the reaction under observation occurs. Selection of WE is done on the basis of several features mainly, intact electro-chemical behavior in a wide potential window, renewable and reproducible electrode surface, low ohmic resistance, low residual current, high over potential towards oxygen and hydrogen evolution and non-toxic nature. Electrode fabricated from materials like gold, platinum, mercury, carbon etc. are popular owing to their remarkable properties for example low electrical resistance, high thermal and chemical stability, impermeability to liquids and gases etc.^{11,12}

While using a bare electrode for the quantitative analysis, the electrochemists come across various problems such as high overpotential, lethargic electrode kinetics, fouling of electrode surface and low electrode stability¹³. In late 20th century, it was observed by Murray and team that upon modification of the electrode surface, its properties could be retained or even improved.¹⁴

1.3.5 Chemically modified electrodes (CMEs) – The recognition element

The CMEs drew more attention after the chemical modification of the electrode through introduction of functional groups by Murray et al.^{15,16} Compared with other electrode concepts in electrochemistry, the distinguishing feature of a CME is that a quite thin film (from a molecular monolayer to perhaps a few micrometers-thick multilayer) of a selected chemical is bonded to or coated on the electrode surface. This is to bestow

the electrode with the electrochemical, chemical, electrical, optical and other desirable properties of the film. Modification of the electrode is accomplished via covalent bonding, sorption, heterogeneous multilayer formation, coating with a polymer film etc. Various nanoparticles, polymers, ionic liquids, organic molecules and inorganic complexes are generally used for modification purpose.¹⁷

1.3.5.1 Nano materials and/or polymers modified electrodes

Among electrode modifiers, nano-structured materials are preferred owing to their appreciable electronic conductivity, high surface area, high mechanical strength and electro-catalytic properties¹⁸. Owing to the small size of nanoparticles, a large number of constituent atoms are not entirely participated in chemical bonding with nearby atoms, which in turn increases their reactivity as well as catalytic activity. Although the direct electrical and electrochemical detection of biomolecules is possible, many have benefited from the electroactive or catalytic properties of NPs for biosensing with unprecedented levels of sensitivity¹⁹. Synthetic nanomaterials of diverse chemical composition are widely used in sensor applications. Such nanomaterials are of different origin - chemical elements (metals, carbon or silicon), inorganic compounds (metal oxides) or organic compounds (polymers).

Another class of modifier, polymer films evoke considerable interest due to their chemical stability, strong adherence to electrode surface, reproducibility and availability of more electro-active sites. Different types of polymers are used as chemical modifiers. Natural polymers (dextran,

chitosan) and synthetic polymers (polymers of aniline, toluene sulphonic acid, amino benzene sulphonic acid, amino naphthalene sulphonic acid, amino hydroxy naphthalene sulphonic acid) are among the most popular modifiers²⁰. These polymers are layered on the electrode surface by means of dip casting, drop casting or electro-polymerisation. The electro polymerisation of the electrode is achieved by dipping the electrode in a solution containing desirable concentration of the monomer or monomers followed by the execution of appropriate electrochemical technique.

Electro-deposition of metal nanoparticles followed by polymerisation on the electrode surface yields nano-polymer composites which synergise the properties of both nanoparticles and polymer films, which inturn can act as excellent electrochemical sensors.²¹

1.4 Optical sensors

The changes in optical properties of the recognition element induced by an analyte acts as the basis for optical sensing. Depending on the characteristic changes studied, they are broadly classified as spectrophotometric/ colorimetric and fluorimetric sensors.

1.5 Colorimetric sensors

1.5.1 Colorimetry/Spectrophotometry – The transduction technique

Colorimetry/Spectrophotometry is a technique based on Beer-Lamberts law. The most attractive feature of this technique is its ease of use. The desirable feature of the target molecule is that it should absorb in the

UV-vis range or it should produce appreciable changes in the absorption of a molecule which otherwise will absorb in the mentioned range.²²

In spectrophotometry, an electromagnetic radiation of desirable wavelength is passed through the solution and the amount of light transmitted or the light absorbed is measured. The relative amount of a particular wavelength of light absorbed by a species is termed absorbance and the unimpeded fraction of light which passes through the solution is called the percentage transmittance. The wavelength of light with which the sample is irradiated may belong to UV, visible or even IR region and the quality of light absorbed gives an idea about the type or kind of the species. Whereas the quantity of light absorbed is correlated to the concentration of the species with the help of Beer- Lamberts law.²³

If the irradiated light is of visible region, the technique is termed colorimetry. In some cases, the target molecule may not absorb from the visible region. In such instances, various reagents are added to impart colour to the solution. The interaction between the reagent and the target species can reduce, enhance or even change the colour of the solution which acts as the back bone of colorimetric quantifications.²⁴

1.5.2 Processes leading to sensing

In the modern era of nanotechnology, different nanomaterials owing to their special features especially the Surface Plasmon Resonance, are used widely in colorimetric sensing applications. In a nanoparticle, Localized Surface Plasmon Resonance (LSPR) arises from the electromagnetic waves that propagate along the surface of the conductive metal²⁵. The excitation of a nanoparticle with light produces an intense absorption and scattering due

to the collective oscillation of the conduction electrons located at the NPs' surface.

Though these LSPR bands roughly depend on the size of the particle and refractive index of the medium, they are strongly affected by the inter particle distance. In presence of the analyte, the nanoparticles undergo aggregation, changing the Plasmon coupling among the particles, producing red shift of the LSPR band leading to colour change²⁶. More specifically, analyte induces surface effects such as detachment of stabilizing / capping agent, binding of analyte to surface or to stabilizing groups. Sometimes analytes functions as cross linkers between particles, resulting in aggregation of nanoparticles. Rarely, analytes remove the capping agents from surface of nanoparticles through bond formation and this will lead to reduction in their stability resulting in aggregation.²⁷

Most of the colorimetric biosensors based on gold and/or silver NPs have been developed on the basis of these changes in color generated by the plasmon coupling between NPs upon aggregation, while other methods have used the LSPR properties of the noble metal NPs just as a colorful reporter.²⁸ Some are based on the unspecific adsorption of biomolecules to non-functionalized noble metal NPs, while others are based on functionalized noble metal NPs for increased specificity.

Those nanoparticles of gold or silver origin, shows extremely high absorption coefficients and scattering properties within the UV/visible wavelength range which imparts higher sensitivity in optical detection methods than conventional organic dyes. This provides them ideal candidature for colorimetric biosensing applications.^{27, 29}

1.5.3 Silver nanoparticles- The recognition element

1.5.3.1 Synthesis and Functionalization of Nanoparticles

A large number of techniques are available for the synthesis of nanoparticles. They include chemical methods for example hydrolysis, thermal decomposition, chemical reduction, photochemical reduction etc. and physical methods including laser ablation, vapor deposition, grinding etc.^{27,28,29} These methods ultimately aim at the synthesis of homogeneous nano particles having controlled size, shape and surface functionalities which is done to extract the best properties for sensing applications.

Colorimetric sensors based on silver nanoparticles (AgNPs) are more affordable but less explored compared to gold nanoparticles. Owing to their unique properties, for instance, high extinction coefficient and narrow surface plasmon resonance band in the visible region, AgNPs are gaining attention these days.³⁰ These silver nanoparticles, also identified as colloidal silver may be synthesized effortlessly in varying sizes and shapes. Normally they possess quasi-spherical shape, primarily due to the lower surface energy of spherical particles. Commonly, the silver nanoparticles are synthesised by the chemical reduction of Ag^+ ions to Ag^0 ions using the reducing agent sodium citrate. Here the citrate group acted both as reducing as well as capping agent which protects the NPs from the formation of particles with larger size owing to electrostatic repulsion among citrate-capped silver NPs.^{31,32} Different methodologies are available for the synthesis of different noble metal NPs having different size, shape and constitution^{33,34,35}. Inorder to satisfy the various conditions like

biocompatibility and specificity in targeting, functionalization with different moieties have been experimented by many groups.^{36,37}

The interaction between the biomolecule (analyte) and the nanoparticles may be electrostatic, chemisorptions or affinity based. Though the electrostatic interactions are very simple and straightforward to perform, they are restricted to opposite charged biomolecules and NPs and are very sensitive to matrix properties. If the analyte is capable of better adsorption than the capping agent without any chemical modification, chemisorption provides excellent results. For instance, in the case of thiol functionalized biomolecule, quasi-covalent binding of the analyte to the silver nanoparticles acts as a better option. In rare cases, it may be subjected to interference by other chemical groups available for adsorption within the biomolecule.³⁸

1.6 Fluorescence sensors

1.6.1 Fluorescence- the transduction technique

A molecule upon electronic excitation, jump from a ground singlet state (S_0) to an excited singlet state (S_n). After spending a period of time in the excited state, it relaxes to the ground state may be through radiative or non-radiative decay. The decay pathway followed by a molecule to reach the ground state is depicted by Jablonski diagram. They include, non-radiative transitions from an excited state to a lower energy level of same spin multiplicity (internal conversion), states of different multiplicity (Inter system crossing) and vibrational states of same electronic level (vibrational relaxation).³⁹

Radiative decay happening from S_1 to S_0 state is termed as fluorescence. It is a spin allowed process and usually the decay occurs in a time span of 10^{-12} to 10^{-9} second. Another Radiative transition occurs from T_1 to S_0 is named as phosphorescence. Here the decay process is delayed due to intersystem crossing and the molecule takes around 10^{-8} second to reach the ground state upon excitation.⁴⁰

1.6.2 Irradiation of light- The input

When a molecule is irradiated with an electromagnetic radiation of appropriate energy, the molecule gets excited to the higher energy level. It spends a time period before getting relaxed by emitting photons. The period of time spent by a fluorescent molecule (fluorophore) in the excited energy level is known to be its fluorescence lifetime⁴¹. It usually ranges from pico to nano seconds. The ratio of number of photons emitted by a fluorophore to the number of photons absorbed by it is its quantum yield⁴². Fluorophores having longer lifetime are preferred for sensor applications.⁴³

Being in the higher energy level, fluorophore undergo non-radiative transition preceding the radiative transitions. Thus the emitted energy will be always lesser than the excitation energy.⁴⁴ This inturn results in a change in the emission wavelength compare to the absorption wavelength. The difference between spectral position of band maxima of absorption and emission is called as Stokes shift.⁴⁵ Sometimes the solvent reorganisation, excited state reaction, energy transfer and complex formation can also bring out remarkable Stokes shift.⁴⁶ For sensing purposes, fluorophores having larger Stoke shift are preferred.⁴⁷

1.6.3 Processes leading to sensing

Introduction of an analyte into the fluorophore solution results in changes in the fluorescence intensity of the fluorophore. Sometimes an enhancement or sometimes a decrease in the fluorescence intensity of the fluorophore occurs. Various processes accompanying a decrease in the fluorescence intensity of a given sample is called quenching. Different molecular interactions leading to quenching are molecular rearrangements, energy transfer and excited state interactions. A decrease in the amplitude of lifetime by fluorophore itself or by some other molecules present in the system (non-molecular interaction) can also lead to quenching. Mechanisms behind quenching are broadly classified into static and dynamic quenching.⁴⁰

1.6.4 Contact or static quenching

The presence of an analyte in close proximity to the fluorophore can induce ground state interactions. Since these interactions occur at the ground state, the lifetime of the fluorophore which undergo excitation will not be affected. Absence of any change in the lifetime is a characteristic of static quenching.

Concentration of the analyte (quencher) and fluorescence intensity of the fluorophore in the presence of the quencher is correlated with the help of Stern - Volmer equation.

$$\frac{I_0}{I} = K_s C + 1$$

I_0 and I indicate the fluorescence intensity of the fluorophore in the absence and presence of the analyte, K_s is the Stern – Volmer constant, C is the analyte concentration

1.6.5 Collisional or dynamic quenching

Analyte which is much closer to the fluorophore can undergo diffusing encounter in the excited state. This will change the period of time spent by the fluorophore in its excited state. Thus altered lifetime of fluorophore in presence of the analyte is a characteristic of dynamic quenching.

The lifetime of fluorophore in presence of the analyte may be correlated to the concentration of the analyte using Stern – Volmer relation.

$$\frac{I_0}{I} = K_q \tau_0 C + 1$$

$$\frac{I_0}{I} = K_d C + 1$$

I_0 and I indicate the fluorescence intensity of the fluorophore in the absence and presence of the analyte, K_d is the dynamic quenching constant, C is the analyte concentration, τ_0 is the lifetime.

It has been observed that variations in the temperature of the system can alter the quenching of fluorophore in presence of the analyte. An increase in temperature can increase the dynamic quenching as the number of collisions between the analyte and the fluorophore may get increased.

1.6.6 Combination of both static and dynamic quenching

In rare cases, contributions of both static and dynamic components towards quenching are observed. In such cases, the concentration of the quencher may be correlated to the fluorescence intensity of the fluorophore as follows.⁴²

$$\frac{I_0}{I} = 1 + (K_s + K_d)[Q] + K_s K_d [Q]^2$$

Since the concentration of the quencher is related to the intensity of the fluorophore through a quadratic equation, the plot will not be linear but will be concave to Y-axis. Therefore in order to quantify the analyte, $\log \frac{I_0}{I}$ vs C is plotted.

To ascertain the values of K_s and K_d , $\left[\frac{I_0}{I} - 1 \right] \frac{1}{[Q]}$ vs. [Q] may be plotted, as the slope of the plot gives $K_s K_d$. The dynamic component of quenching follows the equation,

$$\frac{\tau_0}{\tau} = 1 + K_d [Q]$$

Value of K_d may be obtained from the slope of the plot of $\frac{\tau_0}{\tau}$ vs. [Q]. Thus from $K_s K_d$, value of K_s may also be estimated.

1.6.7 Fluorophores - the recognition element

Those chemical species that can emit photons during relaxation from first excited state to ground state is usually termed as a fluorophore.⁴² A fluorophore which possess high molar absorption coefficient and quantum yield is ideal for sensor applications.⁴⁷ Long lasting stability on continuous

illumination or resistance to photo bleaching is yet another characteristic of an ideal fluorophore. The inherent characteristics of a fluorophore may alter with changes in its matrix. The interaction between the fluorophore and analyte results in a desirable fluorescent signal.

1.6.8 Quantum dots

Among various fluorophores available, quantum dots are widely used owing to its superior features such as remarkably high photo and chemical stability, high quantum yield, broad absorption, tunable emission etc.⁴⁸ These features enable them for various applications such as bio imaging, display device preparation, miniature laser design, labelling, sensing etc.⁴⁹ The eminent properties of QDs are due to quantum confinement compared to bulk. In QDs the electrons are confined within the De Broglie wavelength limit in all the three dimensions. This in turn provides crystalline structure whose behaviour lies between a single atom and bulk.⁵⁰ Moreover, from bulk to zero dimension, the density of states increases thereby producing discrete energy levels of conduction and valence bands.

Transition of electrons between these energy levels imparts unique spectral properties to them. It was discovered by Henglein that the optical properties of QDs are size dependent. The level of QDs are confined to a small space (nm^3) due to which the energy levels and transition between them is highly size dependent.⁵¹ Having lower size than that of bulk exciton Bohr diameter, the band gap of the QDs decreases with increasing size, thus enabling the tunable emission. With decreasing band gap emission of the QDs shifts from blue to red region of the visible spectrum occurs.⁵²

Upon irradiation of QDs with light of suitable energy, the electrons get excited to the conduction band leaving a hole in the valence band. Then the excited electrons relax to get recombined with the hole together with emission of light. But, the irregularities present on the QD surface can create other energy levels within the band gap. These energy levels are called trap states since these states induce non-radiative recombination of excited electrons. This in turn can decrease the quantum yield of the QDs. Due to the presence of various trap states; the lifetime of QDs also can have different components.

In some cases the emission dynamics may be highly complicated - di, tri or tetra exponential decay owing to the surface defects that can produce the trap states which lie within the band gap^{53,54,55}. The shortest decay time (fastest emission) may be ascribed to the immediately populated core-state recombination and reveal the fluorescence produced by radiative relaxation of the electrons to the ground state.^{56,57} In some cases the conduction band electrons or the excited electrons may get localized in trap states, resulting in non radiative decay. The slowest decay may be correlated to the surface states as well as the radiative recombination of the electrons and holes.^{58,59} These different processes in combination with disparities possessed by each nano crystal in a matrix produces highly complicated multi-exponential emission dynamics.⁶⁰

Non-radiative decays can be lowered by adopting different approaches like surface functionalisation, surface passivation, proper designing and execution of synthetic procedure etc.

1.6.9 Surface functionalised QDs

QDs were synthesised from its precursors mainly through bottom up or top down approaches. Considering the practical difficulties in handling top-down procedures, bottom-up procedures are commonly used. Early stages of synthesis were based on non-aqueous solvents. But, to extend their utility in aqueous matrices, the QDs should be made hydrophilic.⁶¹ Among a large number QDs based on cadmium, CdTe QDs are more attractive owing to their narrow band gaps. Rajh and his team developed a method for the aqueous synthesis of 3-mercapto-1,2-propane-diol stabilised, CdTe QDs.⁶¹ Later various groups were indulged in aqueous synthesis of CdTe QDs functionalised with carboxyl, amine or imine end groups.⁶²⁻⁶⁵ These were specifically used for sensing applications.

1.7 Objectives of the present investigations

Real time analysis is a primary need of modern era. Identification and quantification of various targets from complex matrices like food and physiological fluids are gaining remarkable attention. Development of methods for highly sensitive, interference free, simple and cost effective determination of these targets is a challenge to the researchers of this field. Significant efforts have been invested in solving these problems. Use of sophistic instruments and adoption of new methods are bringing breakthrough in the field of sensing.

The most prioritized objective of the present research is to develop sensors for antioxidants and biomarkers. Individual, dual or simultaneous determination of these analytes may be accomplished with the help of voltammetric or optical sensors.

It also aimed at the development of sensor for target molecules which are functionally or structurally similar or coexisting in the real matrix.

Another objective of the present investigations was to probe the efficiency of various metallic and non-metallic nanomaterials as sensing elements of different sensors.

1.8 Literature review of different voltammetric sensors utilizing acetylene black nanoparticles or poly (4-amino 3-hydroxy naphthalene sulfonic acid) (pAHNSA) modified electrodes as the recognition element

We are currently witnessing a remarkable revolution in various fields of science and technology as a result of the development of nanomaterials ^{66,67}. This line of development has a considerable impact on the state-of-the-art of chemical sensors and considerable progress in this area has already been achieved by the application of nanomaterials ⁶⁸⁻⁷⁰ alone or in combination with natural or electro-polymers.

1.8.1 Acetylene black nanoparticles as modifiers

In a voltammetric sensor, the working electrode undergoes chemical modification to improve its performance characteristics. Thus chemically modified electrode - the recognition element, is one of the most important parts of the sensor. From 1993 onwards acetylene black (AB) has been used to enhance the electrochemical response of various target molecules. ⁷¹

Acetylene black (AB) is a non-extensively used nano form of carbon. AB possesses characteristic features such as cost-effectiveness,

chemical stability, electrical conductivity, catalytic property etc. The properties compatible with the electrochemical studies helps it to be widely used in electrode modification purpose ⁷². Various forms of carbon have been used for the fabrication of carbon paste electrodes, widely graphite powder. In 2004, AB was utilized to fabricate carbon paste electrode, after mixing with graphite or as such.

Widely AB is mixed with paraffin oil to make it into a paste which is filled in the cavity of the electrode to produce a carbon paste electrode (ABPE). Electrodes fabricated with the aforementioned procedure has been used for the Voltammetric determination of pharmaceutical – tetracycline ⁷³, neurotransmitter –adrenaline ⁷⁴, various metal ions- lead ⁷⁵, molybdenum ⁷⁶ O₂/O₂⁻ couple ⁷⁷ in DMF and bisphenol A ⁷⁸.

In some cases, in order to improve the efficiency of the electrode, various surfactants are also being used. For example, the electrochemical behaviour of adrenaline at the acetylene black electrode in the presence of sodium dodecyl sulfate (SDS) was investigated. The results indicated that the electrochemical responses of adrenaline were apparently improved by SDS, due to the enhanced accumulation of protonated adrenaline via electrostatic interaction with negatively charged SDS at the hydrophobic electrode surface. This was verified by the influences of different kinds of surfactants on the electrochemical signals of adrenaline ⁷⁴.

In a method developed by Yang et al. the determination of sodium nitroprusside (SNP) was carried out in presence of cetyltrimethylammonium bromide (CTAB) ⁷⁹. Voltammetric studies showed that SNP exhibited a pair of quasi-reversible redox peaks at the electrode in the presence of CTAB

while no redox peak was observed in the absence of CTAB. This was attributed to the enhanced adsorption of SNP at AB through electrostatic interactions between SNP and CTAB as well as hydrophobic adsorption of CTAB at the hydrophobic surface of ABPE.

In one of the methods developed for the determination of trace amounts of vanadium (V) adsorptive anodic stripping voltammetry has been used. The method was based on the preconcentration of the V(V)–alizarin violet (AV) complex at open circuit while stirring the solution for 90 s in 0.15 M hexamethylenetetraamine–hydrochloric acid buffer (pH 4.4). The adsorbed complex was then oxidized, producing a response with a peak potential of 0.56 V in the potential window between 0 V and 1 V. The optimised sensor was successfully applied for the determination of V (V) in natural water samples.⁸⁰

As the efforts in improving the performance of the carbon paste electrodes have been progressed, mixture of AB with various nano materials or polymers were experimented. In 2012, a novel method has been developed by Deng et al. for the determination of p-nitrophenol (p-NP), which was based on the enhanced electrochemical response of p-NP at acetylene black paste electrode coated with salicylaldehyde-modified chitosan (S-CHIT/ABPE). In 0.2 M HCl, p-NP yielded a reduction peak at -0.348 V. Compared with the poor response at conventional carbon paste electrode, S-CHIT/ABPE remarkably increased the peak current of p-NP.⁸¹

In order to understand the role of different components in the performance of composite electrode, cyclic voltammetry was performed with isolated MnO₂ powder and mixed acetylene black/MnO₂ powder.

Crystallized manganese dioxide powder was electrochemically investigated in mild aqueous electrolytes with the cavity microelectrode (CME) technique. High electrochemical performance is achieved exhibiting large, intense and more defined peaks, than for a composite electrode.⁸²

Electrochemical behaviors of methocarbamol (MET) at the bare carbon paste electrode (CPE), acetylene black (AB) modified carbon paste electrode (ABPE), an ionic liquid 1-benzyl-3-methylimidazole hexafluorophosphate ([BnMIM]PF₆) modified carbon paste electrode ([BnMIM]PF₆/PE) and AB-[BnMIM]PF₆ modified carbon paste electrode (AB-[BnMIM]PF₆/PE) in PBS (pH = 6.8) were investigated by cyclic voltammetry (CV) and square wave voltammetry (SWV). The experimental results showed that MET at the above mentioned four electrodes showed an irreversible electrochemical oxidation process, but at the AB-[BnMIM]PF₆/PE, the oxidation peak potential keep almost constant and the oxidation peak current of MET increased greatly.⁸³

The electrode fabricated with the composite of AB and reduced graphene oxide (GR) resulted in highly improved determination of the food contaminant bisphenol A (BPA). This modified electrode was obtained by one-step potentiostatic reduction of exfoliated graphene oxide sheets on the surface of ABPE. Due to the unique structure and extraordinary properties of GR and AB, the fabricated sensor displayed greatly improved voltammetric response to BPA compared with the conventional carbon paste electrode.⁸⁴

In a sensor developed by Deng et al. for BPA determination, acetylene-black paste electrode modified with a chitosan film molecularly

imprinted for BPA was used. The use of a molecular imprint provides an efficient way for eliminating interferences from potentially interfering substances. The high sensitivity for the determination of the analyte in the nano molar range, selectivity and stability of the sensor demonstrated its practical application⁸⁵

Again Deng et al. fabricated graphene–polyvinylpyrrolidone composite film modified acetylene black paste electrode (GR–PVP/ABPE) and it was used to determine vanillin. In 0.1 M H₃PO₄ solution, the oxidation peak current of vanillin increased significantly at GR–PVP/ABPE compared with bare ABPE, PVP/ABPE and GR/ABPE. The oxidation mechanism was discussed. Under the optimal experimental conditions, the oxidation peak current was proportional to vanillin concentration in the range of 0.02–2.0 μM, 2.0–40 μM and 40–100 μM. The detection limit achieved was 10 nM. This sensor was used successfully for vanillin determination in various food samples.⁸⁶

In 2012, Guo et al. put forward a new and highly-sensitive analytical method for insulin based on electrochemically anodic pretreated carbon paste electrode modified with acetylene black nanocarbon particles (ABPE). The results have shown that the pretreated ABPE represented high accumulation efficiency to insulin and promoted its direct electron transfer rate owing to the presence of nanocarbon particles and anodic pretreatment. It was found that insulin exhibited a very sensitive anodic peak at 0.47 V on the pretreated AB/CPE, with a six times increased peak current on the pretreated carbon paste electrode (CPE). A limit of detection as low as 5 nM was obtained on pretreated ABPE.⁸⁷

An indirect electrochemical method was proposed by Huang et al. for the sensitive detection of glutathione (GSH).⁸⁸ By fabricating acetylene black spiked carbon paste electrode (ABPE), the electrocatalytic oxidation of GSH in the presence of rutin at the surface of ABPE was studied. Rutin at the modified electrode showed efficient catalytic activity towards the electrochemical oxidation of GSH. Quantitative detection of GSH was established based on the linear relationship between electrocatalytic current and GSH concentration with the detection limit of 0.08 μM . Some kinetic constants such as diffusion coefficient and rate constant were obtained by chronoamperometry. The proposed method was applied to GSH determination in pharmaceutical sample.

If the fore mentioned methods were based on acetylene black paste electrodes fabricated in different ways and combinations, the following methods discussed are based on the fabrication of acetylene black film (with or without different combinations of other nano materials or polymers) on the glassy carbon electrode. Among these the widely used one is the film of AB produced on the surface of GCE with the aid of DHP (AB-DHP/GCE). The fabricated electrode has been used for the determination of different targets by varying the influencing parameters.

Sensors for different target molecules including the pharmaceutical- lovastatin⁷², the plant hormone- 6-benzyl purine⁸⁹, the environmental pollutant- 2-chlorophenol⁹⁰, the alkaloid drugs- colchicines⁹¹, honokiol⁹², paeonol⁹³, rutin⁹⁴, the trace metal- zirconium⁹⁵, the food colorants- ponceau 4R, tartrazine⁹⁶ and various neurotransmitters⁹⁷ were developed.

In 2004, the determination of lovastatin was accomplished with sub micromolar sensitivity by Zhang et al. In order to enhance the sensitivity, the presence of the surfactant, triton -X was utilized⁷². In 2011, Deng et al. reported a method for the sensitive determination of trace zirconium (Zr) at a glassy carbon electrode modified with a film of acetylene black containing dihexadecyl hydrogen phosphate and in the presence of alizarin violet (AV). The method was based on the preconcentration of the Zr (IV)-AV complex at a potential of -200 mV (vs. SCE). The adsorbed complex was then oxidized, producing a response with a peak potential of 526 mV. Compared to the poor electrochemical signal at the unmodified GCE, the electrochemical response of Zr (IV)-AV complex was greatly improved. The method was successfully employed to the determination of zirconium in standard ore samples.⁹⁵

In 2013, Lin et al. used the AB-DHP/GCE as the working electrode for the electrochemical detection of HPLC method. The results indicated that the modified electrode exhibited efficient electrocatalytic oxidation for monoamine neurotransmitters and their metabolites with relatively high sensitivity, long life, and stability. The linear ranges spanned four orders of magnitude and the detectability was on the level of 0.1 nM.⁹⁷

Wang et al. dispersed AB in N,N-dimethylformamide (DMF) and dropcasted on GCE to determine racoptamine.⁹⁸ However any modification on gold electrode with AB was not observed which is commonly found in the case of carbon nanotubes.^{99,100}

AB was mixed with different ionic liquids to determine various pesticides¹⁰¹ and pharmaceuticals⁸³. In some cases MIPs of different molecules were mixed with AB to improve the selectivity of the sensor.¹⁰²

In 2016, Shuai et al. synthesized a 2-dimensional tungsten disulfide–acetylene black (WS₂–AB) composite by a simple hydrothermal method. The biosensor for DNA was fabricated based on the Au nanoparticles (AuNPs) and WS₂–AB composite modified electrode, which was subsequently used to couple with a capture probe by an Au–S bond, then modified with target DNA, auxiliary DNA and bio-H1–bio-H2 (H1–H2) to perform hybridization chain reaction for signal amplification. Under optimum conditions, the as-prepared biosensor showed a good linear relationship between the current value and logarithm of the target DNA concentration ranging from 0.001 pM to 100 pM and a detection limit as low as 0.12 fM. Moreover, the fabricated biosensor exhibited good selectivity so as to differentiate the one-base mismatched DNA sequence. Thereby it creates a pathway for ultrasensitive detection of other biorecognition events and gene-related diseases based on layered WS₂–AB and hybridization chain reaction.¹⁰³

Some researchers have attempted and succeeded in showcasing the efficiency of AB as an electrode modifier among the various carbon materials. Lahcen et al. did a comparative study of the performance of various carbonaceous material-based electrochemical sensors in order to identify the most appropriate sensor for determination of sulfonamides. The electrooxidative power of carbon paste electrodes prepared using carbon black, graphite, carbon nanopowder, acetylene black, multiwalled carbon

nanotubes and glassy carbon powder was investigated by square-wave voltammetry at pH 6.0 using sulfamethoxazole as the model analyte.¹⁰⁴

Lee et al. tried the electrochemical stabilization of methyl viologen cations on a variety of carbon materials using a glassy carbon electrode. Three different types of voltammetry (potential hold, triangular wave and square wave voltammetry) were used to stabilize the methyl viologen cation. Methyl viologen cation-modified multi-walled carbon nanotubes (MWCNTs) of different diameters and with various functional groups were examined to observe the effects of carbon particle size and surface modification. Various carbon materials containing MWCNTs, acetylene black, Super P, Vulcan XC-72, and Ketjenblack were modified by methyl viologen and then electrochemically characterized. Their electrochemical behaviors were discussed in terms of carbon properties, such as pore structure and electrical conductivity. Carbon with immobilized methyl viologen cation and glucose oxidase was assessed to confirm its feasibility for enzyme electrode applications.¹⁰⁵

Though AB had been used as a modifier film, the fabrication of a uniform film on the electrode surface had been a challenge. In order to overcome this, AB was homogenized in the solution with the help of different reagents. Among which the most attractive one is the natural polymer chitosan owing to its wonderful film forming ability.

Yazhen et al. developed an electrochemical sensor for the determination of methyl parathion, which was based on the enhanced redox response of methyl parathion at a novel acetylene black–chitosan composite film modified glassy carbon electrode (AB-C/GCE). The electrochemical

behavior of methyl parathion at the sensor was investigated by cyclic voltammetry and differential pulse voltammetry. The redox currents of methyl parathion at the acetylene black–chitosan film electrode were significantly higher than that at the bare electrode. The enhanced redox current of methyl parathion was owned to the nano-porous structure of the composite film and the enlarged effective electrode area. The high sensitivity and selectivity of the sensor were demonstrated by its practical application to the determination of residual methyl parathion in spiked cabbage sample.¹⁰⁶ The same group has reported a similar sensor for the determination of methimazole¹⁰⁷ which also showed similar effects.

In 2017, Huang et al. proposed a voltammetric method for simultaneous determination of glutathione (GSH) and L-tyrosine (Tyr) at acetylene black and chitosan modified glassy carbon electrode (AB-C/GCE). By introducing chlorogenic acid (CGA) as a new electrocatalytic mediator, GSH could be detected at much lower potential with symmetric peak shape. Acetylene black and chitosan composite served as current signal amplifier for sensitive detection. The electrochemical behavior of GSH and Tyr in the presence of CGA was studied at AB-C/GCE and complete separation of anodic peaks was achieved. The established method was applied to the simultaneous determination of GSH and Tyr in human urine with satisfactory results.¹⁰⁸

In 2018, a sensitive conductive nanobiocomposite sensor consisting of Au–In₂O₃ nanocomposite and chitosan (C) was successfully prepared and used for the modification of acetylene black paste electrode (Au-In₂O₃-C/ABPE) by Ibrahim et al. The modified electrode showed an excellent

electrochemical activity toward the electro-oxidation of the antimycotic ciclopirox olamine (CPX) leading to a significant improvement in sensitivity as compared to the bare ABPE. The proposed biosensor demonstrated linearity in the range $0.199 - 16.22 \mu\text{mol L}^{-1}$, with high sensitivity ($64.57 \mu\text{A } \mu\text{mol L}^{-1} \text{cm}^{-2}$) and detection limit of $6.64 \times 10^{-9} \text{ mol L}^{-1}$ CPX. The analytical performance of this biosensor was evaluated for detection of CPX in pharmaceutical formulations with good accuracy and precision. This proposed method was validated by HPLC and the results are in agreement at the 95% confidence level.¹⁰⁹

AB modified electrodes has been used for the simultaneous determination of various co-existing and structurally similar species. Deng et al. studied the possibilities for simultaneous determination of ascorbic acid and rutin at an acetylene black paste electrode coated with cetyltrimethyl ammonium bromide film.¹¹⁰ They have tried again to explore the possibilities for the simultaneous determination of structurally similar 2-nitro phenol and 4-nitro phenol. It was based on an acetylene black paste electrode modified with a graphene-chitosan composite film (Gr-C/ABPE). The reduction peak currents of 2-nitrophenol (at -252 mV) and of 4-nitrophenol (at -340 mV) in pH 1 solution increased significantly at the Gr-C/ABPE in comparison to a bare ABPE.¹¹¹

From all the above reports, it may be concluded that among various carbon materials used for the electrode modification, AB is an efficient modifier which enhances the kinetics of electro oxidation/reduction of various molecules, which also brings forward the possibilities for simultaneous determination of structurally similar species.

1.8.2 poly (4- amino 3- hydroxy naphthalene sulfonic acid) (pAHNSA) as modifiers

Among the various modifiers used for development of sensors naphthalene based electron conducting polymers have been reported to be efficient in electrochemical sensing applications due to their stability,¹¹² selectivity,¹¹³ catalytic activity,¹¹⁴ surface reactivity etc. The network of the polymer with different groups, amino (-NH₂), hydroxy (-OH) and sulfonic acid (-SO₃H) have been of much interest in electrochemical application owing to their distinguished features such as hydrophilic nature¹¹⁵ and proton doping ability.¹¹⁶

pAHNSA as an electrode modifier was came into action through the works led by Geto. Geto and team reported the synthesis, characterization and properties of various - polymer networks based on naphthalene sulfonic acid. As per them, the electropolymers generated from naphthalene sulfonic acid monomers having amino and hydroxy groups showed promising result that they could be effectively used in different fields mainly sensing.¹¹⁷

A voltammetric sensor based on pAHNSA modified GCE was reported by Amare et al. for the determination of ephedrine in human urine samples with a detection limit of 7.9×10^{-7} M.¹¹⁸ A year later the same group developed pAHNSA modified GCE based voltammetric sensor for the individual determination of caffeine,¹¹⁹ theophylline,¹²⁰ quinine¹²¹ and nicotine¹²². The sensor for caffeine showed linearity over a decade range of concentrations and it provided an efficient platform for its sensing without any interference from co-existing species. The sensor for theophylline enabled micromolar range determination in pharmaceutical formulations.

1.0×10^{-5} M to 1.0×10^{-7} M of quinine in spiked urine samples and pharmaceutical formulations was determined with its sensor based on pAHNSA/GCE. Square wave voltammetric determination of micromolar level nicotine in cigarette tobacco samples was achieved by Geto et al. with the sensor based on pAHNSA in 2012. Later they reported a voltammetric sensor for the determination of Fenitrothion in water samples in nanomolar range.¹²³

In 2015, Gupta et al. reported the determination of domperidone in biological fluids using the sensor based on pAHNSA. It enabled nanomolar level determination and effectively masked the interference from ascorbic acid, uric acid, xanthine, hypoxanthine etc. which may coexist in the given matrix.¹²⁴

In 2016, Tefera and coworkers put forward a sensor which facilitated the simultaneous determination of paracetamol and caffeine at micro molar range.¹²⁵ They successfully established the quantification of these analytes in cool drinks and tea using the developed sensor.

In 2017, Jesny from the group of Girish Kumar used pAHNSA/GCE for the simultaneous determination of three DNA bases guanine, adenine and cytosine together with their metabolite uric acid. The developed sensor was reported to be effective in enabling the quantification of the analytes in micromolar range.¹²⁶ The quantification of these compounds in artificial physiological fluid samples and denatured herring sperm DNA was successfully achieved with the sensor.

Amare et al. again, successfully used pAHNSA/GCE for the determination of salbutamol sulfate in clinical analysis.¹²⁷

Some researchers have modified the pAHNSA/GCE with various other modifiers including various nanomaterials, aptamers, polymers etc. to improve the performance characteristics.

Yadav and group from India developed an aptamer based sensitive and selective sensor for chloramphenicol at nano molar levels. The sensor was fabricated in such a way that the aptamers were fixed on the pAHNSA modified electrode surface.¹²⁸

Incorporation of multiwalled carbon nanotubes and graphene oxide nanoparticles were found to greatly enhance the electrocatalytic property of the polymer film. Sensitive, stable and reproducible results were obtained for the determination of histamine in fish samples using multi walled carbon nanoparticle- pAHNSA composite modified GCEs.¹²⁹ Rosy et al. in 2016 reported reduced Graphene oxide - pAHNSA composite modified glassy carbon electrode to be an efficient probe for the determination of tryptophan in presence of 5-hydroxytryptamine.¹³⁰ Graphene- pAHNSA composite modified screen printed carbon sensor have been reported as an efficient sensor for the simultaneous determination of dopamine and 5-hydroxytryptamine which showed a detection limit of 2.0×10^{-9} M and 3.0×10^{-9} M respectively for each of the species.¹³¹

Furthermore, a molecularly imprinted polymer-based sensor was developed for the sensitive determination of melatonin which is based

on composite of graphene (Gr) and a co-polymer of AHNSA and melamine. The sensor showed sub-nanomolar level detection limits.¹³²

Afore discussed sensors lead to a conclusion that pAHNSA is a fantastic electrode modifier which may be used alone or in conjunction with other nanomaterials for the highly sensitive determination of single or multiple analytes, individually or even simultaneously.

1.9 Literature review of various colorimetric sensors based on silver nanoparticles (AgNPs) as the recognition element

Noble metal nanoparticles exhibit a strong UV-visible absorption band which is not present in the spectrum of the bulk metal. This absorption band results when the incident photon frequency resonates with the collective excitation of the conduction electrons and is known as the localized surface plasmon resonance (LSPR). LSPR excitation results in wavelength selective absorption with extremely large molar extinction coefficients.¹³³

AgNPs possess some advantages over gold nanoparticles (AuNPs) to a certain degree since they have higher extinction coefficients relative to AuNPs of the same size.¹³⁴ However, compared with AuNPs, little attention has been paid to AgNPs-based colorimetric assays. Sensitive and selective colorimetric detection of DNA,^{135,136} metal ions¹³⁷ and proteins¹³⁸ have been reported using AgNPs functionalized with appropriately ligands. The limitations of employing AgNPs can be attributed to the facts that (a) the

functionalization of AgNPs usually causes chemical degradation and (b) the AgNPs' surface could be easily oxidized.

In a communication Xiong et al. reported a colorimetric sensor to probe histidine in water based on para-sulfonatocalix[4]arene modified silver nanoparticles. This sensor provided a rapid quantitative assay of histidine down to a concentration of 5 μM .¹³⁹ Bae et al. utilized lysine-functionalized silver nanoparticles for visual detection and separation of histidine and histidine-tagged proteins.¹⁴⁰ An antibody-free diagnostic reagent has been developed based on the aggregation-induced colorimetric change of Ni(II)NTA-functionalized colloidal gold and silver nanoparticles. This diagnostic strategy utilized the high binding affinity of histidine-rich proteins with Ni(II)NTA to capture and cross-link the histidine-rich protein which mimics with the silver and gold nanoparticles.¹⁴¹

Silver nanoparticles synthesized by a reagent less method involving only UV radiation have been used in colorimetric assay for the detection of ammonia in solution. The silver nanoparticles were synthesized by the exposure of a silver nitrate solution to a low-power UV source in the presence of poly(methacrylic acid) (PMA), which acted both as reducing and capping agent. Transmission electron microscopic measurements confirmed the formation of spherical particles with an average particle size around 8 nm. Interestingly, the silver nanoparticles solution was found to display a strong color shift from purple to yellow upon mixing with increasing concentration of ammonia ranging from 5 to 100 ppm.¹⁴²

In 2008, Wei et al. utilized AgNPs for the detection of enzymatic reactions. Enzymatic reactions concerning adenosine triphosphate (ATP)

dephosphorylation by calf intestine alkaline phosphatase (CIP) and peptide phosphorylation by protein kinase A (PKA) were studied. In the absence of the enzymes, unreacted ATP could protect AgNPs from salt-induced aggregation, whereas in the presence of the enzymes, the reaction product of ATP (i.e., adenosine for CIP and ADP for PKA) could not. Via this method, dephosphorylation and phosphorylation was readily detected by the color change of AgNPs, with a detection limit of 1 unit/mL for CIP and a detection limit of 0.022 unit/mL for PKA. More importantly, the enzymatic inhibition by inhibitors and enzymatic activity in complex biological fluids could also be realized.¹⁴³

Biothiols modified AgNPs have been used for the sensing of various targets adopting different strategies. Selective colorimetric sensing of histidine in aqueous solutions using cysteine modified silver nanoparticles in the presence of Hg^{2+} was reported by Li et al.¹⁴⁴ The same group has reported the application of glutathione stabilized AgNPs for the sensing of Nickel.¹⁴⁵

Nidya et al. utilized L-cysteine modified AgNPs as a probe for the selective colorimetric detection of Hg^{2+} .¹⁴⁶

Sung et al. proposed a highly sensitive colorimetric sensing platform for the selective trace analysis for Co^{2+} ions, based on glutathione (GSH)-modified AgNPs. The shape of metallic nanoparticles used in colorimetric detection, using the unique optical properties of plasmonic nanoparticles, was almost spherical. Therefore, in this work they investigated the selective detection of heavy metal ion (Co^{2+}), by changing the shape of AgNPs (nanosphere, nanoplate, and nanorod). GSH-AgNPs having spherical shape

showed a high sensitivity for all of the metal ions (Ni^{2+} , Co^{2+} , Cd^{2+} , Pb^{2+} and As^{3+}) but poor selective recognition for target metal ions. Whereas, AgNPs solution containing rod-type GSH-AgNPs showed a special response to Co^{2+} , and its selective detection might be based on the cooperative effect of CTAB and GSH. Therefore, Co^{2+} ion could be selectively recognized using rod-type GSH-AgNPs.¹⁴⁷ Yao et al. synthesized bifunctionalized silver nanoparticles (triazole-carboxyl Ag NPs) through a click reaction and have a cooperative effect on recognition of Co^{2+} , resulting in appreciable changes in color and absorption properties over other metal ions tested. The functionalized silver nanoparticles aggregated in Co^{2+} solution through cooperative metal-ligand interaction. The colorimetric sensor established a rapid quantitative assay of Co^{2+} down to the concentration of 7.0×10^{-6} M.¹⁴⁸

Wang et al. developed a colorimetric thiourea (TU) sensor utilizing citrate modified silver nanoparticles (AgNPs). Since common steps such as modification and separation could be successfully avoided, the developed sensor provided a simple, cost-effective measurement tool for TU detection, and may provide new opportunities in the development of sensors for food safety and environmental monitoring in the future.¹⁴⁹ Citrate stabilized AgNPs were used to study the antioxidant capacity of polyphenols by Ozyurek et al.¹⁵⁰

Elavarasi and team presented a simple colorimetric probe for detecting chromium species, i.e. Cr(VI) and Cr(III), in aqueous solution using as-synthesized citrate capped silver nanoparticles without further functionalization. Two types of silver nanoparticles, AgNP-I (10 ml sodium

borohydride) and AgNP-II (30 ml sodium borohydride) were synthesized by varying the volume of the reducing agent. AgNP-I was proven to be specific for Cr(III) only, whereas AgNP-II would measure total chromium in a binary mixture of Cr(III) and Cr(VI). The probe was tested in a binary mixture at a 1 : 1 ratio, containing the total chromium concentrations in the range of 500–5000 ppb.¹⁵¹ Wang et al. used citrate capped AgNPs for Hg⁺ ion determination.¹⁵² It was again used by vaishnav et al. for medicinally important thiol determination.¹⁵³ In the presence of triazophos, the AgNPs was aggregated, resulting in the obvious color change from yellow to prunosus via hydrogen bonding, π - π interactions and substitution. The theoretical investigations between the triazophos and AgNPs were also validated with density functional theory (DFT) approach by Ma et al.¹⁵⁴

In 2013, Chen et al. developed Chitosan-capped silver nanoparticles as a highly selective colorimetric probe for visual detection of aromatic ortho-trihydroxy phenols. The visual sensing of aromatic polyphenols such as gallic acid, pyrogallol and tannic acid, was based on the intensified plasmon absorbance signals and visual changes from yellow to orange due to hydrogen-bonding recognition and subsequent catalytic oxidation of the target phenols by chitosan-capped Ag NPs.¹⁵⁵

Ma et al. reported a colorimetric sensor for Cu²⁺ using dopamine/silver nanoparticles. Dopamine can self-polymerize under alkaline conditions and the generated polydopamine can adsorb on noble metals, metal oxides, polymers and ceramics. In addition, dopamine is reported to have the ability to reduce metal ions to metal nanoparticles, such as Au³⁺ and Ag⁺. For instance, dopamine can reduce Ag⁺ to monodispersed

AgNPs and functionalize the formed AgNPs. Considering that the nitrogen and oxygen atoms of dopamine have certain coordination ability with Cu^{2+} , the AgNPs functionalized with dopamine would have the ability to link with Cu^{2+} . The binding reaction of dopamine and Cu^{2+} result in the aggregation of AgNPs and the color change response.¹⁵⁶

In 2014, Rohit et al. reported the use of dopamine dithiocarbamate functionalized silver nanoparticles (DDTC-Ag NPs) as a colorimetric probe for sensing of mancozeb in environmental water and fruit juice samples. It was observed that the mancozeb induces the aggregation of DDTC-Ag NPs via Michael addition and enamine formation between DDTC-Ag NPs and mancozeb, leading to a color change from brownish orange to bluish.¹⁵⁷

Highly selective label free colorimetric sensor based on AgNPs stabilized by phenolic chelating ligand, N, N₀-bis(2-hydroxybenzyl)-1,2-diaminobenzene (HBDB), for NO_2^- anions was developed by Kumar et al. Addition of NO_2^- showed selective decolourisation of brownish yellow colour of HBDB-AgNPs with the detection limit of the order of 10^{-7} M. Absorption studies showed the complete disappearance of HBDB-AgNPs peak at 426 nm due to the conversion of AgNPs to silver ions. The presence of silver ions was confirmed by white precipitates of AgCl formation with NaCl. The interference studies confirmed the high selectivity of NO_2^- sensing in presence of anions as well as cations by HBDB-AgNPs. A linear relationship was observed between the change of absorption and concentration of NO_2^- . The present approach could be performed at room temperature and ambient conditions. The practical applications of HBDB-

AgNPs for selective sensing of NO_2^- in different water samples such as ground, river, pond and tap water had also been demonstrated.¹⁵⁸

Determination of Hg^+ was achieved by different groups with the help of AgNPs functionalized with various molecules such as folic acid,¹⁵⁹ citrate,¹⁶⁰ bile acid-based 1,2,3-triazole ligands¹⁶¹ silanes,¹⁶² redox phytoproteins,¹⁶³ cysteine,¹⁶⁴ starch,¹⁶⁵ mercaptobenzoheterocyclic compounds,¹⁶⁶ cyclodextrins¹⁶⁷ and even un modified AgNPs¹⁶⁸

Determination of other metal ions like Co^{2+} , Cr^{3+} , Ba^{2+} ^{169,170}, Cr^{4+} ¹⁷¹, Al^{3+} ¹⁷²⁻¹⁷⁴, Mn^{2+} ¹⁷⁵⁻¹⁷⁸, Cu^{2+} ¹⁷⁹⁻¹⁸¹, Fe^{3+} ¹⁸², Zn^{2+} ^{183,184}, Pb^{2+} ¹⁸⁵⁻¹⁸⁷ etc and different anions including Cl^- ¹⁸⁸, Br^- , I^- ¹⁸⁹, S^{2-} ¹⁹⁰, CN^- ¹⁹¹ also had been achieved by different research groups utilizing AgNPs.

In 2014, Xavier and co-workers developed silver nanoparticles functionalized using a single reducing and functionalizing agent b-cyclodextrin and the prepared silver nanoparticles were exploited as probes for the colorimetric sensing of melamine. The monodispersed and spherical-shaped silver nanoparticles were obtained with an average particle size of 10 nm, and the addition of melamine induced the aggregation of nanoparticles, as evidenced from the morphological characterizations. The toxic melamine was effectively sensed through the colorimetric response, owing to the host-guest inclusion of melamine into the hydrophobic cavities of b-cyclodextrin functionalized silver nanoparticles.¹⁹² Ma et al. also used cyclodextrines modified AgNPs for the determination of riboflavin.¹⁹³

In 2015, Ferreira et al. demonstrated the use of AgNPs for colorimetric quantification of ascorbic acid (AA) through a paper-based

sensor. This device was constituted by spot tests modified with AgNPs and silver ions bordered by a hydrophobic barrier which provided quantitative and fast analysis of AA. AgNPs paper-based sensor changed from light yellow to grey colour after the addition of AA.¹⁹⁴ Peng et al. also determined ascorbic acid using AgNPs.¹⁹⁵

Glutathione was determined by D'souza et al. using ascorbic acid capped silver nanoparticles (AA–AgNPs) as a probe for selective colorimetric detection of glutathione (GSH) in aqueous solution. This detection system was based on the GSH-induced aggregation of AA–Ag NPs, resulting in drastic changes in the absorption spectra and color of the AA–Ag NPs system.¹⁹⁶

Parmer et al. established a new approach to the traditional Jaffe's reaction for the determination of creatinine, by coating Ag NPs with picric acid (PA) to form an assembly that can selectively detect creatinine. The Ag NPs based sensor proficiently and selectively recognized creatinine owing to the ability of picric acid to bind with it and to form a complex.¹⁹⁷

A sensitive assay for the detection of biothiols was reported based on biothiol-induced aggregation of silver nanoparticles (Ag NPs). In the presence of biothiols, such as cysteine (Cys), homocysteine (Hcy) and glutathione (GSH), the aggregation of AgNPs resulted in the colorimetric change of the nanoparticles, which could be observed by the naked eye and measured with UV-vis spectroscopy. More importantly, the report also discussed electrochemical sensing of biothiols. In the electrochemical analysis, the biothiol induced aggregation of Ag NPs resulted in the decrease of electrochemical current.¹⁹⁸

A colorimetric and fluorometric dual channel sensor had been developed for the determination of norepinephrine (NE). Visual detection was made possible due to the formation of brown AgNPs in the presence of NE, which further resulted in strong metal enhanced fluorescence signals. Furthermore, application of the developed approach in synthetic blood serum had been demonstrated.¹⁹⁹

In 2017, a colorimetric sensing platform for the detection of glutathione (GSH) in dietary supplements was developed using phthalic acid (PTA) assisted synthesis of AgNPs. The di-carboxylic functional groups of PTA were used to modify the surface of AgNPs. AgNPs stabilized with PTA could cause the strong affinity to GSH. As the GSH concentration increased, the color of AgNPs solutions gradually changed from yellow to orange and light purple as well as the SPR shifted from 400 nm to 556 nm upon an aggregation of AgNPs.²⁰⁰

Gao et al. coupled gold nanoparticles (AuNPs) with silver nanoparticles (AgNPs) to assemble a plasmonic sensing platform for colorimetric detection of glucose. In this system, small AuNPs (~4 nm) acted as glucose oxidase (GOD) mimic enzyme to catalytically oxidize glucose in the presence of oxygen, producing hydrogen peroxide, which dissolved AgNPs leading to color changes. Glucose was detected with spectrophotometer in the concentration range of 5–70 μM , with detection limit of 3 μM .²⁰¹

Colorimetric method for the sensing of biothiols such as cysteine, homocysteine, and glutathione in biological samples was reported. The selective binding of chitosan capped silver nanoparticles to biothiols

induced aggregation of the chitosan–Ag NPs. But the other amino acids without any thiol group did not aggregate the chitosan–Ag NPs.²⁰²

A self-referenced colorimetric sensor for the quantitative determination of hydrogen peroxide was presented by Rivero et al. The optical sensor was based on the presence of the localized surface plasmon resonances of silver and gold nanoparticles which are capped with the same encapsulating agent - poly (diallylammonium chloride) (PDDA). These metallic nanoparticles were synthesized by a chemical reduction method from their corresponding inorganic precursors. A remarkable difference in sensitivity related to both LSPR absorption bands was observed as a function of variable molar concentration of the target molecule. The LSPR band of the silver nanoparticles gradually decreased, whereas the LSPR of the gold nanoparticles remained practically unaltered upon increasing the molar concentration of H₂O₂. The LSPR band of the AuNPs was used as an optical reference and the molar concentration of the target molecule was obtained by the ratio of absorption maxima of both NPs.²⁰³

Rajar and coworkers reported a sensing system which relied on the application of succinic acid as a selective recognition probe functionalized over Ag NPs. The AgNPs were modified with cysteamine were synthesized to induce positively charged surface which allowed easy and favourable functionalization of succinic acid. The di-carboxyl nature of succinic acid enabled its binding to both cysteamine and melamine. The strong and favorable linkage between carbonyl group of succinic acid and amine moieties of melamine triggered aggregation of silver NPs producing a significant shift in the absorption maxima.²⁰⁴

Zor developed silver nanoparticles embedded nanopaper as a colorimetric chiral sensing platform. To this aim, nanopaper was prepared by environment-friendly approach using bacterial cellulose made of nanofibers and silver nanoparticles were embedded within nanopaper by an in-situ generation method. AgNPs showed a discriminative sensing response toward D-cysteine with a LOD value of 4.88 μM . For practical use, the obtained plasmonic nanopaper was punched into circular pieces and put on wax-printed PET film to produce disposable two-dimensional cuvette which could be inserted in an ordinary spectrophotometer. The enantiomeric percentage of D-cysteine was successfully determined by the fabricated nanopaper-based cuvettes.²⁰⁵

Rostami et al. introduced a platform for detection of dopamine (DA) based on morphology transition and etching strategy of hexagonal platelet shaped silver nanoparticles (Ag NPs) functionalized with task-specific ionic liquid (TSIL). A pyridinium based TSIL was used for surface functionalization. According to the etching strategy, hexagonal TSIL-Ag NPs were converted to round-shape nanoparticles in the presence of DA. This etching process caused a blue shift in the localized surface plasmon resonance (LSPR) peak of TSIL-Ag NPs. The absorption maxima shifted from 585 nm to 500 nm. Color change from green to red was also observed as a consequence of morphology transition of TSIL-Ag NPs.²⁰⁶

Amirjani and team illustrated the colorimetric determination of ammonia using smartphones. The mechanisms were based on the manipulation of the surface plasmon band of AgNPs via the formation of $\text{Ag}(\text{NH}_3)_2^+$ complex. The complex decreased the amount of AgNPs in the

solution and consequently, the color intensity of the colloidal system decreased. UV–vis spectrophotometer as well as smartphone was employed to monitor the color intensity variation by RGB analysis. Ammonia, in the concentration range of 10 – 1000 mg L⁻¹, was successfully quantified spectrophotometrically (UV–vis spectrophotometer) and colorimetrically (RGB measurement) with the detection limit of 180 and 200 mg L⁻¹, respectively. Both of the colorimetric and spectrophotometric methods showed a reliable performance for determination of ammonia in the real samples within a response time of 20 s.²⁰⁷

Urinary creatinine concentration is a critical physiological parameter that enables reliable assessment of patient renal function and diagnosis of a broad spectrum of diseases. In this study, a simple and inexpensive sensor comprising monodisperse, citrate-capped silver nanoparticles (cc-AgNPs) was developed. The mechanism of this sensor entails the creatinine-mediated aggregation of the cc-AgNPs (within 1 min) under alkaline conditions (pH 12). This was attributed to the tautomerization of creatinine to its amino anionic species at alkaline pH, which cross-link the cc-AgNPs via hydrogen bond networks with the negatively charged citrate caps. Creatinine elicited visibly-discernable color changes of the cc-AgNPs colloids in a concentration-dependent manner up to 10 mM. UV-visible spectroscopic analyses of the cc-AgNPs revealed that creatinine elicited a concentration-dependent decrease in intensity of the localized surface plasmon resonance (LSPR) band centered around 403 nm, with a concomitant increase in intensity of the red-shifted LSPR band at 670 nm. The cc-AgNPs sensor exhibited a linear correlation between the A_{670}/A_{403}

extinction ratio and creatinine concentration range of 0-4.2 μM in aqueous solutions and a low detection limit of 53.4 nM.²⁰⁸

A colorimetric sensor was developed for chiral recognition of tryptophan enantiomers using chitosan-capped silver nanoparticles. The function of the sensor was based on scanometry and spectrophotometry of the colored product of a reaction solution containing a mixture of chitosan-capped silver nanoparticles, phosphate buffer and tryptophan enantiomers. The image of the colored solution was taken using the scanometer and the corresponding color values were obtained using Photoshop software which subsequently was used for optimization of the experimental parameters as the analytical signal. Two types of color values system were investigated: RGB (red, green and blue values) and CMYK (cyan, magenta, yellow and black values). The color values indicated that L-tryptophan had better interaction than D-tryptophan with chitosan-capped silver nanoparticles.²⁰⁹

The discriminative determination of glutathione (GSH) over cysteine (Cys) and homocysteine (Hcy) is still challenging in bioassays due to their similar functional groups. Li et al. proposed colorimetric method for the selective determination of GSH over Cys and Hcy. In this assay, o-phenylenediamine (OPD) was used to oxidize silver ions (Ag^+) to produce silver nanoparticles (AgNPs) and pale yellow colored 2,3-diaminophenazine (OPDox) with absorbance peak center at 429 nm. The as formed AgNPs could further catalyze the redox reaction between OPD and Ag^+ . Upon introduction of GSH into the system, it could chelate with Ag^+ , inhibiting the oxidation ability of Ag^+ , and link with AgNPs, influence the catalytic ability of AgNPs. Furthermore, GSH possesses strong reducibility to reduce

OPDox, resulting in color fading of the detection solution and decrease in absorbance intensity. The proposed Ag^+ -OPD based sensing system exhibited a wide linear range from 2 nM to 1 μM for GSH detection, with the limit of detection as low as 1.7 nM. Moreover, this developed method was successfully applied to GSH detection in plasma and urine samples with satisfied results.²¹⁰

A strategy based on Fenton reaction coupled by silver nanoparticles (AgNPs) was designed to establish a multi-functional platform for colorimetric determination of Fe^{2+} , H_2O_2 and glucose. For this purpose, AgNPs were synthesized in a green manner using agar and ascorbic acid and then utilized as a colorimetric sensor. Addition of H_2O_2 to the mixture of Fe^{2+} and AgNPs caused the production of hydroxyl radical, oxidation of AgNPs and discoloration of the solution. Changing the amount of Fe^{2+} affected on discoloration of the solution, while other metallic ions did not show such this effect. So, a selective colorimetric sensor with a detection limit of 0.54 μM was provided for Fe^{2+} measuring. On the other hand, the concentration of H_2O_2 affected both on the oxidation of AgNPs and discoloration of the solution. These conditions was used to measure H_2O_2 with a LOD as low as 0.032 μM . Owing to the fact that glucose oxidase produces H_2O_2 from glucose, this system was also applied for determination of glucose.²¹¹

Hydrophilic amine ($-\text{NH}_2$) protected Au@Ag nanoparticles (NPs) were developed and fabricated as colorimetric paper sensor for delicate detection of TNT. The as developed nanoprobe selectively reacted with TNT through classic Meisenheimer complex formation by means of charge

transfer process from an electron-rich NH_2 group of β -cysteamine to an electron deficient nitro group on TNT.²¹²

1.10 Literature review of various fluorescence sensors based on cadmium telluride quantum dots (CdTe QDs) as the recognition element

A remarkable momentum in optical sensing has been brought about by the introduction of nanomaterials with distinguished photophysical properties. In many aspects, these materials are superior to the traditional molecular fluorophores and hence could replace them in many applications. There are many reports so far which successfully utilized these materials for the sensing purpose. Those results upon further integration with various optical properties can bring about better chemical sensors.

CdTe QDs with MPA capping was modified with bovine serum albumin (BSA) to sense Ag^+ ions selectively by Wang et al. They have proved its sensing applications in various samples containing Ag^+ .²¹³

Various capping agents can impart charge on the QD surface and the presence of an oppositely charged species can quench its fluorescence. This possibility was utilized by Diao et al. in 2007 for the determination of surfactants such as dodecyltrimethylammonium bromide (DTAB), cetylpyridinium chloride (CPC), cetyltrimethylammonium bromide (CTAB) etc (positively charged surfactants) with negatively charged CdTe QDs as the sensing element.²¹⁴

In 2007, Wang et al. used MPA capped CdTe as the fluorophore for the determination of ovalbumin. Here the enhancement in fluorescence

intensity of the QDs was correlated to the concentration the analyte. Determination of ovalbumin in the range 4.0×10^{-6} M – 1.3×10^{-7} M was obtained with the sensor.²¹⁵

The same year itself, MPA capped CdTe/CdS QDs were used for the determination of the protein- BSA by Yu et al.²¹⁶ Also, TGA capped CdTe nanocrystals were used for the determination of methomyl by Li et al.²¹⁷

Fluorescence quenching induced by the introduction of Hg^{2+} in to the BSA functionalized TGA CdTe QDs was utilized for the development of a sensor for the metal by Xia et al. in 2008. The developed sensor enabled selective determination of Hg^{2+} even in solutions containing various metals.²¹⁸

A sensor based on TGA-CdTe was developed by Sun and coworkers for the determination of vitamin B₆. The authors have tried to elucidate the mechanism underlying the quenching of fluorescence intensity and it was concluded to be an electron transfer processes between analyte and CdTe.²¹⁹

Mercaptosuccinic acid (MSA) capped CdTe QDs were used as the fluorophore in the study conducted by Yuan et al. In this system they have used horse radish peroxidase enzyme to convert phenolic compounds to benzoquinone which easily quenched the fluorescence of the QDs. Dopamine, hydroquinone etc. were determined at submicromolar levels with the help of the developed sensor.²²⁰

Determination of Tiopronin present in pharmaceutical formulations was accomplished with a fluorescence sensor based on MPA- CdTe by

Wang et al.¹²⁷ Zeta potential of the QD was decreased in presence of the analyte, which induced aggregation followed by quenching of fluorescence. Folic acid induced quenching of TGA capped CdTe fluorescence. This was owing to the interaction between amino group of folic acid and acid group on the surface of the QDs²²². Various pharmaceuticals quantified at micromolar level and even at nanomolar level by different research group with the help of sensors based on CdTe QDs.²²³⁻²²⁷

Fluorescent sensors for the determination of various metal ions as well as anions have been reported. Ghogh et al. utilized the enhancement in fluorescence of dendrimer functionalized CdTe QDs for the determination of Cu^{2+} ions. Whereas GSH capped QDs were used for the determination of Fe^{3+} ²²⁸ Zhang et al. used the similar QDs for Cr^{3+} quantification²²⁹. CN^- ions were determined by CdTe- Cu^+ assembly by Shang et al.²³⁰ TGA capped CdTe was used by Hou et al. for the determination of V^{5+} and the similar QDs were used by Ge et al. for the determination of Sb^{3+} .²³¹ Wang et al. used CdTe for the determination of As^{3+} ²³². BSA modified bi colour QD's multilayer facilitated the determination of Hg^{2+} ²³³. Pb^{2+} ions present in spinach and citrus leaves were determined by CdTe²³⁴. 10^{-7} to 10^{-8} M range quantification of Br^- was accomplished by Adegoke et al. in 2012 with the help of 4-amino-2,2,6,6-tetramethyl piperidine-N-oxide functionalized CdTe QDs.²³⁵ Rodrigues et al. utilized the S^{2-} induced quenching of fluorescence of CdTe QDs to quantify it successfully.²³⁶

In a number of sensors, the interaction of the metal present in a macromolecule with QDs was explored. Cao et al. developed a sensor for

the determination of cytochromes with glutathione capped CdTe as the probe.²³⁷

In a sensor developed by Wu et al., the fluorescence of CdTe QDs was quenched with the help of Ni²⁺ and then it was enhanced by the addition of histidine. This was due to the metal binding affinity of histidine with Ni²⁺ ions.²³⁸

Glucose sensors were developed by Yuan et al. and Li et al. by quenching of fluorescence of CdTe QDs by the interaction of the same with hydrogen peroxide generated enzymatically. They have used the sensor for the determination of glucose in serum.^{239,240}

Calixarene functionalized CdTe was used for the determination of the insecticide acetamipride with very low detection limits.²⁴¹ Zhang et al. developed a sensing strategy based on formation of the film containing layer by layer assembly of acetyl choline esterase, choline oxidase and CdTe QDs for the determination of various pesticides.²⁴²

It has already been identified the presence of bisphenol A in food taken in plastic containers. Kuang et al. determined bisphenol A using CdTe QDs capped with cysteamine.²⁴³

In 2010, trinitrotoluene was determined with the probe l-cysteine capped CdTe. Using the probe Chen et al. achieved nanomolar level detection of TNT.²⁴⁴

AuNPs effectively quench the fluorescence of the TGA capped CdTe QDs due to inner filter effect. Upon addition of melamine into the

system, it gets attached to the AuNP surface. This inturn retrieves the fluorescence of QDs, which acted as the basis for the fluorescence sensor developed by Zhang et al.²⁴⁵

Lysozyme binding DNA was used to modify the surface of CdTe QDs to induce DNA-lysozyme interaction and thereby the quenching of fluorescence of QDs.²⁴⁶

Nanomolar level quantification of DNA was achieved by a number of groups utilising the quenching of CdTe fluorescence induced by DNA.
247-249

In 2017, Han et al. reported a glucose sensor based on the enzymatic reaction of glucose oxidase to produce hydrogen peroxide and thereby the quenching of fluorescence of QDs induced by it.²⁵⁰

.....❧.....

Chapter 2

Materials and Methods

Contents

- 2.1 *Reagents*
- 2.2 *Instruments*
- 2.3 *Preparation of sensing element*
- 2.4 *Preparation of stock solutions*
- 2.5 *Preparation of buffer solutions*
- 2.6 *Analytical procedure*
- 2.7 *Preparation of real/artificial samples*
- 2.8 *Reference methods*

This chapter encompasses a description about the various materials, instruments and methods employed for the development of various sensors detailed and discussed in the following chapters of the thesis.

2.1 Reagents

All reagents used were of analytical grade. Acetyl choline and 5-hydroxyindol-3-acetic acid, L-cysteine hydrochloride, acetylene black, chitosan, serotonin, serotonin hydrochloride, nafion, propyl gallate and tert-butyl hydroquinone, cadmium chloride hemipentahydrate, sodium tellurite, tetrabutylammonium hexafluorophosphate and bovine serum albumin were obtained from Sigma Aldrich, India.

Dextrose, ascorbic acid, silver nitrate, uric acid and phosphoric acid were purchased from s. d. fine chemicals, India. Epinephrine, norepinephrine and dopamine hydrochloride were procured from Himedia laboratories Pvt. Ltd, India.

3-Mercapto propanoic acid and 4-amino-3- hydroxy naphthalene -1-sulphonic acid were supplied by Alfa Aesar, England.

The suppliers of the chemicals cysteamine hydrochloride, histidine, l-proline, l-alanine, l-dopa, glycine, sodium borohydride, mercapto succinic acid, creatinine, cysteine and n-acetyl l-cysteine was Spectrochem Private Ltd, India.

Merck life sciences pvt. Ltd., Germany furnished the chemicals sodium chloride, tri-sodium citrate dihydrate, sodium hydroxide pellets, potassium chloride, sodium nitrate, fructose, acetic acid, sodium acetate trihydrate, monosodium dihydrogen orthophosphate, disodium hydrogen orthophosphate.

Glutathione reduced, 1,3,5-trimethylbenzene and fluorescein were obtained from Loba Chemie Pvt. Ltd., India. TCI Chemicals (India) Pvt.

Ltd., India was the suppliers of Melatonin. Cobaltous chloride hexahydrate, creatine, l-tyrosine, l-tryptophan and l-serine were purchased from Sisco Research Laboratories pvt. ltd., India.

Millipore water (resistivity greater than 18 MΩcm) was used to prepare the solutions.

2.2 Instruments

Electrochemical measurements were performed on a CHI electrochemical work station (CHI6023D, CH Instruments, USA) and electrochemical impedance studies were carried out on CHI6017D electrochemical analyser. A three-electrode system consisting of glassy carbon electrode (GCE) or gold electrode (GE) (Bare/Modified) as the working electrode, Ag/AgCl as the reference and Pt wire as the counter electrode was used. Different voltammetric techniques such as linear sweep voltammetry, cyclic voltammetry and square wave voltammetry were used to study the electrochemical processes.

Fluoromax - 4 and Fluorolog TCSPC from HORIBA scientific was used to acquire Fluorescence spectra and fluorescence decay curves respectively. Absorption studies were performed on Evolution 201, UV–visible spectrophotometer from Thermo scientific. The FTIR spectra of the samples were recorded on JASCO-4100 FTIR using KBr discs.

Morphology of the bare/modified electrodes or nanoparticles or quantum dots was investigated by instruments such as JEOL/JEM 2100 (for TEM imaging), JEOL 6390LV (for SEM imaging) and Karl Ziess instruments (for FESEM imaging). Particle size distributions (DLS) and

zeta potentials were measured using 'nano partical', nanoparticles size analyzer, SZ-1000, from HORIBA Scientific.

ELICO, LI 120, pH meter was used to carry out the pH measurements. Centrifugations were performed with Elteck labospin centrifuge (TC 450 C). An ultrasonicator (Oscar Ultrasonics Pvt. Ltd., Mumbai) and HPLC-UV (LC-20AT, SPD-20A, Shimadzu) were also used.

Software such as ZimpWin for fitting electrochemical impedance spectra and DAT station for fitting fluorescence decay traces were used.

2.3 Preparation of sensing element

2.3.1 Cleaning of electrodes

Prior to use, glassy carbon electrode (GCE) was cleaned by polishing the electrode surface on a micro cloth polishing pad with alumina slurry (0.05 μm) followed by sonication in methanol, 1:1 HNO_3 , acetone and water successively.

The gold electrode (GE) was mechanically polished with aqueous slurries of alumina (1 μm) on a flat pad prior to modification. Polished GE was rinsed ultrasonically with water and absolute ethanol to remove residual alumina particles from the surface, then with a piranha solution ($\text{H}_2\text{O}_2:\text{H}_2\text{SO}_4=1:3$ v/v) for 10 min when required. This was followed by an electrochemical cleaning process which included the performance of cyclic voltammetry from 0 to 1.5 V in 0.50 M sulphuric acid solution at a scan rate of 100 mVs^{-1} until a stable cyclic voltammogram was obtained.

2.3.2 Fabrication of CoNP/GCE

The cleaned GCE was subsequently immersed in 10 mL of 0.1 M phosphate buffer solution (PBS) (pH 7) containing 1 mM CoCl₂. A film of cobalt nano particles (CoNP) was electrodeposited on the electrode surface by 20 segments of cyclic voltammetric scan between 1.1 V to -1.1 V at a scan rate of 0.1 Vs⁻¹. Cyclic voltammograms in accordance with reported literature was obtained¹⁸. CoNP/GCE was then washed with distilled water and dried in air. A yellowish film on the surface of the electrode evidently points to the successful electrodeposition of a thin film of CoNP.

2.3.3 Fabrication of pAHNSA/CoNP/GCE

CoNP/GCE was immersed in 0.1 M HNO₃ (10 mL) containing 2 mM 4-amino-3-hydroxy-1-naphthalene sulphonic acid (AHNSA). Polymer film of AHNSA (pAHNSA) was grown on the electrode surface by cyclic voltammetry (CV) (30 segments) with potential scanning ranging between -0.5 V to 2.0 V at a scan rate of 0.1 Vs⁻¹²⁵¹. The resultant pAHNSA/CoNP/GCE was washed with distilled water so as to remove any residual specks of monomer. After drying in air, a blue film of pAHNSA was visible on the electrode surface.

The modified electrode was then activated in PBS (pH 7) by CV (10 segments) scanned over a potential range of -0.5 V to 0.6 V. This pAHNSA/CoNP modified GCE was employed for the determination.

2.3.4 Fabrication of acetylene black modified gold electrode (AB/GE)

5.0×10^{-3} g of AB was dispersed in a solution of 3.0×10^{-4} L nafion (15%) and 3.7×10^{-3} L water to get a black homogenous suspension. $3.0 \times$

10^{-6} L of AB suspension was dropped on cleaned GE surface and solvent was evaporated to obtain modified GE.¹⁰⁰

2.3.5 Fabrication of AB-C modified gold electrode (AB-C/GE)

5.0×10^{-3} g chitosan was dissolved in 5.0×10^{-3} L of 0.02 M acetic acid to get 1 mg/mL solution. To the chitosan solution (5.0×10^{-3} L), 5.0×10^{-3} g of AB was added and sonicated for 24 h to form homogenous black suspension. 4.0×10^{-6} L of AB-C suspension was dropped on cleaned GE surface and solvent was evaporated to obtain acetylene black-chitosan composite modified GE (AB-C/GE).^{106,107,108}

2.3.6 Synthesis of tyrosine capped silver nanoparticles (AgNP - Tyr)

2.4 mL of freshly prepared aqueous solution of NaBH_4 (5.0×10^{-2} M) was added to 24.6 mL of water placed in an ice bath with continuous stirring. Then 30 mL of 4.0×10^{-4} M silver nitrate solution was dropped slowly (almost 1 drop per second). Colour of the solution changed from colourless to bright yellow which indicates the formation of silver nanoparticles. Finally the capping agent, L-Tyrosine (3 mL of 3.0×10^{-3} M) solution was added to stabilize the synthesized nanoparticles. The AgNP-Tyr solution was refrigerated at 4°C .¹⁸⁰

2.3.7 Synthesis of MPA capped CdTe quantum dots

Synthesis of MPA capped CdTe QDs was done based on a reported procedure. Briefly in a one necked RB flask containing 50 mL water, 91.6 mg of $\text{CdCl}_2 \cdot 2.5\text{H}_2\text{O}$, 200 mg of tri sodium citrate dehydrate, 52 μL of 3-mercaptopropanoic acid was added successively with stirring. pH of the solution was adjusted to 10 using 1 M NaOH. Finally, 22.1 mg of sodium

tellurite followed by 50 mg of sodium borohydride were added and stirring was continued for 5 min. Then the mixture was refluxed at 100⁰C for about four hours and allowed to cool to room temperature. Quantum dots were precipitated with the help of ethanol and re-dissolved in 100 mL water.²⁵²

2.4 Preparation of stock solutions

1.0×10⁻² M stock solutions of the various analytes studied were prepared by weighing 18.96 mg of dopamine hydrochloride, 30.73 mg of glutathione, 11.36 mg cysteamine hydrochloride, 21.27 mg serotonin hydrochloride, and 19.11 mg 5-hydroxyindole-3-acetic acid and dissolving in 10 mL water separately. Also 21.22 mg propyl gallate, 16.62 mg tert-butyl hydroquinone, 17.62 mg serotonin and 23.23 mg melatonin was weighed and dissolved in 10 mL methanol separately to obtain corresponding 1.0×10⁻² M stock solutions. All these stock solutions were diluted to get solutions of lower concentrations.

2.5 Preparation of buffer solutions

Buffer solutions of definite pH were prepared by weighing different components as given in the following tables (Table 2.1, 2.2, 2.3) and dissolving them in 100 mL water.

Table 2.1 0.1 M Phosphate buffer solution

| pH | NaH ₂ PO ₄ (g) | Na ₂ HPO ₄ (g) |
|----|--------------------------------------|--------------------------------------|
| 2 | 1.3799 | 0.0001 |
| 3 | 1.3790 | 0.0003 |
| 4 | 1.3780 | 0.0036 |
| 5 | 1.3615 | 0.360 |
| 6 | 1.2143 | 0.3218 |
| 7 | 0.5836 | 0.5466 |
| 8 | 0.0940 | 2.4970 |
| 9 | 0.0100 | 2.6605 |
| 10 | 0.0010 | 2.6781 |

Table 2.2 0.1 M Acetate buffer solution

| pH | CH ₃ COOH (mL) | CH ₃ COONa (g) |
|----|---------------------------|---------------------------|
| 2 | 0.5709 | 0.0024 |
| 3 | 0.5619 | 0.0237 |
| 4 | 0.4855 | 0.2054 |
| 5 | 0.2058 | 0.8711 |
| 6 | 0.0304 | 1.2885 |
| 7 | 0.0034 | 1.3534 |

| | | |
|----|--------|--------|
| 8 | 0.0032 | 1.3602 |
| 9 | 0.0036 | 1.3609 |
| 10 | 0.0000 | 1.3609 |

Table 2.3 0.1 M Citrate buffer solution

| pH | Citric acid (g) | Sodium citrate (g) |
|----|-----------------|--------------------|
| 2 | 2.0544 | 0.0652 |
| 3 | 1.7963 | 0.4265 |
| 4 | 1.3115 | 1.1051 |
| 5 | 0.7819 | 1.8642 |
| 6 | 0.2650 | 2.5700 |
| 7 | 0.0375 | 2.8880 |
| 8 | 0.0039 | 2.9355 |
| 9 | 0.0003 | 2.9404 |

2.6 Analytical procedure

Procedures followed for distinct analyses have been discussed below.

2.6.1 Voltammetric measurements

In a voltammetric cell, 10 mL of supporting electrolyte containing the analyte was taken and was de-aerated with N₂ gas. Potential in a specific range was applied between the working electrode and reference electrode, the current response produced by various analytes was recorded. Various electrochemical processes at the working electrode were accomplished with the help of suitable electrochemical techniques and were studied by assimilating the output obtained from the instrument.

2.6.2 Colorimetric measurements

Colorimetric studies were carried out by mixing sensing probe (nano particle) in suitable medium in the absence or presence of analyte retaining the resultant volume as 2 mL. Absorption spectra were obtained by scanning wave length in the range from 300 nm to 800 nm in each case.

2.6.3 Fluorescence measurements

Fluorescence studies were conducted by mixing fluorophore (quantum dots) in suitable medium in the absence or presence of analyte preserving the resultant volume as 2 mL. Emission spectrum of the mixture was obtained by exciting the sample at 380 nm with the help of a xenon lamp.

2.7 Preparation of real/artificial samples

Diverse artificial samples which are chemically similar to the physiological samples were prepared by standard methods. Studied analytes were spiked into these samples to investigate the utility of the developed sensor in determining these analytes.

2.7.1 Preparation of artificial urine

Synthetic urine was prepared by dissolving 1.5 g of NaCl, 0.9 g of KCl, 3.64 g of urea and 0.96 g of Na₂HPO₄ in 150 mL of water. 0.1 M HCl was used to maintain the pH of the solution between 5.5 and 6.5.²⁵³

2.7.2 Preparation of artificial blood serum

Artificial blood serum was made by dissolving by 0.017 g of CaCl₂, 0.037 g of KCl and 0.720 g of NaCl in 100 mL of water. pH of the solution was adjusted between 7.3-7.4.²⁵⁴

2.7.3 Preparation of artificial cerebrospinal fluid

Artificial CSF was prepared by dissolving 8.66 g NaCl, 0.224 g KCl, 0.163 g MgCl₂.6H₂O and 0.206 g CaCl₂.2H₂O in 500 mL water. It was then mixed with a 500 mL solution containing 0.027 g NaH₂PO₄.H₂O and 0.214 g Na₂HPO₄.7H₂O.²⁵⁵

2.7.4 Treatment of coconut oil/butter sample

5.0×10^{-3} g of the coconut oil/butter sample was placed in a 0.1 L Erlenmeyer flask and pure methanol (0.01 L) was added. The mixture was then shaken vigorously for 30 min, transferred to a 0.025 L centrifuge tube and centrifuged at 3000 rpm for 10 min. After a settling time of 2 min, the extracts were transferred to a sample bottle. Methanol was again added to oil and the whole procedure was repeated 5 times to completely extract the antioxidants from oil/butter. 1.0×10^{-4} L aliquot of this sample was analyzed by voltammetric procedure.²⁵⁶

2.8 Reference methods used for validation of the developed methods

A number of reference methods were adopted to determine the studied analytes in different matrices. The results obtained from these methods were compared with that obtained from the developed methods to confirm the validity of the latter.

2.8.1 Spectrophotometric determination of glutathione (GSH) and cysteamine (Cyste)

3.96 mg DTNB (1 mM) make up 10mL PBS. Add 500 μ L of DTNB (5,5-dithio-bis-(2-nitrobenzoic acid)), the Ellman's reagent into 25 mL std flask containing required quantity of GSH/Cyste and made up with 0.2 M PBS 7. Solution was incubated for 30 min and resultant absorption at 412 nm was noted.²⁵⁷

2.8.2 HPLC-UV determination of dopamine (DA)

A mixture of water, methanol and acetic acid was used as the mobile phase in 85:10:5 ratios. Stock solution of DA was prepared and injected in reverse phase HPLC column. The flow rate was maintained at 1mL/min. UV detection of dopamine was done at 280 nm. Peak areas obtained for dopamine was plotted against its concentration to get a calibration graph. Dopamine present in spiked samples was determined.²⁵⁸

2.8.3 Spectrophotometric determination of propyl gallate (PG)

In a standard flask, adequate amount of stock solution of PG was added and 2.5 mL of 10% ammonium acetate solution was added to it. Then

1 mL of ferrous sulphate was added and made upto 25 mL with water. Incubated for 5 min. Resultant absorbance at 540 nm was recorded.²⁵⁹

2.8.4 HPLC-UV determination of tert-butyl hydroquinone (TBHQ)

The chromatographic conditions for the determination of TBHQ using methodologies previously proposed by Lin et al. (2013) was used with some modifications. An HPLC instrument equipped with UV–VIS detection at 280 nm was used. The mobile phase was a combination of (A) methanol and (B) 1% orthophosphoric acid. A gradient was developed as follows: the solution A (v/v) ratio was varied from 40% to 80% during 0 -15 min, 100% during 15 -20 min. The flow rate was kept at 1 mLmin⁻¹ and under these conditions, the retention times was 13.99 min for TBHQ. Each sample solution (20 µL) was injected, and the concentrations were calculated on the basis of peak area.²⁵⁶

2.8.5 Spectrophotometric determination of serotonin (ST) and melatonin (MT)

Ehrlich's reagent (0.20 mg/mL) was prepared by dissolving p-dimethylaminobenzaldehyde in 17:3 (v/v) glacial acetic acid - con. hydrochloric acid mixture (100 mL) and was refrigerated before use. An aliquot of ST/MT in methanol (1mL), 2.50 mL Ehrlich's reagent and 1.50 mL of 0.1 M HCl were mixed and warmed at 50°C for 30 min. The mixture was allowed to cool to room temperature and the absorbance at 625 nm was measured.²⁶⁰

2.8.6 HPLC-UV determination of 5-hydroxyindole-3-acetic acid (HIAA)

Aliquots (usually 20 μ L) of the HIAA samples were injected into the chromatograph, and eluted with a mobile phase (acetate buffer/methanol, 95/5 v/v) pumped at 3.0 mL/min. UV detection of HIAA was carried out at 254 nm. A peak was obtained after a retention time of 15 min. The peak areas obtained were plotted against the concentration of HIAA to get the calibration graph.²⁶¹

.....✂.....

Chapter 3

Voltammetric sensor for the determination of dopamine

| | |
|--|----------------------------|
| C o n t e n t s | 3.1 Introduction |
| | 3.2 Experimental |
| | 3.3 Results and discussion |
| | 3.4 Conclusions |

This chapter discusses the development of a sensor based on a single probe for the determination of a single analyte dopamine (DA). A voltammetric sensor for the simple and rapid determination of DA, a vital neurotransmitter, has been developed using a glassy carbon electrode modified with cobalt nano/poly (4-amino-3-hydroxy-1-naphthalenesulphonic acid) composite. On square wave voltammetric mode, the modified electrode was found to efficiently catalyse the electrochemical oxidation of DA in 0.1 M PBS (pH 7). Peak current obtained at 0.164 V for the oxidation of DA increased linearly with its concentration in the range 5.0×10^{-5} M to 5.0×10^{-7} M with a limit of detection (LOD) 1.75×10^{-8} M. Reliability of the developed sensor in real sample analysis was ascertained successfully by determining DA in artificial blood serum, urine and cerebrospinal fluid (CSF)

3.1 Introduction

Dopamine (DA), belonging to catecholamine family, is a vital neurotransmitter in the central nervous system of mammals. DA (2-(3,4-dihydroxyphenyl)ethylamine)²⁶², is derived from tyrosine and is a precursor to epinephrine and norepinephrine. It administers several functions such as movement and cognition. Being an excitatory chemical neurotransmitter, excess amounts of DA in the brain causes delight and elation²⁶³. A loss in DA-secreting neurons results in an adverse neurological disorder, called Parkinson's disease²⁶³, which is a degenerative condition causing tremor and motor impairment. Altered levels of DA can also lead to Schizophrenia²⁶⁴ and attention deficit hyperactivity disorder (ADHD). Employment of hydrochloric salt of DA as a medication to renal failure and congestive heart failure is widely in practice. Considering these factors, development of sensitive and specific sensors for monitoring DA has always been a well focused area of research.

Till date, several analytical methods have been reported for the determination of DA including high performance liquid chromatography (HPLC)²⁶⁵, fluorescence⁴³, chemiluminescence²⁶⁶, spectrophotometry²⁶⁷, capillary electrophoresis (CE)²⁶⁸ and competitive enzyme-linked immunosorbent assay (ELISA)²⁶⁹ method. Many of these techniques pose difficulties such as high cost, longer detection time, and in some cases poor sensitivity and selectivity. In this regard, electrochemical analysis is a better alternative mainly due to its better sensitivity, selectivity, quick response and ease of operation.²⁷⁰ Among different electro-analytical methods, voltammetry has been widely used for the analysis of various inorganic and organic entities, owing to its advanced features.

Voltammetric methods for the determination of DA using different electrodes have been reported. In order to overcome the demerits posed by bare electrodes such as high overpotential, lethargic electrode kinetics, fouling of electrode surface and low electrode stability,¹³ chemically modified electrodes have been used. Among electrode modifiers, nano-structured materials, especially metal nanoparticles are preferred modifiers owing to their appreciable electronic conductivity and electro-catalytic properties.¹⁸ Another class of modifier, polymer films evoke considerable interest due to their chemical stability, strong adherence to electrode surface, reproducibility and availability of more electro-active sites.²⁰ Electro-deposition of metal nanoparticles followed by polymerisation on the electrode surface yields nano-polymer composites which synergise the properties of both nanoparticles and polymer films, which in turn can act as excellent electrochemical sensors.²¹ Cobalt-based oxides in their nano form are least explored as electrode modifiers even though they exhibit high electro-catalytic activity.¹⁸ pAHNSA is a conducting polymer which contains different functional groups mainly sulphonic acid groups which helps the polymer to be a wonderful electro-catalytic agent.¹³

The present study illustrates the development of an efficient and selective electrochemical sensor for DA with wide linear range and excellent detection limit. This work includes the development of an electrochemical sensor for the determination of DA by monitoring its oxidation on a glassy carbon electrode modified with pAHNSA/CoNP composite which was used for the sensor development. In addition, this study aims at the utilisation of developed sensor for the determination of

DA in artificial physiological samples such as blood serum, urine and cerebrospinal fluid.

3.2 Experimental

Cleaning of GCE, fabrication of CoNP/GCE and pAHNSA/CoNP/GCE were carried out according to the procedures described in chapter 2, sections 2.3.1, 2.3.2 and 2.3.3. Electrochemical measurements were conducted using these electrodes as follows.

3.2.1 Electrochemical measurements

A stock solution (1.0×10^{-2} M) of DA was prepared by dissolving 19.0 mg dopamine hydrochloride in 10 mL of water. Lower concentrations (1.0×10^{-3} M and 1.0×10^{-4} M) were prepared by sequential dilution of the stock solution with water. Adequate amount of prepared solutions were transferred into an electrochemical cell and diluted to 10 mL with 0.1 M PBS (pH 7). Square wave voltammetry was employed for the electrochemical determination of DA within the potential range from -0.2 V to 0.8 V at a scan rate of 0.1 Vs^{-1} .

3.3 Results and Discussion

3.3.1 Electrocatalytic action of pAHNSA/CoNP/GCE on electro-oxidation of DA

Electrochemical behaviour of DA (1.0×10^{-4} M) was monitored at bare GCE, CoNP/GCE and pAHNSA/CoNP/GCE in 0.1 M PBS (pH 7) at a scan rate of 0.1 Vs^{-1} using cyclic voltammetry (CV).

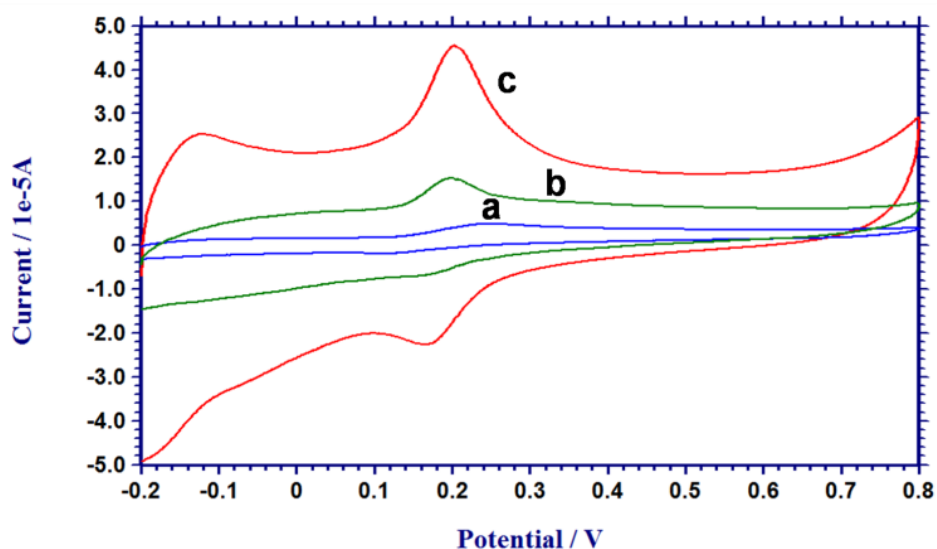


Figure 3.1 Overlay of cyclic voltammogram of 1.0×10^{-4} M DA at (a) bare GCE (b) CoNP/GCE and (c) pAHNSA/CoNP/GCE

Cyclic voltammograms obtained at different electrodes are given in Figure 3.1. At bare GCE, 1.0×10^{-4} M DA gave anodic peak at $E_{pa}=0.25$ V and cathodic peak at $E_{pc}=0.11$ V. Quasi-reversible nature of oxidation at bare electrode is revealed from a 0.14 V ($\Delta E=E_{pa}-E_{pc}$) separation between anodic and cathodic peaks. On modification of GCE with CoNP, anodic ($E_{pa}=0.20$ V) as well as cathodic ($E_{pc}=0.13$ V) peaks shift so as to give a decrease in their separation ($\Delta E=0.07$ V). It reveals the quasi-reversible kinetics followed by the electro-oxidation of DA at CoNP/GCE. A remarkable change was obtained on electro-polymerisation of AHNSA upon CoNP/GCE. A perfectly reversible oxidation of DA was obtained at pAHNSA/CoNP/GCE with $E_{pa}=0.20$ V, $E_{pc}=0.17$ V and $\Delta E=0.03$ V. This ratifies the efficiency of pAHNSA/CoNP composite on electro-oxidation of

DA. Moreover, the number of electrons involved in the electro-oxidation of DA is calculated to be two ($\Delta E = \frac{0.059 V}{\text{no. of electrons}}$, for a reversible reaction).

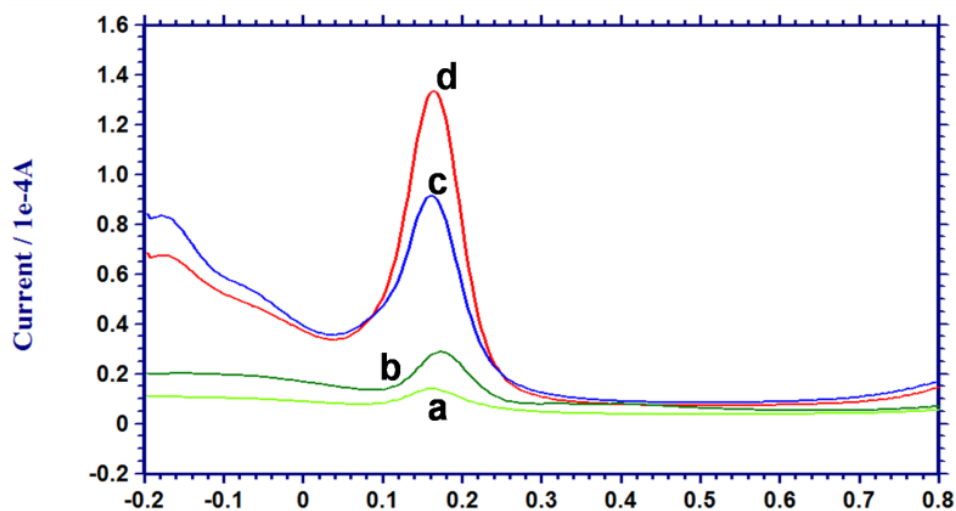


Figure 3.2 Overlay of square wave voltammogram of 1.0×10^{-4} M DA at (a) bare GCE (b) CoNP/GCE (c) pAHNSA/GCE and (d) pAHNSA/CoNP/GCE.

In order to get more information about the electro-oxidation of DA, square wave voltammetric responses were also recorded (Figure 3.2). At bare GCE, an anodic peak current (I_{pa}) of 7.5×10^{-6} A ($E_{pa} = 0.196$ V) was obtained for 1.0×10^{-4} M DA. I_{pa} was increased to 1.8×10^{-5} A and 8.5×10^{-5} A, upon modification of GCE with CoNP and pAHNSA respectively. A tremendous enhancement in peak current to 1.2×10^{-4} A compared to bare GCE (**16fold** increment) was noted when pAHNSA/CoNP/GCE was used. CoNPs increase the electro-active surface area as well as act as an efficient mediator between the analyte and electrode. In case of pAHNSA, hydroxyl as well as sulphonic acid groups can form hydrogen bond with the

functional groups of dopamine. Furthermore π - π interaction between the polymer and dopamine can enhance the peak current. When CoNP and pAHNSA was used to modify the electrode, the properties were synergized in catalysing electro-oxidation of DA.

3.3.2 Performance characteristics of the sensor

Effects of various factors such as supporting electrolyte, pH of supporting electrolyte were studied and conditions were optimised.

3.3.2.1 Supporting electrolyte

The electrochemical response of DA (1.0×10^{-5} M) at pAHNSA/CoNP/GCE was studied using SWV in various media (0.1 M) such as phosphate buffer solution (PBS), citrate buffer solution (CBS), acetate buffer solution (ABS), KCl, HCl, acetic acid, perchloric acid and NaOH. The highest peak current for oxidation of DA was obtained in PBS hence it was selected as the supporting electrolyte for further studies.

3.3.2.2 pH of supporting electrolyte

Influence of pH of PBS on electro-oxidation of DA (1.0×10^{-5} M) was studied using SWV. Different solutions of 0.1 M PBS within a pH range of 3-9 were used and corresponding anodic peak potentials and peak currents were noted.

Figure 3.3a represents the plot of anodic peak potential versus pH of supporting electrolyte. Anodic peak potential showed a linear negative shift with increase in pH of PBS. Peak potentials were observed to be the highest in acidic pH. This could be attributed to the uneasiness of electron transfer

in a medium of excess protons.²⁷² Since physiological samples possess a pH around 7 and PBS (pH 7) gave appreciable current at low potential, it was chosen for the electrochemical oxidation of DA in this study.

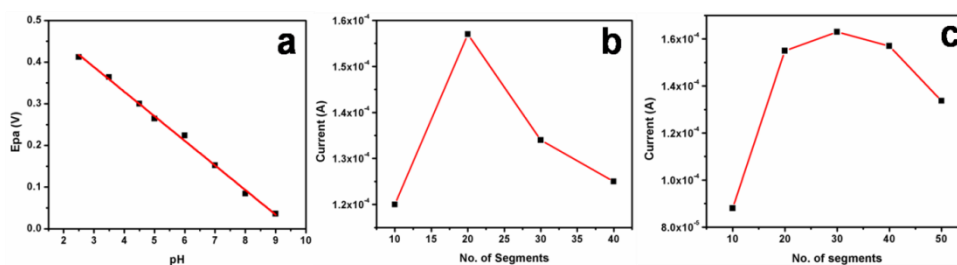


Figure 3.3 (a) Plot of peak potential with pH of the supporting electrolyte (b) Plot of anodic peak current 1.0×10^{-4} M DA with varying number of cycles for the electro-deposition of CoNP (c) Plot of anodic peak current 1.0×10^{-4} M DA with varying number of cycles for the electro-polymerisation of pAHNSA

A linear relationship between peak potential (E_{pa}) and pH was observed following the equation $E_{pa} = -0.06\text{pH} + 0.61$ with $R^2 = 0.99$. A slope of 0.06 was obtained, which is close to the theoretical value of 0.059 indicating that electrochemical oxidation of DA involves equal number of protons and electrons.¹⁰⁰

3.3.2.3 Thickness of film (number of cycles for electro-deposition and electro-polymerisation)

Thickness of the modifier film is proportional to the number of cycles for electro-deposition/polymerisation of the modifier.

3.3.2.3.1 Optimisation of number of cycles for electro-deposition of CoNP

CoNP was electrodeposited on GCE at varying thicknesses by altering the number of cycles for deposition while keeping the number of cycles for polymerisation of pAHNSA as twenty (Figure 3.3 b). Influence of thickness of CoNP layer on the oxidation peak current of 1.0×10^{-4} M DA was studied by recording square wave voltammograms after deposition of CoNP with various number of cycles. On increasing the number of cycles for electro-deposition of CoNP, it was observed that peak current for oxidation of DA was increased to a maximum value at ten cycles. Further increase in number of cycles gave a decrease in peak current. Number of cycles required for the electro-deposition of optimum quantity of CoNP on GCE was fixed to be ten, as it gave the best response for electro-oxidation of DA.

3.3.2.3.2 Optimisation of number of cycles for electro-polymerisation of AHNSA on CoNP-modified GCE

Effect of varying film thickness of the electro-polymer pAHNSA on anodic peak current of DA (1.0×10^{-4} M) was also monitored (Figure 3.3 c). AHNSA was electro-polymerised on cobalt-nano-modified GCE by varying the number of cycles for polymerisation from 10 to 50. Maximum anodic peak current for oxidation of DA was obtained when CoNP/GCE was modified with fifteen cycles for electro-polymerisation of pAHNSA. Thus number of cycles for the electro-polymerisation of AHNSA was optimised to be fifteen.

3.3.2.4. Characterisation of the electrode-pAHNSA/CoNP/GCE

SEM images of bare GCE, CoNP/GCE and pAHNSA/CoNP/GCE given in Figure 3.4 depicts the successful modification of the electrode.

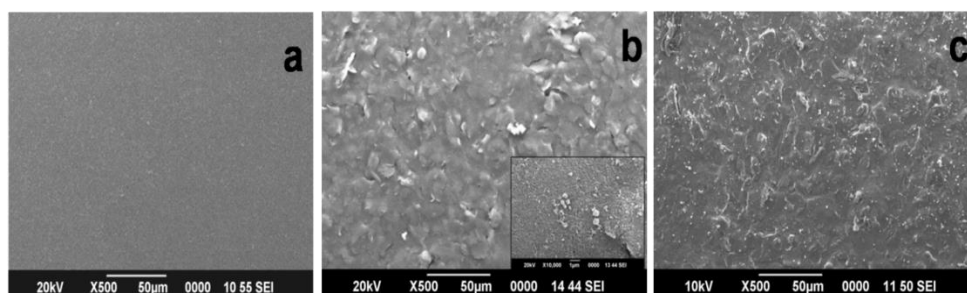


Figure 3.4 SEM images of (a) bare GCE (b) CoNP/GCE and (c) pAHNSA/CoNP/GCE.

Cyclic voltammograms of 2.0×10^{-3} M $K_3[Fe(CN)_6]$ was obtained at different scan rates (Figure 3.5). For a reversible system, the relationship between the current and scan rate is given by the Randles–Sevcik equation.⁵

$$I = 2.69 \times 10^5 A n^{3/2} D^{1/2} C v^{1/2}$$

Where A refers to the electro-active surface area of the electrode, I is peak current, D is diffusion coefficient, n is number of electrons transferred, C is concentration of $K_3[Fe(CN)_6]$ and v refers to scan rate. Here, $n=1$, $D=7.6 \times 10^{-6} \text{ cm}^2 \text{ s}^{-1}$. Variation in peak current with square root of scan rate was plotted. From the slope of the plot **electro-active surface area, A** was calculated.

Electro-active surface area obtained for bare GCE and pAHNSA/CoNP/GCE are 0.0385 cm^2 and 0.0513 cm^2 . Enhancement in

electro active surface area indicates the increase in number of catalytic sites on the surface.

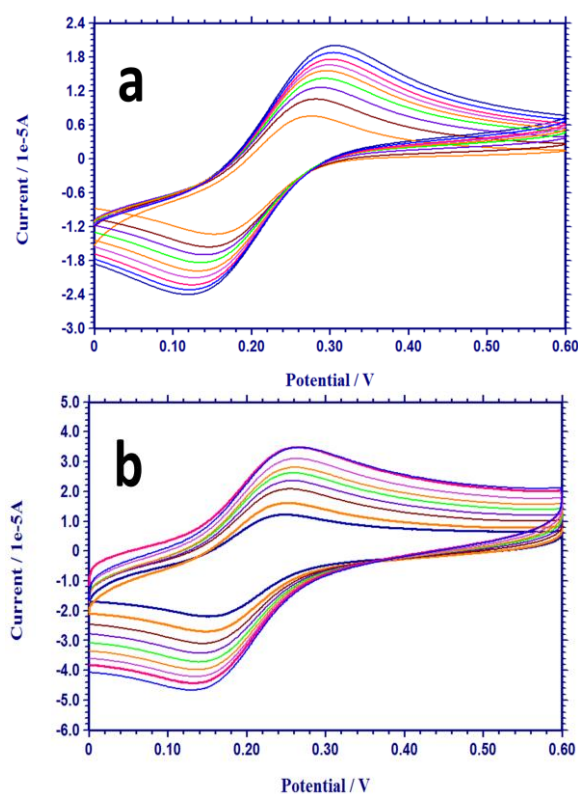


Figure 3.5 Overlay of cyclic voltammograms of 2.0×10^{-3} M $K_3[Fe(CN)_6]$ on (a) bare GCE and (b) pAHNSA/CoNP/GCE at various scan rates.

Faradaic Impedance Studies were employed to compare the electrochemical behaviour of pAHNSA/CoNP/GCE with that of bare electrode. Nyquist plots of modified as well as bare electrode was obtained at +0.22 V using 5mM $[Fe(CN)_6]^{3-/4-}$ as the probe (Figure 3.6 A). Nyquist plot shows a semicircular region which is attributed to the resistance offered by the electrode towards the electron transfer reaction and

a linear region which depicts the diffusion of the analyte to the electrode. Nyquist plots were fitted with an equivalent circuit $Rs[QRct]W$ where Rct is the charge transfer resistance, Q is the constant phase element and W is the Warburg constant. It is seen that the Rct value of GCE decreases from 4387 Ω to 1219 Ω upon modification. It indicates the feasibility offered by the modified electrode towards channelizing of electron.

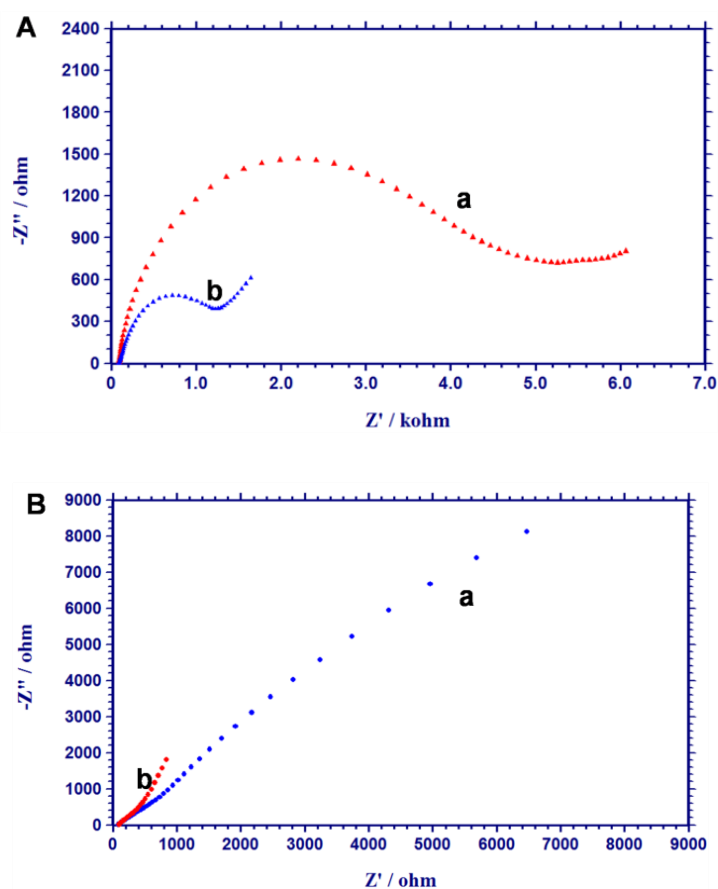


Figure 3.6 A. EIS spectra of 0.1 M KCl containing 5 mM [Fe(CN)₆]^{3-/4-} at (a) bare GCE and pAHNSA/CoNP/GCE. B. EIS spectra of 0.1 M PBS (pH 7) containing 1.0 × 10⁻⁵ M DA at (a) bare GCE and pAHNSA/CoNP/GCE.

In order to confirm the electro-catalytic activity of the modifier towards the oxidation of DA, impedimetric changes produced by GCE upon modification was studied in 0.1 M PBS (pH 7) containing 1.0×10^{-5} M DA (Figure 3.6 B). Nyquist plots obtained were fitted with an equivalent circuit. The charge transfer resistance was found to be decreased from 8448 Ω to 782 Ω when the electrode was modified with the nano-polymer composite. This evidently points to the catalytic activity offered by the modifier towards the electro-oxidation of DA.

3.3.3 Kinetic and mechanistic aspects of electrooxidation

3.3.3.1 Diffusion controlled electro-oxidation of DA

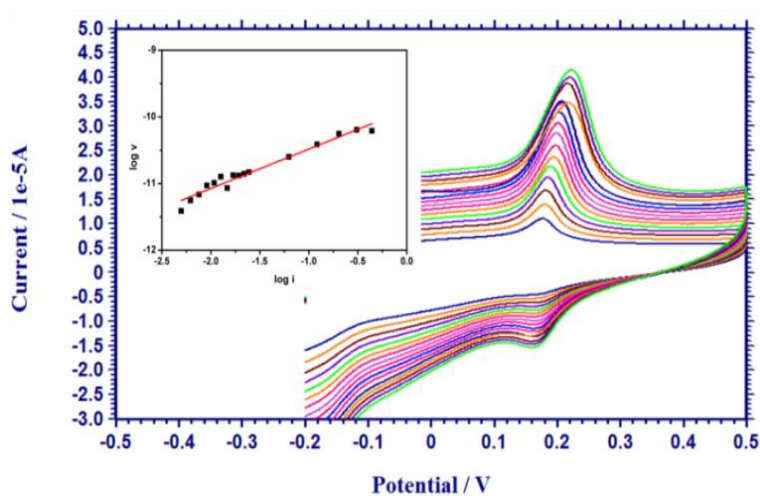


Figure 3.7 Cyclic voltammograms of 5.0×10^{-6} M DA at various scan rates, inset: Plot of $\log i$ vs. $\log v$

Effect of **varying scan rates** on oxidation peak current of DA (5.0×10^{-6} M) was investigated in 0.1 M PBS (pH 7) using cyclic voltammetry (Figure 3.7). Linear dependency of square root of scan rate

($v^{1/2}$) with peak current signifies that the oxidation of DA at pAHNSA/CoNP/GCE is controlled by the bulk transport of analyte from solution to electrode surface. Moreover, the plot of $\log I_{pa}$ vs $\log v$ was observed to be linear with a slope of 0.60 over a range of scan rates 0.1 to 0.7 Vs^{-1} . The value of slope is in agreement with the theoretical value of 0.5 indicating that the electrochemical oxidation of DA is diffusion controlled.²⁷³

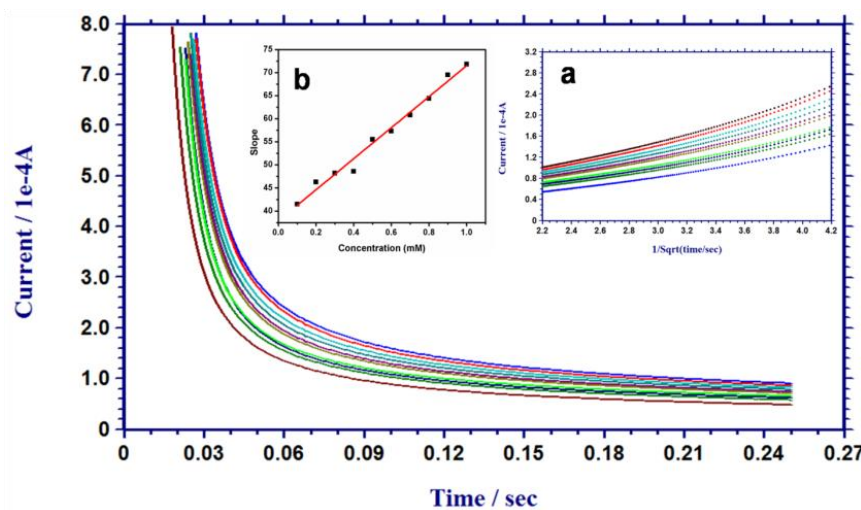


Figure 3.8 Chronoamperograms of various concentrations of DA, inset (a) plot of I_{pa} for DA vs. $t^{-1/2}$ (b) plot of slope of (I vs. $t^{1/2}$) vs. concentration of DA.

In order to determine the diffusion coefficient, **chronoamperometric studies** were carried out. Decay of Faradaic current with time, generated by the electrochemical oxidation of DA in the range 1.0×10^{-4} M to 1.0×10^{-3} M was recorded and the chronoamperograms are given in Figure 3.8. Variation in current with $t^{-1/2}$ was found to be linear, which was in accordance with Cottrell equation.

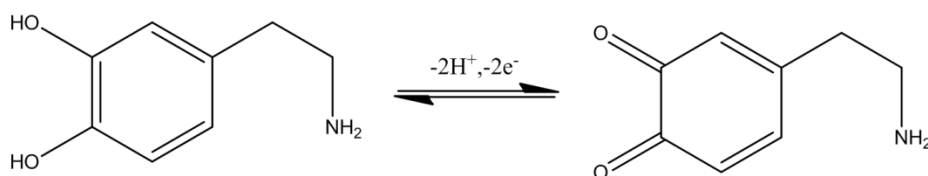
$$I_p = nFAD^{1/2}C\pi^{-1/2}t^{-1/2}$$

Slopes of these experimental plots (I_{pa} vs. $t^{-1/2}$) were plotted against the concentration of DA.

Slope of the resultant plot was utilised to calculate diffusion coefficient and the value obtained was $3.6 \times 10^{-5} \text{ cm}^2 \text{ s}^{-1}$.

3.3.3.2 Calculation of number of electrons and protons

From earlier sections it can be seen that electrochemical redox reaction of DA is perfectly reversible with 2 electrons transfer. From the plot of pH with anodic peak potential, it is confirmed that equal no of electrons and protons are involved in the redox reaction of DA. Thus the possible mechanism of electrochemical redox reaction of DA is given in scheme 3.1.



Scheme 3.1 Mechanism of electro-oxidation of DA

3.3.4 Concentration Study

Under optimal conditions mentioned above, square wave voltammograms of different concentrations of DA in the range $1.0 \times 10^{-4} \text{ M}$ to $2.0 \times 10^{-7} \text{ M}$ were recorded and results obtained are given in Figure 3.9.

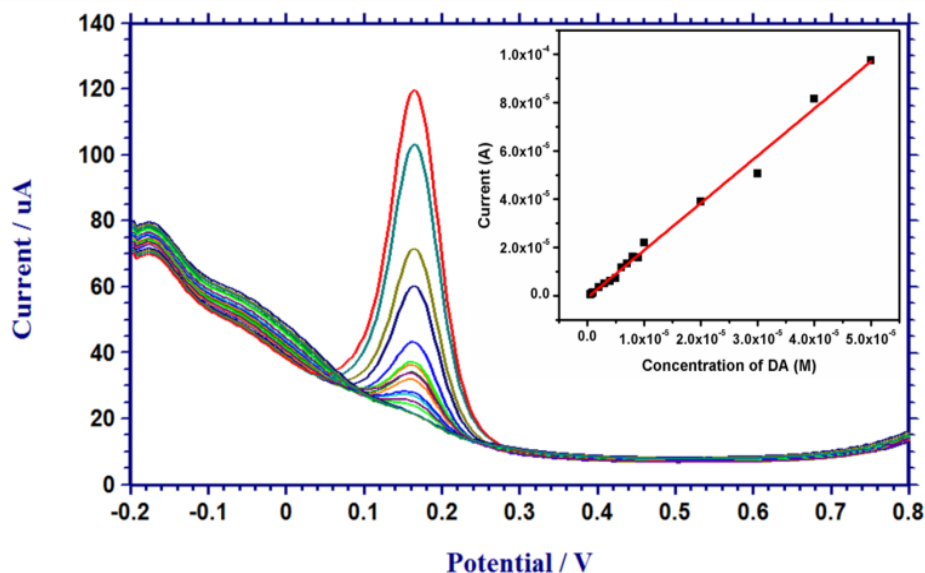


Figure 3.9 Overlay of square wave voltammograms of DA at varying concentration from 1.0×10^{-4} M to 2.0×10^{-7} M. Inset: calibration plot of DA in the range 5.0×10^{-5} M to 5.0×10^{-7} M.

Within the concentration range 5.0×10^{-5} M to 5.0×10^{-7} M increase in peak current with increasing concentration of DA fitted the following equation, $I_{pa} = 1.95 C - 7 \times 10^{-7}$, with a correlation coefficient of 0.99. The limit of detection calculated using the equation $3s/m$, where s is the standard deviation of current responses of lowest concentration of DA in the linear range and m is the slope of calibration plot. Limit of detection (LOD) achieved for the developed sensor is 1.75×10^{-8} M. The results obtained for various reported sensors based on GCE are enlisted in Table 3.1. Comparison with different sensors reveals that the lowest LOD was achieved by the developed sensor.

Table 3.1 Comparison of the linear range and LOD of the existing DA sensors based on chemical modification of GCE.

| Electrode | Techniques used | Linear range (M) | LOD (M) |
|---|-----------------|---|----------------------|
| LB-CUCR/GCE(ox) ^a ₂₇₄ | DPV | 6.0×10^{-8} - 8.0×10^{-8} | 2.0×10^{-8} |
| C-dots/IL-graphene/GCE ^b ₂₇₅ | CV, DPV | 6.0×10^{-4} - 1.0×10^{-7} | 3.0×10^{-8} |
| GNS-CNT's/MoS ₂ /GCE ^c ₂₇₆ | CV, DPV, EIS | 1.0×10^{-4} - 1.0×10^{-7} | 5.0×10^{-8} |
| Carbon/tyrosinase/Nafion/GCE ^d ₂₇₇ | CV, Amperometry | 1.0×10^{-3} - 5.0×10^{-5} | 5.0×10^{-5} |
| Poly(PCV)/GCE ^e ₂₇₈ | DPV, EIS | 2.0×10^{-4} - 1.5×10^{-5} | 9.7×10^{-6} |
| ICDACH/GCE ^f ₂₇₉ | CV, DPV, EIS | 9.0×10^{-5} - 6.0×10^{-7} | 1.9×10^{-7} |
| DDTCAg/GCE ^g ₂₈₀ | CV | 6.0×10^{-5} - 5.0×10^{-7} | 1.0×10^{-7} |
| PTH/GCE ^h ₂₈₁ | CV, DPV | 3.5×10^{-5} - 5.0×10^{-6} | 2.0×10^{-7} |
| Proposed sensor | CV, SWV, EIS | 5.0×10^{-5} - 5.0×10^{-7} | 1.8×10^{-8} |

a: Langmuir-Blodgett film of calixarene modified GCE, **b:** Ionic liquid functionalised graphene and carbon dots modified GCE, **c:** GCE modified with a graphene and carbon nanotube hybrid decorated with MoS₂ flowers, **d:** GCE modified with carbon, tyrosinase and Nafion, **e:** poly(pyrocatechol violet) modified GCE, **f:** N,N'-bis(indole-3-carboxaldimine)-1,2-diaminocyclohexane thin film modified GCE, **g:** Silver-diethyldithio carbamate modified GCE, **h:** poly(thionine)-modified GCE.

3.3.5 Effect of coexisting species

The selectivity of the developed sensor towards DA was monitored by studying the effects of foreign species such as KCl, NaNO₃, dextrose, fructose, glycine, serotonin, uric acid, l-dopa, adrenaline, tyrosine and ascorbic acid on the electrochemical response of DA (5.0×10^{-6} M) in 0.1 M PBS (pH 7). It was found that KCl, NaNO₃, dextrose, fructose and glycine did not interfere with the analysis of DA even when present in 100fold excess concentrations. Tyrosine did not generate any interference up to 10fold excess concentration of DA. Another neurotransmitter serotonin did not produce interference in equimolar concentrations but interfered when present in higher concentrations than that of DA. Equimolar concentrations of adrenaline, uric acid, l-dopa and ascorbic acid interfered with the response of the sensor.

3.3.6 Application study

Efficiency of the sensor in real sample analysis was successfully ascertained by carrying out determination of DA in artificial samples of blood serum, urine and cerebrospinal fluid (CSF). Prepared samples spiked with DA were subjected to square wave voltammetry and concentrations were obtained from the calibration curve. Appreciable recoveries were obtained with relative standard deviations (RSD's) below 5% (Table 3.2), establishing the reliability of the sensor in real sample determination of DA.

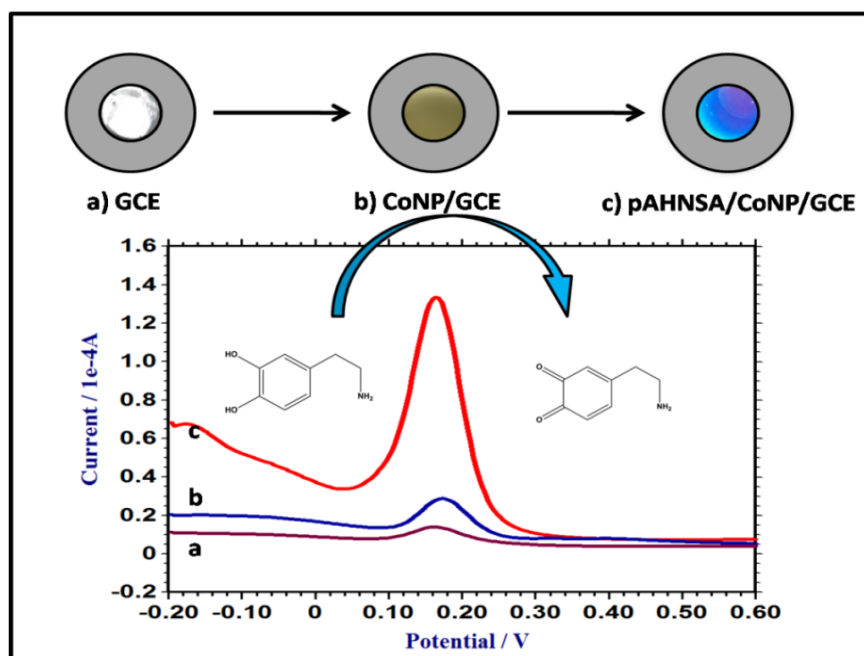
Table 3.2 Determination of DA in artificial biological samples

| Sample | Added (M) | Found (M) | Recovery (%) | RSD (%) |
|------------------------|---|---|--------------|---------|
| Artificial blood serum | 2.0×10^{-6} - 4.0×10^{-5} | 2.1×10^{-6} - 4.1×10^{-5} | 103 | 1.9 |
| Artificial urine | 9.0×10^{-7} - 2.0×10^{-6} | 9.1×10^{-7} - 2.1×10^{-6} | 102 | 3.1 |
| Artificial CSF | 7.0×10^{-7} - 3.0×10^{-6} | 7.0×10^{-7} - 3.1×10^{-6} | 101 | 3.2 |

In order to validate the developed sensor, results obtained for urine analysis were compared with that obtained by HPLC analysis. DA in artificial urine gave recovery of 101% when studied with HPLC method. This is comparable with the recovery obtained (102%) for developed sensor which validates the developed sensor.

3.4 Conclusions

The present study reports the development of a pAHNSA/CoNP/GCE with high conductivity and electro-catalytic efficiency towards the oxidation of DA compared to bare GCE. A pronounced increase in peak current (16fold) at modified electrode implicates the synergic effect of cobalt nano particle - pAHNSA composite. The fabricated sensor exhibits wide linear range, 5.0×10^{-5} M to 5.0×10^{-7} M with very low detection limit, 1.75×10^{-8} M. The developed sensor was successfully applied to the quantification of DA in artificial samples of blood serum, urine and cerebrospinal fluid (CSF).



Scheme 3.2 Schematic representation of voltammetric sensor for dopamine

.....*OR*.....

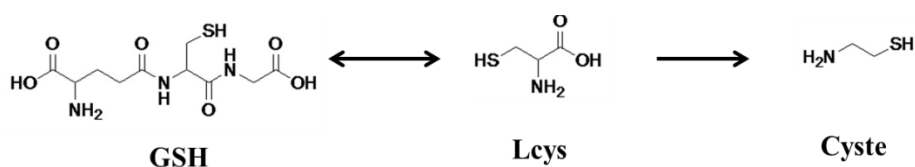
Colorimetric sensor for the determination of biothiols - glutathione and cysteamine

| | |
|--|-----------------------------------|
| C o n t e n t s | 4.1 <i>Introduction</i> |
| | 4.2 <i>Experimental</i> |
| | 4.3 <i>Results and discussion</i> |
| | 4.4 <i>Conclusions</i> |

This chapter details the development of a sensor for the determination of dual analytes. A sensor for the detection and determination of bio-thiols (glutathione (GSH) and cysteamine (Cyste)) has been developed by integrating the distinguished distance related optical characteristics of silver nanoparticles with the simplicity of colorimetric technique. In presence of these analytes, shift in surface plasmon resonance (SPR) absorption of silver nanoparticles (AgNPs) with change in its colour was observed. Yellow coloured AgNPs solution becomes colourless in presence of GSH and changes to red in presence of Cyste. The difference in absorption of AgNPs in the absence and presence of GSH was found to vary linearly in the range 1.0×10^{-5} M to 5.0×10^{-7} M concentration range with limit of detection at 3.68×10^{-7} M. The method can also be applied to quantify Cyste in the range 1.1×10^{-6} M to 5.0×10^{-8} M with limit of detection at 1.80×10^{-8} M. The utility of the proposed colorimetric assay is validated by determination of GSH and Cyste in artificial blood serum.

4.1 Introduction

Low molecular weight bio-thiols are a very important class of molecules distributed in living cells. Individually as well as collectively, they are involved in maintaining the redox homeostasis of the cell. Of these, the most active and abundant thiol is glutathione (GSH). GSH is biosynthesized from its core metabolite l-cysteine (Lcys) which is a major intracellular sulfur donor. Another thiol cysteamine (Cyste) is obtained by the decarboxylation of Lcys.²⁸² Structures of these inter related thiols are given in Scheme 4.1.



Scheme 4.1 Structures of GSH, Lcys and Cyste

GSH, the mother of all antioxidants, is widely distributed in living species in very high concentrations.²⁸³ It prevents cell damaging by inhibiting the action of free radicals and peroxides. Different biological functions of GSH include detoxification, elimination (or transportation) of metal ions, regulation of oxidative stress, removal of foreign particles from the liver etc.²⁸⁴ Clinically, levels of GSH give implications of diseases such as AIDS, neurodegenerative disorder, chronic lung diseases, cardiovascular disorders, rheumatoid arthritis, and diabetes.²⁸⁵ GSH is found at milli molar levels in tissues and at micro molar levels in biological fluids such as plasma.²⁸⁶ Therefore, sensitive method for the determination of GSH is highly demanded.

Cyste (2-aminoethanethiol) the degradation product of Lcys is a short, simple and reactive amino thiol present in living organisms.²⁸⁷ Cyste is generated during the enzymatic hydrolysis of panthetheine to pantothenic acid (vitamin B₅) which is an interim step in the metabolism of co-enzyme A.²⁸⁸ It is used as a radio protective agent which gives protection from lethal effects of X-rays, γ -radiations, LET radiations, intracellularly localized auger electrons, α - particle emitters, β - particle emitters, etc.²⁸⁹ By decreasing the DNA damage, Cyste protects the cells from both mutation induction and cell death caused by radiation. It has been approved by FDA in the US since 1994 and in the EU since 1997 for the treatment of nephropathic cystinosis in children and adults.²⁹⁰ It was found to be effective in the treatment of Huntington's disease.²⁹¹ It may be used as a feed additive to enhance the growth rate of animals in farms.²⁹² These facts leads to the elevated demand of sensitive methods for the determination of above mentioned thiols.

Several methods are available to estimate the amount of GSH present in biological samples. They are capillary zone electrophoresis,²⁹³ HPLC with different detection methods^{284,294} and fluorescence sensors.²⁹⁵ However analytical methods for the determination of Cyste in biological samples are scarcely found. The available methods are based on ion-exchange column chromatography,²⁹⁶ high voltage electrophoresis,²⁹⁷ HPLC methods,^{298,299} gas chromatography with flame photometric detection²⁸⁷ and electrochemical methods.³⁰⁰

Metallic nanoparticles have been widely used to design different types of sensors for the determination of biologically important molecules.

Colorimetric assays based on these nanoparticles received significant interest due to their simplicity, visual detection, low cost, cheap instrumentation and easy operation. Colorimetric sensors based on silver nanoparticles (AgNPs) are more affordable but less explored compared to gold nanoparticles. Owing to their unique properties, for instance, high extinction coefficient and narrow surface plasmon resonance band in the visible region, AgNPs are gaining attention these days.¹⁹⁹ Moreover, development of chemo sensors for the determination of multi-analyte is found to be an interesting research area.^{301,302}

Colorimetric determination of bio-thiols using a sensor based on tyrosine capped AgNPs (AgNP-Tyr) has not yet been reported. In continuation to the development of sensors for the determination of different biologically important molecules,^{43,199,297, 303} the present work is an attempt to fuse the outstanding properties of AgNPs with the simplicity of colorimetric technique for the determination of two prominent bio thiols. Development of detection strategies of two inter related thiols GSH and Cyste based on their interaction with AgNPs builds the core content of this work. These interactions produce variations in the SPR absorptions of AgNPs, thereby forming a platform for their colorimetric analysis. Developed method is applied to determine GSH and Cyste in artificial blood serum.

4.2 Experimental

Tyrosine capped silver nanoparticles (AgNP - Tyr) were synthesized as per the procedure discussed in chapter 2, section 2.3.6.

4.2.1 Colorimetric detection and determination of Cyste and GSH

A stock solution of 1.0×10^{-2} M Cyste was prepared by dissolving 11.36 mg of cysteamine hydrochloride in 10 mL water. 1.0×10^{-2} M solution of Cyste was diluted with water to get a 1.0×10^{-5} M Cyste. To 500 μ L of as – synthesized AgNP-Tyr solution, required amount of 1.0×10^{-5} M Cyste was added and made up to 2 mL using 0.01 M PBS. Absorbance of the mixture was measured from 200 nm to 900 nm. The ratio of absorbance at 530 nm to that at 400 nm (A/A_0) was plotted against the concentrations of Cyste.

30.73 mg of GSH was dissolved in water to get 1.0×10^{-2} M GSH. Solutions with lower concentrations were prepared by serial dilution. Then, mixtures of AgNPs solution, varying concentrations of GSH and 0.01M PBS were subjected to absorbance measurements. Difference in absorbance at 400 nm in the absence and presence of GSH ($A_0 - A$) was plotted against the concentrations of GSH.

4.2.2 Electrochemical measurements of GSH

The conventional three electrode system includes a working electrode (glassy carbon electrode), a reference electrode (Ag/AgCl), and a counter electrode (platinum wire). The glassy carbon electrode (GCE) was polished using 0.05 μ m alumina, and ultra-sonicated in ethanol, water, 1:1 HNO₃, water, acetone and water to remove the unspecific adsorption. Oxidative stripping voltammetry was used to detect the Ag⁺ ions. The experimental conditions employed were as follows: electrochemical deposition at -0.80 V for 400 s and the potential scan from -0.40 to 0.80 V at a rate of 1 Vs^{-1} .

4.2.3 Application study

Artificial blood serum was prepared as per the procedure discussed in section 2.7.2. A stock solution of 1.0×10^{-5} M Cyste / 1.0×10^{-4} M GSH was prepared in artificial blood serum. Required amount of these solutions added to 500 μ L of the AgNPs solution was diluted to 2 mL with 0.01 M PBS (pH 7.4) and absorbance was recorded.

4.3 Results and discussion

4.3.1 UV – visible study of AgNPs in presence of Cyste and GSH

The as-synthesized tyrosin capped AgNPs are yellow coloured with typical SPR band maximum at 400 nm (Figure 4.1 a). The size and shape of the nanoparticles were evaluated by processing micrographs obtained from TEM of AgNPs solution. From TEM images it is clear that the AgNPs are dispersed and spherical in shape with an average diameter around 10 nm (Figure 4.2 a). This is again confirmed by the hydrodynamic volume (18.80 nm) obtained in the DLS measurements. During capping, -OH terminal of tyrosine gets attached to the nanoparticles surface with carboxyl and amino group projected out. In alkaline conditions, AgNPs bear -ve charge at its surface by virtue of $-\text{COO}^-$ group of tyrosine which stabilizes the particles. Zeta potential value of -52 mV supports the above inference.

Absorption spectra of AgNPs at 400 nm in the absence and presence of GSH and Cyste each are given in Figure 4.1. As mentioned earlier, in the absence of any foreign species, AgNP-Tyr is yellow in colour. Upon addition of a particular concentration of Cyste into AgNP-Tyr, the latter turns to red. From Figure 4.1 b, it is clear that the new absorption at 530 nm imparts red colour to the solution. In presence of GSH, colour of the AgNP-

Tyr solution diminishes and becomes colourless. Absorption measurements (Figure 4.1 c) reveal decrease in the absorbance at 400 nm.

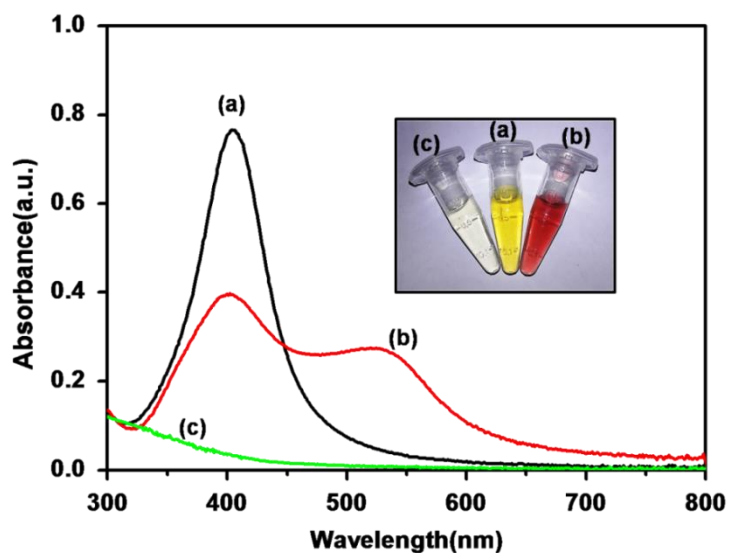


Figure 4.1 Absorption spectra of (a) AgNP-Tyr (b) AgNPs in presence of 3.0×10^{-6} M Cyste and (c) AgNPs in presence of 1.0×10^{-4} M GSH; inset: photographs of solutions of (a) AgNP-Tyr (b) AgNPs with Cyste and (c) AgNPs with GSH

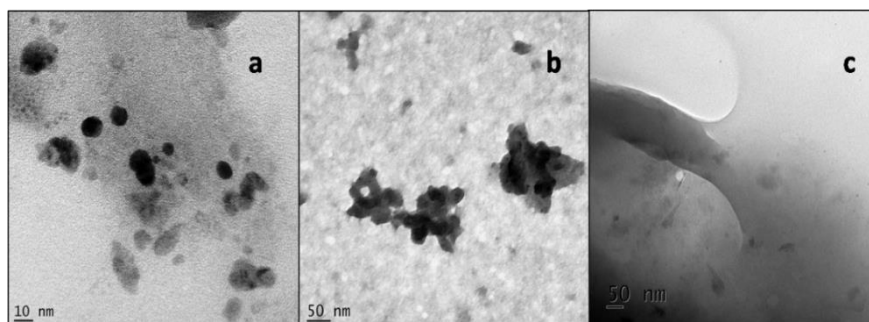


Figure 4.2 TEM images of (a) AgNP-Tyr (b) AgNPs in presence of Cyste and (c) AgNPs after reaction with GSH

4.3.2 Sensing mechanism of Cyste

When Cyste is added to AgNPs solution, $-NH_2$ or $-SH$ group may bind to the metal surface. The amino group can bind to AgNPs effectively at lower pH whereas $-SH$ group at relatively higher pH ($pH > 5$).³⁰⁴ Hence at pH 7.4, $-SH$ group of Cyste may easily displace tyrosine moiety binding itself to the nanoparticles surface. Comparison of FT - IR spectra of Cyste and Cyste capped AgNPs (AgNP- Cyste) support the above deductions. The band at 2500 cm^{-1} corresponding to $-SH$ group of Cyste (Figure 4.3a) is absent in the IR spectrum of AgNP- Cyste (Figure 4.3b) which may be due to the formation of Ag-S bond.

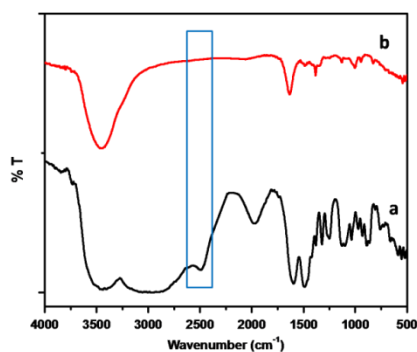
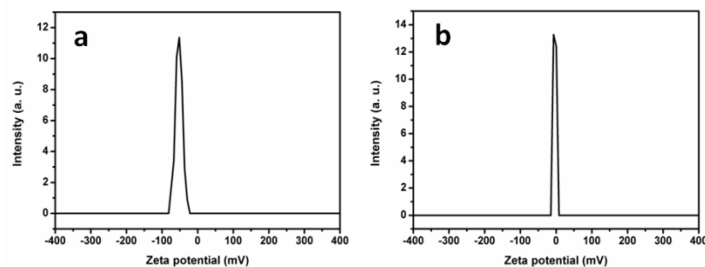


Figure 4.3 FTIR spectra of (a) Cyste alone and (b) Cyste after reaction with AgNPs



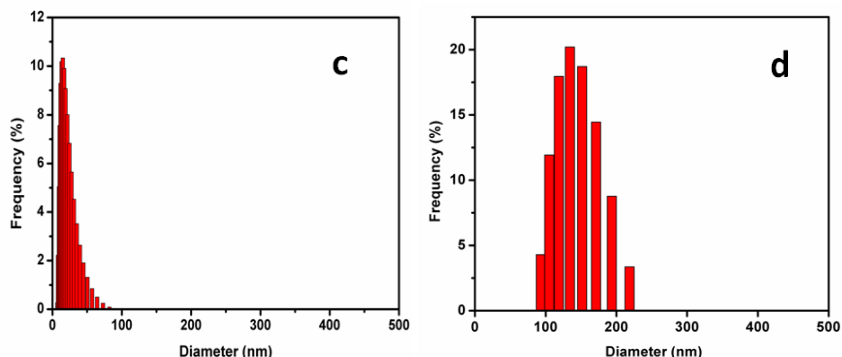


Figure 4.4 Zeta potential analysis of AgNPs in the (a) absence and (b) presence of Cyste and DLS spectrum of AgNPs in the (c) absence and (d) presence of Cyste

Due to the absence of -ve charge ($-\text{COO}^-$) on Cyste, surface charge on the AgNP- Cyste is lower than that on AgNP-Tyr. It is clearly evidenced by the reduction of zeta potential from -52 mV to -3 mV on addition of Cysteamine to AgNP-Tyr (Fig 4.4 a and b). This in turn lowers their impedance for closer approach. It ultimately results in the aggregation of AgNP - Cyste, with a visible change in the colour of the solution from yellow to red. Hydrodynamic diameter of AgNPs was measured by DLS studies after the addition of Cyste. A change in the hydrodynamic diameter from around 18 nm to approximately 250 nm was observed (Fig 4.4 c and d). Aggregated nano particles may be visualized from TEM images given in Figure 4.2 b. From the data given above, it may be concluded that the red colour of AgNPs solution, reduction in zeta potential and increase in hydrodynamic volume of AgNPs is due to the Cyste induced aggregation of AgNPs.

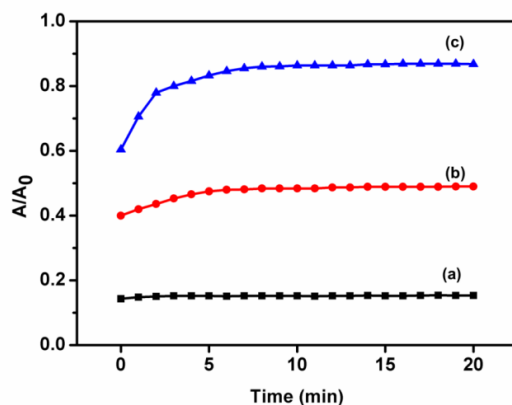


Figure 4.5 Variation in the absorption ratios of AgNPs in presence of (a) 1.0×10^{-6} M (b) 2.0×10^{-6} M and (c) 3.0×10^{-6} M Cysteine with time.

Figure 4.5 (a, b and c) depicts the time required by different concentrations of Cysteine to complete the reaction. Considering this time requirement exhibited in absorption profile, for Ag-S bond formation followed by aggregation of nanoparticles, all measurements were done after giving an incubation time of 10 min.

4.3.3 Sensing mechanism of GSH

GSH when added to AgNP-Tyr may get adsorbed on the surface of AgNPs. During this process colour change (yellow to red) of AgNPs solution was not observed instantaneously. Absence of the development of red colour indicates absence of aggregation. From Figure 4.1 a, it is clear that, silver in its nano form absorbs visible light at 400 nm to give yellow colour. Decrease in intensity of yellow colour (decrease in absorption at 400 nm) in presence of GSH, is an indication of decrease in the number of

nanoparticles. It may be due to the dissolution of nanoparticles, that is the transition of Ag^0 to its oxidized state.

Oxidative stripping voltammetric measurements of AgNO_3 , AgNP-Tyr in presence and absence of GSH were carried out (Figure 4.6). Ag was electrodeposited on GCE from AgNO_3 solution at -0.80 V and stripped oxidatively at 0.28 V (Figure 4.6 a). In the voltammogram of AgNP-Tyr (Figure 4.6 b), the peak at 0.28 V was absent. But, a small increase in the peak current was observed when AgNP-Tyr solution was subjected to voltammetric studies in presence of GSH (Figure 4.6 c). It acts as a worthy evidence for the formation of more number of silver ions in the solution of AgNP-Tyr in presence of GSH.

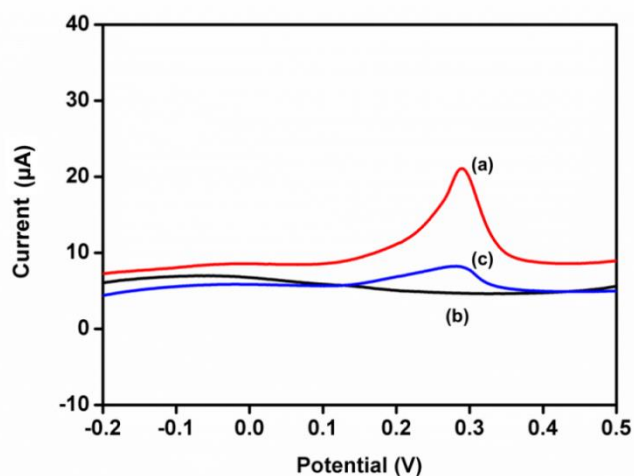


Figure 4.6 Overlay of voltammograms of (a) AgNO_3 (b) AgNP-Tyr and (c) AgNP-Tyr in presence of GSH on GCE.

It is normally accepted that in as-synthesized AgNPs, surface silver atoms are oxidized and likely exist as silver oxide.³⁰⁵ When organo-thiols are allowed to react continuously with AgNPs for a long time, they can

convert silver oxide and silver atoms to silver-thiolate salts.³⁰⁶ Literature also says that the mechanism behind the dissolution of AgNPs is the displacement exchange of Ag^+ ions by reduced cysteinyl residues of the analytes.³⁰⁷ Here, GSH may initially get adsorbed on to AgNPs and forms bond with silver ions on the surface. Incoming GSH moieties displaces the Ag^+ loaded GSH on AgNPs surface. This may progress until each GSH is saturated with silver ion. Since silver – GSH complexes are soluble in basic medium (PBS, pH = 7.4), the solution becomes colourless.³⁰⁸ Absence of metallic nanoparticles in the solution was observed through TEM images (Figure 4.2 c) which support the above deductions. Dissolution of AgNPs may be quantitatively correlated to the concentration of GSH.

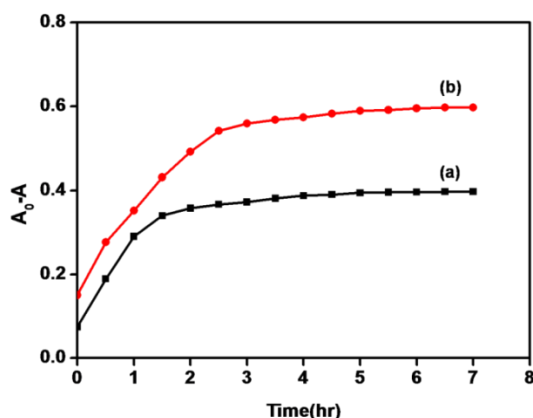


Figure 4.7 Variation in $(A-A_0)$ of AgNPs in presence of (a) 1.0×10^{-5} M and (b) 5.0×10^{-5} M GSH with time.

Time studies show that the reaction reaches equilibrium in almost 5 hours. After 5 hours absorption maximum was stable. Hence all absorption studies were carried out five hours after mixing (Figure 4.7 a and b).

4.3.4 Analytical performance of the sensor

4.3.4.1 Effect of reaction medium and pH

UV - vis absorption characteristics of AgNP-Tyr in absence and presence of Cyste were studied in different media. Among 0.01 M solutions of citrate buffer, acetate buffer, phosphate buffer (PBS), Britton - Robinson buffer and water, best result was obtained in PBS. Colour of AgNP-Tyr solution was found to change from yellow to orange below pH 6. Below pH 6, the zwitter ionic form of tyrosine leads to their entangling, which in turn results in the aggregation of tyrosine capped AgNPs. pH of AgNP solution (containing Cyste/ GSH) was varied from 6 to 10 and absorption measurements were carried out. In basic pH, absorption ratios (A/A_0) in presence of Cyste and absorption difference (A_0-A) in presence of GSH did not show pronounced difference. Hence further studies were conducted in biological pH, 7.4.

4.3.4.2 Concentration study

Absorption of AgNPs in presence of different concentration of Cyste was studied. In presence of Cyste, the absorbance at 400 nm decreased together with the formation of new absorption peak at 530 nm (Figure 4.8 a). The absorption ratio (A/A_0) increased linearly with concentration of Cyste in the range 1.1×10^{-6} M to 5.0×10^{-8} M ($R^2 > 0.99$) (Figure 4.8 b). The limit of detection was calculated as per the equation $3s/m$ where 'm' is the slope of the calibration graph and 's' is the standard deviation of the response offered by the lowest concentration of Cyste. The limit of detection of Cyste for the sensor is found to be 1.8×10^{-8} M.

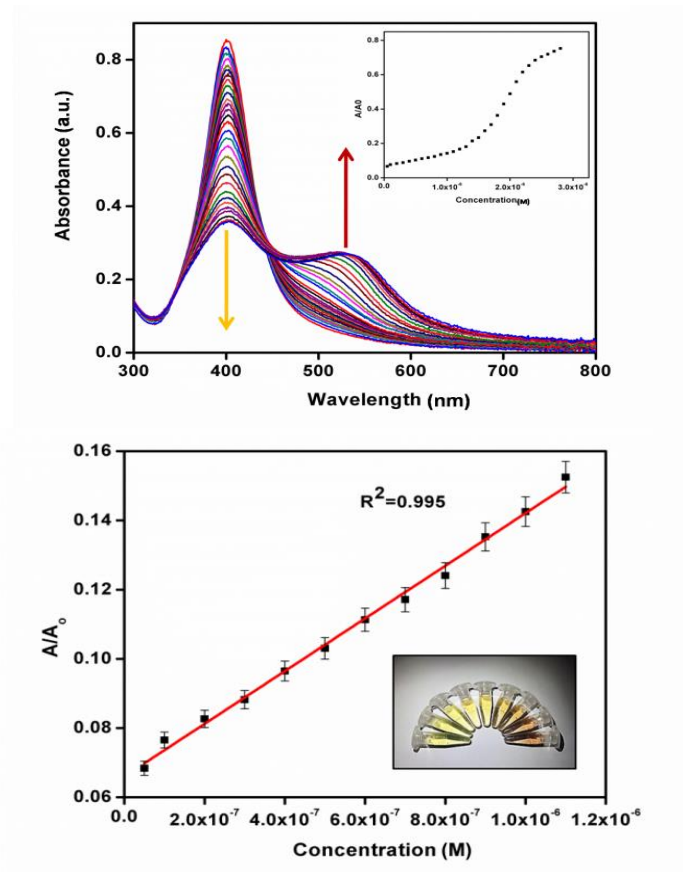


Figure 4.8 (a) Absorption spectra of AgNPs in presence of various concentrations of Cysteine from 3.0×10^{-6} M to 5.0×10^{-8} M; inset: A plot of absorption ratio (A/A_0) with concentration of Cysteine. (b) Calibration graph of Cysteine in the range 1.1×10^{-6} M to 5.0×10^{-8} M; inset: photographs showing colour change of AgNPs in presence of Cysteine.

Under optimum conditions, the sensitivity of the sensor for the detection of GSH was also monitored. The absorbance at 400 nm decreases quantitatively as a function of GSH concentration (Figure 4.9). ($A_0 - A$) varied linearly with concentration of GSH in the range 1.0×10^{-5} M to 5.0×10^{-7} M with a correlation coefficient > 0.99 (Figure 4.9 a). The lowest

limit of detection was calculated using the equation $3s/m$. Limit of detection of GSH obtained is 3.68×10^{-7} M.

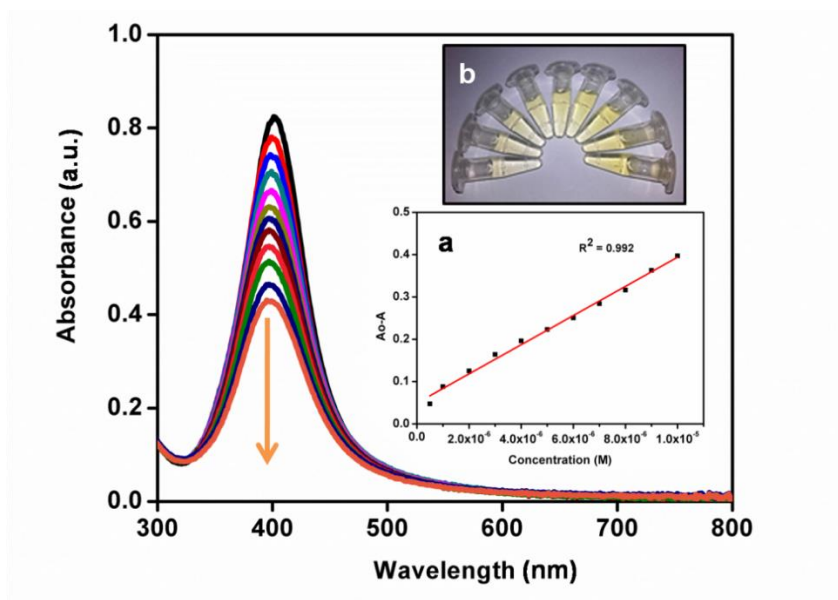


Figure 4.9 Absorption spectra of AgNPs in presence of GSH in the range 1.0×10^{-5} M to 5.0×10^{-7} M; inset(a) Calibration graph of GSH and inset(b) photographs showing colour change of AgNPs in presence of GSH.

4.3.4.3. Selectivity and interference

To assess the selectivity of this sensor, the effects produced by some co-existing species were studied including NaCl, KCl, glucose, urea, uric acid, glycine, alanine, serine, tyrosine, tryptophan, creatinine, histidine, proline, cysteine and ascorbic acid. The response of AgNPs towards each species is given in Figure 4.10. Lcys gave a decrease in the SPR absorption maximum without a peak at 530 nm. Other amino acids did not produce any

change in absorption maxima at 400 nm, since they could not bind to AgNPs at the optimized pH (pH 7.4).

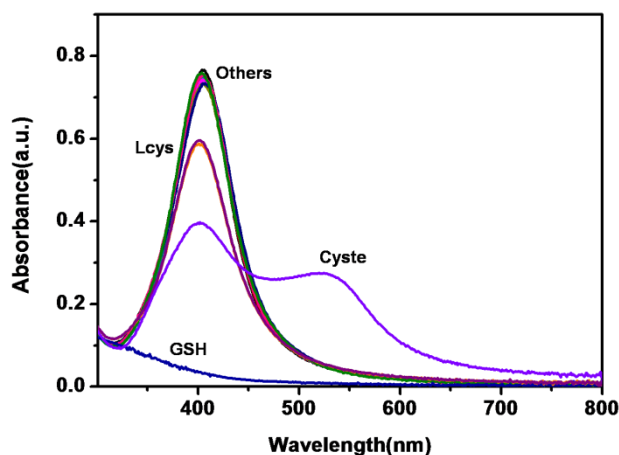


Figure 4.10 Selectivity of AgNP-Tyr towards different species. (Concentration of each species = 1.0×10^{-4} M other than 3.0×10^{-6} M Cyste)

Effect of foreign species on the absorption ratio (A/A_0) produced by Cyste (7.0×10^{-7} M) was investigated. Variation in the maximum concentration of the foreign species which caused an approximately $\pm 5\%$ relative error in the determination of Cyste at 7.0×10^{-7} M was taken as the tolerance limit. The response of AgNPs due to Cyste in presence of different species is given in Figure 4.11. As shown in Figure 4.11, KCl, NaCl, glycine, alanine, urea, uric acid and glucose did not change the absorption ratio when present even at 100 fold excess concentration of Cyste. Ascorbic acid did not interfere at 2 fold excess concentration. Lcys showed interference in the determination of Cyste even at equal concentration.

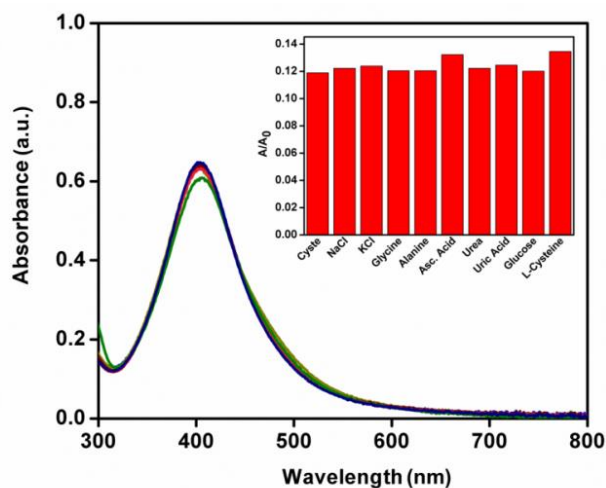


Figure 4.11 Absorption spectra of AgNP-Cyste along with different species; Inset: Bar diagram representing the change in (A/A_0) of AgNP- Cyste, produced by each species.

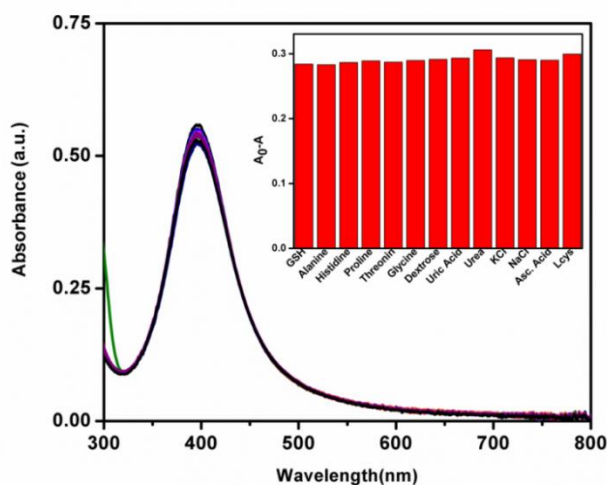


Figure 4.12 Absorption spectra of AgNPs in presence of GSH and different coexisting species; inset: Bar diagram representing the change in $(A_0 - A)$ produced by each species.

Under the optimized experimental conditions, the effects of some foreign species on the determination of GSH at the 7.0×10^{-6} M level were estimated; 100fold concentration of glycine, alanine, histidine, threonine, proline, glucose, uric acid, 10fold excess of urea and ascorbic acid had almost no influence on the response (A_0-A) of GSH (signal change below 5%) (Figure 4.12). Determination of GSH was interfered by Lcys even at equal concentration. These results indicate the better selectivity of the sensor towards Cyste and GSH.

4.3.4.4. Analytical application - Determination of Cyste and GSH in artificial blood serum

In order to evaluate the validity of proposed sensor, it was used to determine Cyste in artificial blood serum. Absorbance of the mixtures of AgNP-Tyr, Cyste in artificial blood serum and PBS (0.01 M, pH 7.4) was recorded and absorption ratio (A/A_0) was calculated. The recovery percentage between 97% and 103% appraises the validity of the sensor (Table 4.1).

Utility of this sensor towards the determination of GSH in artificial blood serum was also evaluated. AgNP solution, GSH in artificial blood serum, 0.01 M PBS (pH 7.4) was mixed. Absorbance of the solution was recorded and absorption difference (A_0-A) was calculated. The recovery percentage was found to be between 98% and 102% (Table 4.1).

Table 4.1 Determination of Cyste and GSH in artificial blood serum

| Analyte | Added (M) | Found (M) | Recovery(%) | RSD ^a |
|---------|---|---|-------------|------------------|
| Cyste | 1.0×10^{-6} - 5.0×10^{-8} | 1.0×10^{-6} - 4.9×10^{-8} | 100 | 3.5 |
| GSH | 1.0×10^{-5} - 5.0×10^{-7} | 1.1×10^{-5} - 4.9×10^{-7} | 100 | 1.3 |

The results are in good agreement with those obtained from Ellman's colorimetric method.²⁵⁷ (Table 4.2).

Table 4.2 Determination of Cyste and GSH in artificial blood serum using reference method

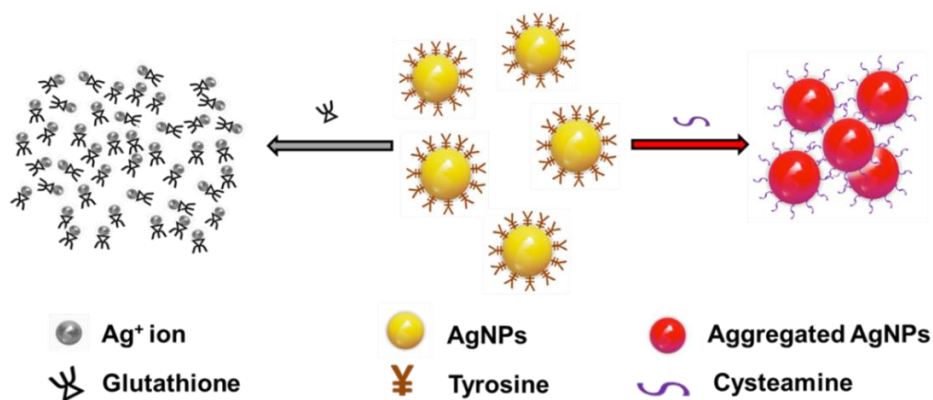
| Analyte | Added (M) | Found (M) | Recovery(%) | RSD ^a |
|---------|---|---|-------------|------------------|
| Cyste | 6.0×10^{-5} - 2.0×10^{-6} | 6.0×10^{-5} - 2.2×10^{-6} | 101 | 2.1 |
| GSH | 8.0×10^{-5} - 5.0×10^{-6} | 7.9×10^{-5} - 5.1×10^{-6} | 101 | 3.2 |

^a Five replicates

4.4 Conclusions

In summary, this work describes simple and cost effective assay based on the colour change of AgNPs. The proposed method may be used for the determination of trace amounts of Cyste and GSH. The colorimetric assay is based on the distance dependent optical characteristics of AgNPs, chemisorption of Cyste on AgNPs and interactions of AgNPs with GSH. Presence of Cyste, rapidly induce aggregation of AgNPs. However GSH

induces dissolution of AgNPs which resulted in different visual observations. The sensor exhibited good sensitivity with a detection limit of 1.80×10^{-8} M for Cyste and 3.68×10^{-7} M for GSH. Compared with other methods, proposed method is cost effective and can be accomplished without any sophisticated instruments. The developed method is simple and sensitive with potential applications for the determination of Cyste and GSH in biological samples.



Scheme 4.2 Schematic representation of colorimetric sensor for the determination of biothiols- glutathione and cysteamine

.....*SC*.....

Voltammetric sensor for simultaneous determination of antioxidants – tert - butyl hydroquinone and propyl gallate

| | |
|--|-----------------------------------|
| C o n t e n t s | 5.1 <i>Introduction</i> |
| | 5.2 <i>Experimental</i> |
| | 5.3 <i>Results and discussion</i> |
| | 5.4 <i>Conclusions</i> |

This chapter describes the simultaneous determination of two analytes. A sensitive voltammetric sensor for the resolution of tert-butyl hydroquinone (TBHQ) and propyl gallate (PG) at submicromolar levels has been developed. Acetylene black modified gold electrode (AB/GE) has been recognized to be a simple yet highly sensitive sensing platform enabling the individual determination of these antioxidants within a wide range of concentration from 1.0×10^{-4} M to 3.0×10^{-7} M and 1.0×10^{-4} M to 7.0×10^{-8} M with detection limits 2.8×10^{-8} M and 4.3×10^{-8} M for TBHQ and PG respectively. Moreover, highly resolved peaks for the oxidation of TBHQ and PG with a separation of 206 mV have been observed on AB / GE which in turn facilitated their simultaneous determination. The potential of the developed sensor towards the quantification of TBHQ and PG in fats and oils has proved its efficacy as a promising tool for food quality control.

5.1 Introduction

Synthetic phenolic antioxidants are added individually or in combination into oils and fats to prevent oxidative rancidity. Common antioxidants used to retard chemical deterioration of food include propyl gallate (PG), tert-butyl hydroquinone (TBHQ), butylated hydroxyl anisole (BHA), butylated hydroxyl toluene (BHT) etc. It has been observed that these antioxidants when used in mixtures could increase antioxidant activity.³⁰⁹ Binary or ternary mixtures of these antioxidants with a total concentration of 200 ppm have been permitted by food regulatory bodies of different countries.³¹⁰ Chronic exposure to these antioxidants even at permissive levels, may impart numerous health hazards to humans.^{100,311}

Till date different methods have been reported for individual as well as simultaneous determination of antioxidants in food, pharmaceuticals, fuels etc. They include most widely used techniques such as chromatography,³¹² spectrophotometry,³¹³ fluorimetry,³¹⁴ photo electrochemical³¹⁵ and electro-analytical techniques.^{99,316} Electro-analytical methods especially voltammetry, by virtue of its characteristic properties such as possibility for miniaturization, simple and rapid detection process and cost effective operation procedure has been widely used for sensor applications. Owing to chemical similarity, it is difficult to determine different antioxidants at lower concentrations without prior separation.³¹⁷ Voltammetry being an outstanding technique could be used for simultaneous determination of chemically similar compounds in a mixture even at trace level. Several sensors have been already reported for individual as well as simultaneous determination of TBHQ and/or PG along with other antioxidants.^{256,318-320} However methods for simultaneous determination of

TBHQ and PG with wide linear range and nanomolar detection limits are rare.³²¹

Acetylene black (AB), a particular type of carbon black, is a highly porous material with very good electrical conductivity, high electro-catalytic activity and electrical stability.^{322,323} It has been attracting the attention of electrochemists as an electrode modifier, owing to its fascinating properties.

Continuing the efforts to develop sensors for natural as well as synthetic antioxidants,^{99,100,316,324-326} an attempt is being made to develop a highly sensitive sensor for simultaneous determination of TBHQ and PG over wide range of concentrations. It further aims at the determination of TBHQ and PG in fats and oils.

5.2 Experimental

Fabrication of AB modified gold electrode (AB/GE) was done as per the procedure described in chapter 2, section 2.3.4.

5.2.1 Analytical procedure

An appropriate amount of the stock solution of TBHQ/PG (1.0×10^{-3} M) in methanol was transferred to electrochemical cell and made up to 1.0×10^{-2} L with supporting electrolyte. Cyclic voltammograms and square wave voltammograms were recorded from 0 V to 0.8 V, at 0.1 Vs^{-1} , using three electrodes setup. All measurements were carried out at room temperature ($\sim 25 \text{ }^\circ\text{C}$).

5.3 Results and Discussion

5.3.1 Electro-catalytic action of AB on the electrochemical behaviour of TBHQ and PG

Electrochemical behaviour of equimolar mixture of TBHQ and PG (1.0×10^{-6} M each) was studied at bare and AB modified GE electrodes using SWV in PBS (pH 2) at a scan rate of 0.1 Vs^{-1} . At AB/GE well separated anodic peaks were obtained at 0.29 V and 0.50 V corresponding to the electro-oxidation of TBHQ and PG. Whereas it was found to be difficult to detect any response for these antioxidants (1.0×10^{-6} M each) using bare electrode. By increasing the concentration of the solution (1.0×10^{-4} M each) peaks at 0.44 V and 0.56 V corresponding to TBHQ and PG were obtained at bare GE.

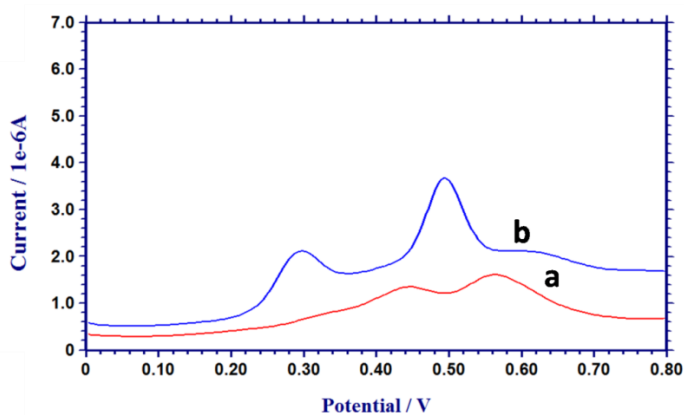


Figure 5.1 SWV of TBHQ and PG (1.0×10^{-6} M each) at bare GE and AB/GE

It may be noted that, while using the bare electrode, separation between the peaks is around 0.09 V, which points to the inaptness of bare GE for simultaneous determination of TBHQ and PG. Comparison of SWV

of TBHQ and PG (1.0×10^{-6} M each) at bare GE and AB/GE are given in Figure 5.1. Appreciable enhancement in peak current for oxidation of the antioxidants on AB modified GE indicates electro-catalytic action of AB towards electro-oxidation. Large surface area, more active sites, higher conductivity and topological effects of AB may be the reason for enhanced sensitivity of the modified electrode, AB/GE.

5.3.2 Performance Characteristics of the Developed Sensor

5.3.2.1 Choice of the supporting electrolyte

Choice of suitable supporting electrolyte is important as it can influence mass transfer, thermodynamics and kinetics of electrochemical processes.³²⁶ In order to choose most suitable supporting electrolyte for voltammetric determination of antioxidant TBHQ/PG, its electrochemical behaviour was compared in various supporting electrolytes of 0.1 M concentration. Among the different electrolytes studied (phosphate buffer solution (PBS), citrate buffer solution, acetate buffer solution, hydrochloric acid, nitric acid and sodium hydroxide), oxidation of antioxidants in PBS gave well defined voltammetric peaks with relatively high sensitivity. Thus, PBS was chosen as the suitable medium for TBHQ/PG determination.

5.3.2.2 Effect of pH

From Figure 5.2, it is clear that E (V) shows a linear relation with pH ($R^2=0.99$) with a slope of -0.061 and -0.069 for TBHQ and PG respectively. The obtained slope is in agreement with the theoretical value (-0.059 V/pH), indicating the involvement of equal number of electrons and

protons in the oxidation of TBHQ as well as PG.³²⁸ Moreover, a gradual decrease in peak current was also observed with increasing pH from 2 to 8. Maximum current for the oxidation of above mentioned antioxidants was obtained in PBS, pH 2.

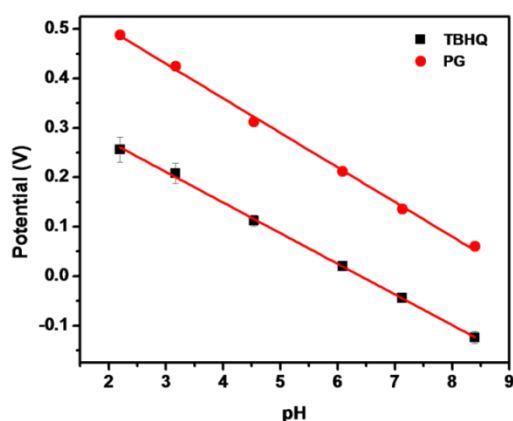


Figure 5.2 Variation of overpotential for the electro-oxidation of TBHQ and PG with pH

When the voltammetric behavior of TBHQ and PG was studied in a mixture at different pH, it is found that the peak separation is greatly influenced by pH of the supporting electrolyte (Figure 5.3). At pH 7 (0.1 M PBS), the peak potential for the oxidation of TBHQ and PG were obtained at -0.04 V and 0.11 V with a separation of 0.15 V. When pH of the supporting electrolyte was changed to 2, it was observed that the separation between anodic peaks increases to 0.206 V with over potentials at 0.29 V and 0.50 V for TBHQ and PG respectively. This again confirms the suitability of 0.1 M PBS with pH 2 as supporting electrolyte for the simultaneous determination of TBHQ and PG.

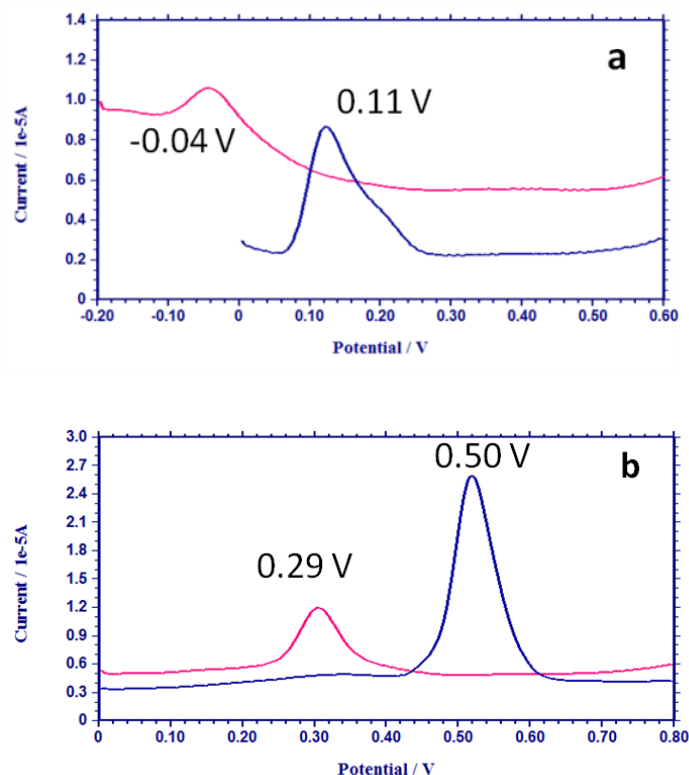


Figure 5.3 Responses of TBHQ and PG in 0.1 M PBS of (a) pH 7 and (b) pH 2

5.3.2.3 Effect of AB- Nafion film thickness and characterization of AB/GE

Thickness of the film is directly proportional to the volume of AB-Nafion suspension (1.25 g L^{-1}) drop casted on the bare GE. It is seen that, peak current for PG increased with increasing the volume of modifier suspension from $1.0 \times 10^{-6} \text{ L}$ to $3.0 \times 10^{-6} \text{ L}$. But peak current was found to decrease with further increase in the volume of modifier.

5.3.2.3.1 SEM Images

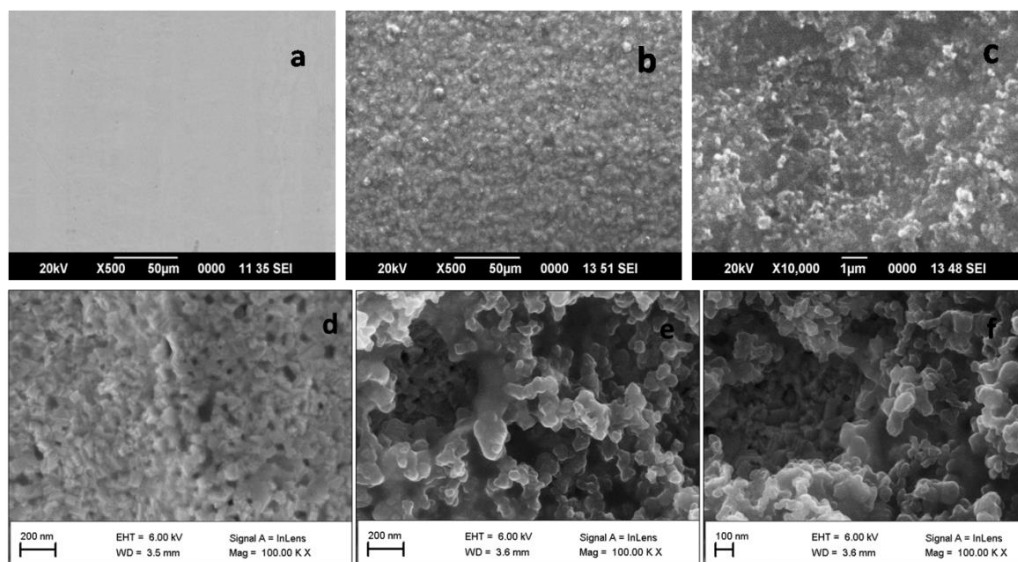


Figure 5.4 SEM images of (a) bare GE (b) AB/GE and (c) AB/GE (zoomed image), FESEM images of (d) bare GE (e) AB/GE and (f) AB/GE (zoomed image)

Figure 5.4 depicts the surface morphology of AB-Nafion film drop casted on GE surface. AB nanoparticles on GE surface show uniform dispersal. Compared to bare GE, surface of AB/GE has become rough which indicates the successful modification of GE surface.

5.3.2.3.2 Surface Area of AB/GE

Electroactive surface area of bare GE and AB/GE with different film thickness was calculated using Randles - Sevcik equation. In order to measure microscopic surface areas of AB modified as well as bare GE, 2.0×10^{-3} M $K_3[Fe(CN)_6]$ was taken as probe. Cyclic voltammograms were recorded at different scan rates (Figure 5.5).

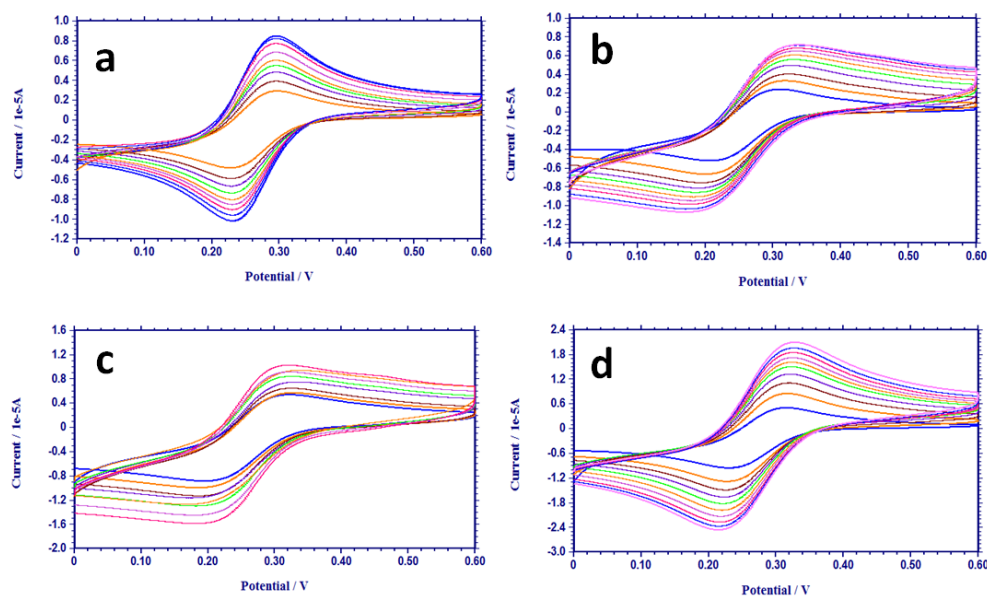


Figure 5.5 Cyclic voltammetric response of 2.0×10^{-3} M $K_3[Fe(CN)_6]$ at different scan rates at gold electrode modified with various amounts of 1.25 gL^{-1} suspension of AB-Nafion; (a) bare GE (b) $1 \mu\text{L}$ (c) $2 \mu\text{L}$ and (d) $3 \mu\text{L}$ of suspension

For a reversible system, the relationship between the current and scan rate is given by the Randles - Sevcik equation.⁵

$$I = 2.69 \times 10^5 A n^{3/2} D^{1/2} C v^{1/2}$$

Where A refers to the geometric surface area of the electrode, I is peak current, D is diffusion coefficient, n is number of electrons transferred, C is concentration of $K_3[Fe(CN)_6]$ and v refers to scan rate. Here, $n=1$, $D=7.6 \times 10^{-6} \text{ cm}^2 \text{ s}^{-1}$. The plot of I vs. $v^{1/2}$ follows linear relationship. From slope of the plot, effective surface areas of bare GE and AB modified GEs were calculated.

Surface area studies reveal that, electro-active area of the electrode increases from 0.0135 cm², 0.0169 cm², 0.0271 cm² to 0.0473 cm² for bare GE and AB/GE electrodes modified with 1.0×10⁻⁶ L, 2.0×10⁻⁶ L and 3.0×10⁻⁶ L of AB-Nafion suspension. Appreciable change in surface area was not obtained on further increase in thickness of the film. A 3.5fold increase in surface area compared to bare GE was observed on modifying GE with 3.0×10⁻⁶ L of AB-Nafion suspension. This increase in surface area may cause enhancement in the response of electro active species.

5.3.2.3.3 *Electrochemical impedance measurements*

Impedance measurements of different electrodes were carried out in 5 mM [Fe(CN)₆]^{3-/4-} mixture in 0.1 M KCl and impedance spectra are given in Figure 5.6. In order to obtain different impedance parameters, each spectrum was fitted with an equivalent circuit ($\chi^2 < 1 \times 10^{-3}$). R_{CT} values represent the resistance offered by the electrode surface towards electrochemical reaction. R_{CT} values corresponding to different electrodes obtained by curve fitting are given in Figure 4. On comparison, it is clear that the bare electrode has highest R_{CT} value. As the quantity of modifier increases (volume of AB-Nafion suspension increases from 1.0×10⁻⁶ L to 3.0×10⁻⁶ L), R_{CT} value decreases to a minimum value. This could be attributed to the increased catalytic activity of the AB on the modified electrode. Further increase in volume of modifier increases the thickness of AB film, which may offer more impedance to the electrochemical process rather than channelizing the flow of electrons.³²⁹

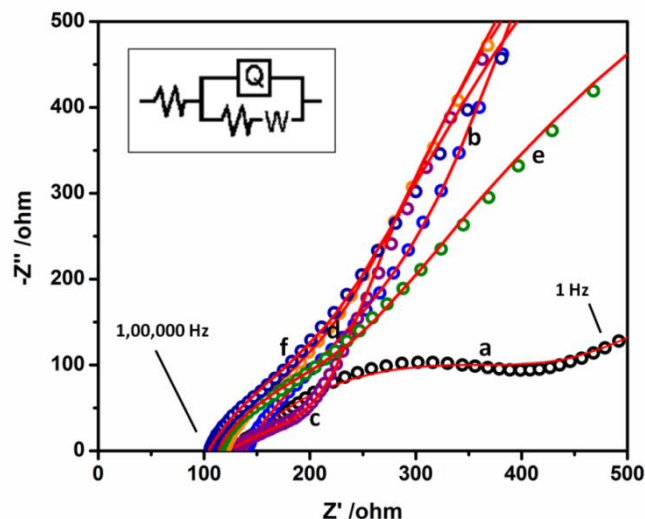


Figure 5.6 Electrochemical impedance spectrum of (a) bare GE and GE modified with (b) 1 μ L (c) 2 μ L (d) 3 μ L (e) 4 μ L and (f) 5 μ L of AB suspension, inset: equivalent circuit.

EIS measurements were repeated in PBS (pH 2) containing 5.0×10^{-5} M PG with bare GE and GE modified with 1.0×10^{-6} L to 5.0×10^{-6} L of AB suspension. Obtained results were fitted with a Faradaic Randles equivalent circuit $R_s(Q_1(R_{CT}W))$, ($\chi^2 < 1 \times 10^{-3}$) (Table I). Similar to the usual notations, bulk properties of solution is represented by R_s . Charge transfer resistance, R_{CT} and constant phase element, Q_1 define the conducting and dielectric properties of electrolyte and electrode. A decrease in R_{CT} value from $4.32 \times 10^5 \Omega$ to $1.35 \times 10^4 \Omega$ obtained on modification of the bare GE with 3.0×10^{-6} L of AB suspension. This implies the enhanced conductivity offered by the modifier towards the electrode surface. Appreciable change was not observed in Q_1 for bare and modified electrode. However a noticeable decrease in the Warburg impedance, resistance offered to

diffusion, was observed which can enhance the electrochemical process with diffusion controlled mechanism at AB/GE compared to bare GE.

Table 5.1 Fitted impedance values for AB modified electrodes with different thickness (experiments were carried out in 0.1 M PBS (pH 2) containing 5.0×10^{-5} M PG)

| Volume of AB suspension | R_s (Ω) | Q | R_{CT} (Ω) | W (Ω) |
|-------------------------|--------------------|-----------------------|-----------------------|------------------------|
| Bare GE | 248.8 | 1.22×10^{-6} | 4.32×10^5 | 2.37×10^4 |
| 1×10^{-6} L | 251 | 4.23×10^{-6} | 2.58×10^5 | 1.56×10^{-4} |
| 2×10^{-6} L | 250.2 | 9.40×10^{-6} | 9.04×10^4 | 2.05×10^{-9} |
| 3×10^{-6} L | 243.2 | 1.28×10^{-5} | 1.35×10^4 | 3.59×10^{-12} |
| 4×10^{-6} L | 263.5 | 1.88×10^{-5} | 2.32×10^4 | 2.94×10^{-11} |
| 5×10^{-6} L | 251.7 | 2.12×10^{-6} | 2.93×10^4 | 1.82×10^{-8} |

5.3.3 Mechanistic and kinetic aspects of electro-oxidation

5.3.3.1 Variation of peak current with scan rate

Influence of scan rate on peak current of TBHQ has been examined using linear sweep voltammetry (LSV). In the studied range (0.02 Vs^{-1} to 0.1 Vs^{-1}), peak current of TBHQ increased with increase in scan rate (Figure 5.7a). A plot of peak current versus square root of scan rate exhibited linear relationship suggesting diffusion controlled process. A plot between $\log I$ and $\log v$ followed linearity with a linear regression equation, $\log I = 0.52$

$\log v$ -12.66; $R^2 = 0.983$. Slope of the plot (0.52) confirms the diffusion controlled process at AB/GE.²⁷³

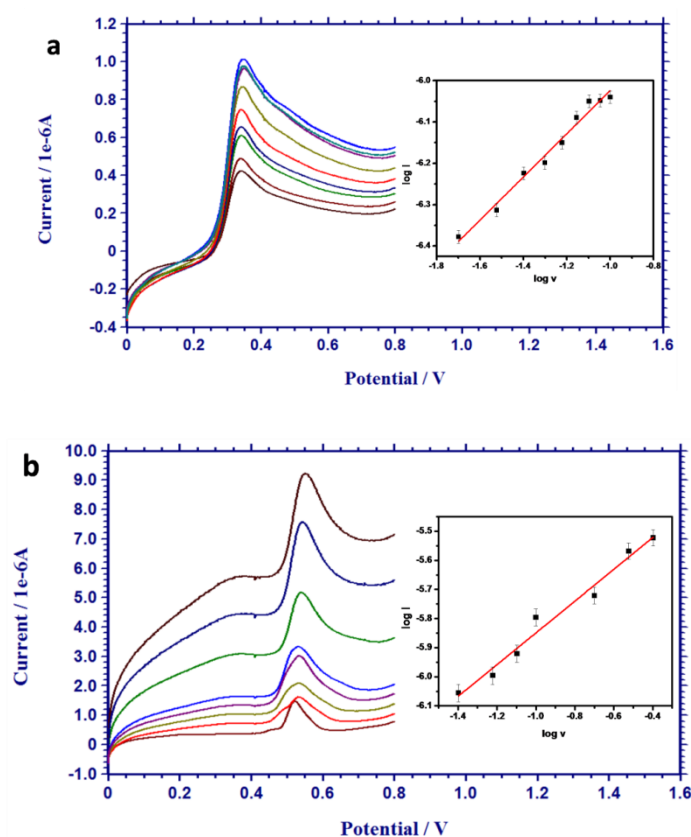


Figure 5.7 LSV response of (a) 1.0×10^{-5} M TBHQ with varying scan rates from 0.02 Vs^{-1} to 0.1 Vs^{-1} , inset : a plot of $\log I$ vs. $\log v$ (b) 1.0×10^{-5} M PG with varying scan rates from 0.04 Vs^{-1} to 0.4 Vs^{-1} , inset : a plot of $\log I$ vs. $\log v$

Similarly anodic peak current for PG was also found to behave linearly with varying scan rate (0.04 Vs^{-1} to 0.4 Vs^{-1}) (Figure 5.7 b). Linearity of the plot I vs. $v^{1/2}$ suggests diffusion controlled process. Moreover, $\log I$ vary linearly with $\log v$, in accordance with the linear

regression equation $\log I = 0.54 \log v - 12.21$; $R^2 = 0.980$. The slope of latter plot (0.54) confirms diffusion controlled process.

5.3.3.2 Calculation of diffusion coefficient from chronoamperometric studies

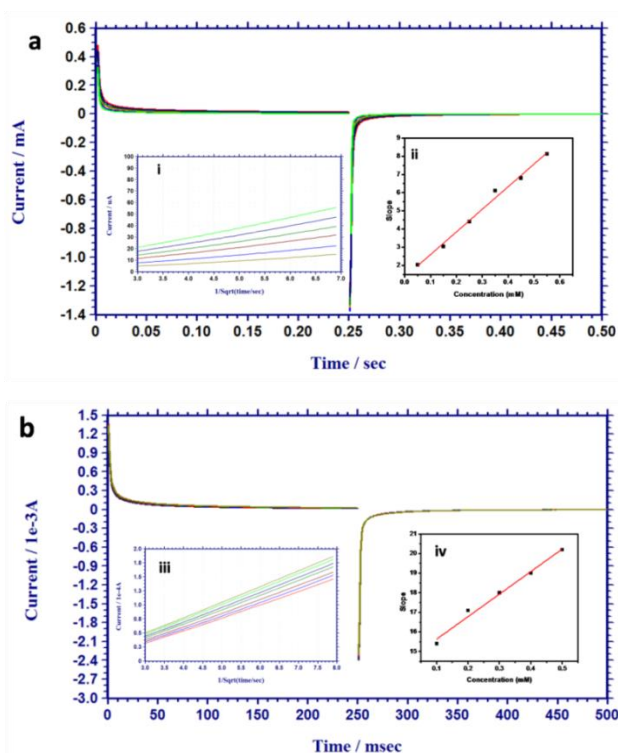


Figure 5.8 Overlay of chronoamperograms for various concentrations of (a) TBHQ and (b) PG, inset (i) plot of current for TBHQ vs. $t^{1/2}$ (ii) plot of slope of (I vs. $t^{1/2}$) vs. concentration of TBHQ (iii) plot of current for PG vs. $t^{1/2}$ (iv) plot of slope of (I vs. $t^{1/2}$) vs. concentration of PG

Chronoamperometric measurements were conducted for TBHQ as well as PG and the chronoamperograms are given in Figure 5.8 a and Figure

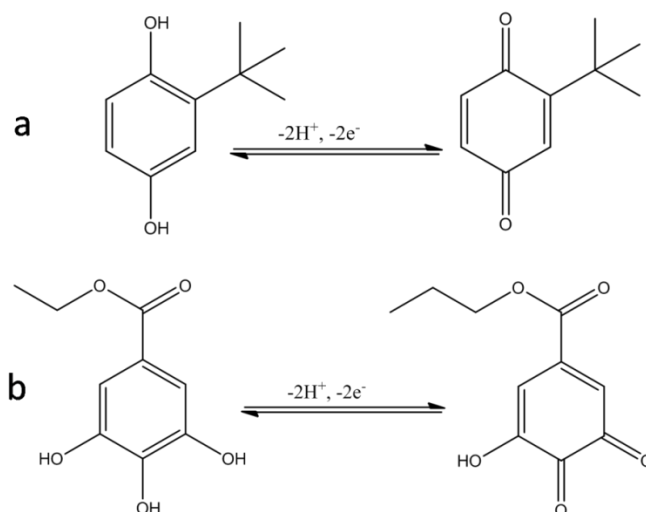
5.8 b. Cottrellian decay of transient current for the oxidation of TBHQ and PG at different concentrations was observed. The slopes of the experimental plots of current vs. $t^{1/2}$ were plotted against their concentration. Slope obtained for the resultant plot was used to calculate D, diffusion coefficient using Cottrell equation,

$$I = nFAD^{1/2}C\pi^{-1/2}t^{-1/2}$$

Diffusion coefficient obtained for TBHQ and PG are 5.94×10^{-6} and $9.36 \times 10^{-6} \text{ cm}^2 \text{ s}^{-1}$. Obtained results are comparable with the reported ones.³¹⁶

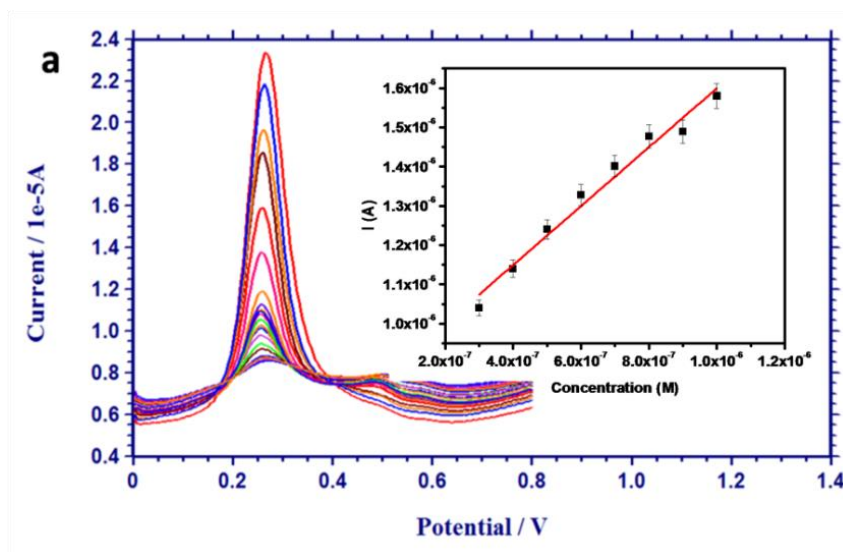
5.3.3.3 Calculation of number of electrons and protons

From Figure 5.7, it is clear that the overpotential for oxidation of TBHQ as well as PG shows very little shift towards higher value on increasing the scan rate. This gives a clear indication of reversibility of oxidation of the antioxidants.¹⁰⁰ Cyclic voltammograms of TBHQ and PG were obtained at AB/GE at a scan rate of 0.1 Vs^{-1} . TBHQ gave reversible peaks at 0.336 V and 0.297 V. Whereas, PG gave redox peaks at 0.545 V and 0.520 V. Total number of electrons (n) involved in the reaction is calculated using the equation, $\Delta E = \frac{0.059}{n}$, where ΔE denotes the difference in potentials for oxidation and reduction.³³⁰ It was obtained that, two electrons are involved in the oxidation of both TBHQ and PG. Since it was already concluded that, equal number of protons and electrons are involved in the reaction, the number of protons involved in the electro-oxidation will also be two. Hence it may be concluded that, TBHQ by a two electron oxidation forms a quinone and PG forms a diketone derivative as shown in Scheme 5.1.



Scheme 5.1 Mechanism of electro-oxidation of (a) TBHQ and (b) PG

5.3.4 Square wave voltammetric responses of TBHQ and PG



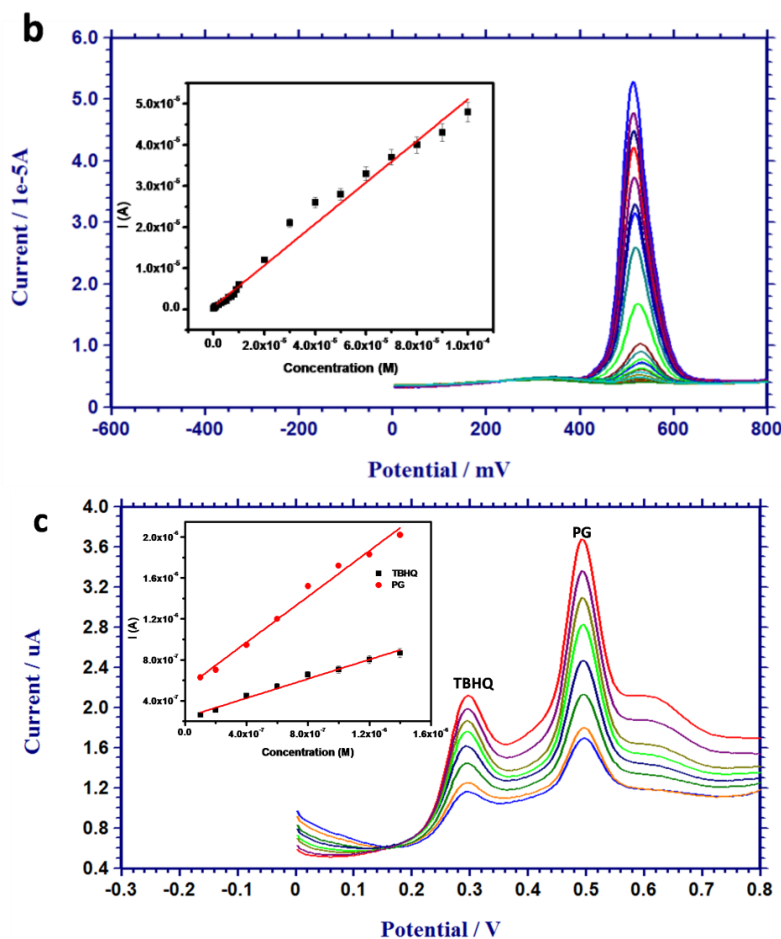


Figure 5.9 SWV response of (a) various concentrations of TBHQ in the range 1.0×10^{-4} M to 3.0×10^{-7} M, inset: plot of anodic peak current vs. concentration (1.0×10^{-6} M to 3.0×10^{-7} M) (b) various concentrations of PG in the range 1.0×10^{-4} M to 7.0×10^{-8} M, inset: plot of anodic peak current vs. concentration (1.0×10^{-4} M to 7.0×10^{-8} M) (c) simultaneous oxidation of TBHQ and PG in an equimolar mixture with concentration of each antioxidant ranging from 1.4×10^{-6} M to 1.0×10^{-7} M, inset: Plot of anodic peak current for simultaneous oxidation of TBHQ and PG vs. concentration (1.4×10^{-6} M to 1.0×10^{-7} M)

At AB/GE, SWV responses of different TBHQ as well as PG concentrations were analyzed under optimized conditions. Figure 5.9 a and Figure 5.9 b represent square wave voltammograms of TBHQ and PG at different concentrations, on AB/GE. It was observed that the anodic peak current for TBHQ and PG varies linearly within a wide range of concentration from 1.0×10^{-4} M to 3.0×10^{-7} M and 1.0×10^{-4} M to 7.0×10^{-8} M respectively. Linear regression equations corresponding to calibration plots are

$$\text{TBHQ: } I (\text{A}) = 0.75 C (\text{M}) + 8.40 \times 10^{-7}; R^2 = 0.986$$

$$I (\text{A}) = 0.16 C (\text{M}) + 1.70 \times 10^{-6}; R^2 = 0.982$$

$$\text{PG: } I (\text{A}) = 0.50 C (\text{M}) + 6.11 \times 10^{-7}; R^2 = 0.986$$

From slope of the graph (m) and standard deviation (s), limit of detection ($3s/m$) was calculated. Limit of detection obtained for TBHQ and PG are 2.80×10^{-8} M and 4.31×10^{-8} M respectively.

Simultaneous oxidation of TBHQ and PG at AB/GE was monitored in the range 1.0×10^{-5} M to 1.0×10^{-7} M (Figure 5.9 c). In an equimolar solution of antioxidants, the peak current varies linearly from 1.4×10^{-6} M to 1.0×10^{-7} M (Figure 5.9 c) following the linear regression equations,

$$\text{TBHQ: } I (\text{A}) = 0.47 C (\text{M}) + 2.31 \times 10^{-7}; R^2 = 0.986$$

$$\text{PG: } I (\text{A}) = 1.12 C (\text{M}) + 5.12 \times 10^{-7}; R^2 = 0.986$$

LODs ($3s/m$) were calculated to be 1.92×10^{-8} M and 2.72×10^{-8} M.

5.3.4.1 Comparison of developed method with reported methods

Table 5.2 Comparison of detection limit and linear range of TBHQ

| Sl. No | Technique | Linear range (M) | LOD (M) | Reference |
|--------|----------------------|--|--|-------------------------------------|
| 1 | DPV | 0.4×10^{-4} - 2.6×10^{-4} | 7.4×10^{-6} | Fuente et al. 1999 ³²⁸ |
| 2 | LSV | 6.2×10^{-4} - 9.1×10^{-5} | 8.6×10^{-7} | Marketa et al. 2014 ³³¹ |
| 3 | FDV | 9.0×10^{-6} - 6.0×10^{-7} | 4.7×10^{-7} | Lin et al. 2013 ²⁵⁶ |
| 4 | DPV | 1.0×10^{-3} - 1.0×10^{-6} | 2.6×10^{-7} | Monteiro et al. 2016 ³¹⁵ |
| 5 | Voltammetry | 1.1×10^{-3} - 1.0×10^{-6} | 6.7×10^{-8} | Wang et al. 2014 ³³² |
| 6 | SWV | 1.0×10^{-5} - 1.0×10^{-6} | 3.4×10^{-8} | Araujo et al. 2011 ³³³ |
| 7 | SWV | 1.0×10^{-4} - 4.0×10^{-6} | 3.2×10^{-8} | Thomas et al. 2015 ¹⁰⁰ |
| 8 | Proposed work | 1.0×10^{-4} - 2.0×10^{-7} | 3.5×10^{-8} | - |

Table 5.3 Comparison of detection limit and linear range of PG

| Sl. No | Technique | Linear range (M) | LOD (M) | Reference |
|--------|----------------------|--|--|------------------------------------|
| 1 | DPV | 1.6×10^{-6} - 1.0×10^{-6} | 9.9×10^{-7} | Diaz et al. 1998 ³¹⁸ |
| 2 | DPV | 1.0×10^{-4} - 1.0×10^{-5} | 6.3×10^{-7} | Vikraman et al. 2012 ⁹⁹ |
| 3 | DPV | 1.0×10^{-5} - 1.0×10^{-6} | 4.0×10^{-7} | Augi et al. 1996 ³³⁴ |
| 4 | DPV | 1.0×10^{-4} - 9.0×10^{-6} | 1.9×10^{-7} | Cyriac et al. 2016 ³¹⁶ |
| 5 | CV | 1.0×10^{-4} - 5.0×10^{-8} | 2.4×10^{-8} | Dai et al. 2016 ³³⁵ |
| 6 | Proposed Work | 1.0×10^{-4} - 7.0×10^{-8} | 4.3×10^{-8} | - |

A large number of electrochemical methods suitable for antioxidant assessment are reported. Of these, none focuses on the simultaneous determination of TBHQ and PG at very low concentrations. To demonstrate the performance of the present work with voltammetric methods reported earlier, a comparison of linear working range and lowest limit of detection of different methods are done and are listed in Table 5.3 and Table 5.4. For the determination of the synthetic phenolic antioxidants-TBHQ and PG, developed method provides widest linear range with lowest detection limit than any other reported works. Moreover, the developed method is fast, cost-effective and easy to handle.

5.3.5 Selectivity and Interference

To assess the selectivity of sensor towards the determination of each antioxidant, SWV response of different concentrations of TBHQ and PG was monitored individually, in presence of a fixed concentration of the other. Overlay of SWV of oxidation of TBHQ in presence of 1.0×10^{-6} M PG is given in Figure 5.10 a. In presence of PG, change in SWV response of TBHQ was studied within a range of concentration from 1.0×10^{-4} M to 5.0×10^{-8} M. It is found that the anodic peak current varied linearly with the concentration of TBHQ from 1.0×10^{-4} M to 4.0×10^{-7} M. A plot between the anodic peak current and concentration of TBHQ in presence of PG is given in Figure 5.10 a, which follows a linear regression equation, $I \text{ (A)} = 0.31 \text{ C (M)} + 2.13 \times 10^{-6}$; $R^2 = 0.994$. LOD ($= 3s/m$) was calculated to be 1.47×10^{-8} M.

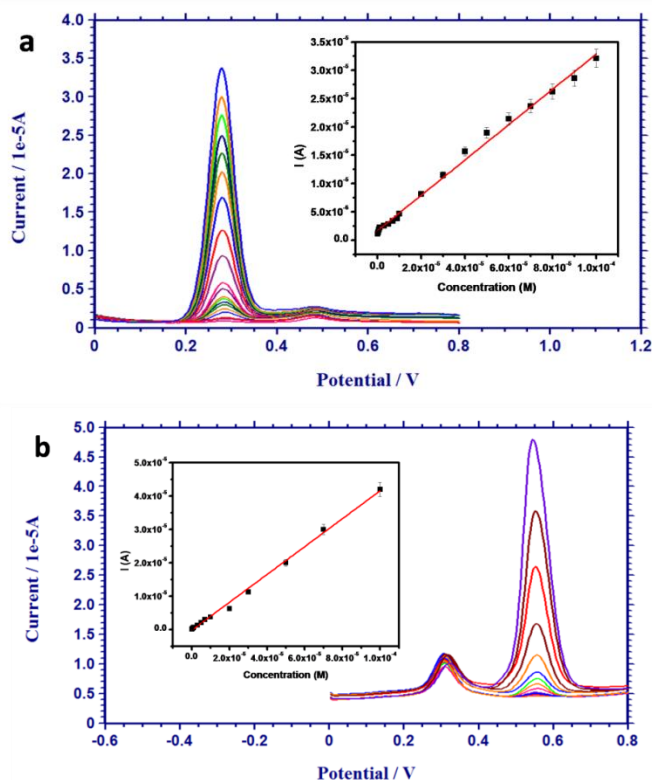


Figure 5.10 Overlay of SWV of (a) TBHQ in the range 1.0×10^{-4} M to 4.0×10^{-7} M in presence of 1.0×10^{-6} M PG, inset: plot of anodic peak current vs. concentration of TBHQ (b) PG in the range 1.0×10^{-4} M to 1.0×10^{-7} M in presence of 5.0×10^{-5} M TBHQ, inset: plot of anodic peak current vs. concentration of PG

Similarly, in presence of 5.0×10^{-5} M TBHQ, SWV responses for PG was obtained from 1.0×10^{-4} M to 5.0×10^{-8} M and the results are given in Figure 5.10 b. It is observed that, the anodic peak current varies linearly with concentration of PG, in the range 1.0×10^{-4} M to 1.0×10^{-7} M (Figure 5.10 b). The linear regression equation for the graph is I (A) = $0.42 C$ (M) - 2.14×10^{-7} ; $R^2 = 0.996$. LOD was calculated to be 5.14×10^{-8} M.

To determine the influence of other foreign species on the determination of TBHQ/PG, some common coexisting substances in food as well as antioxidants such as Na_2SO_3 , ascorbic acid, BHA and BHT were added with TBHQ/PG and changes were studied (Table 5.4). Studies reveal that citric acid, acetic acid, NaCl and KCl did not interfere with the determinations even at 100fold higher concentration than TBHQ/PG. 10fold excess concentration of Na_2SO_3 did not interfere with the determination of TBHQ but interferes at higher concentrations. However, Na_2SO_3 did not offer any interference with the determinations of PG even at 100fold excess concentrations. A common interfering substance, ascorbic acid did not show interference towards the determination of PG at 10fold excess concentration of PG but it interfere the determination of TBHQ even at equimolar concentrations. Other antioxidants such as BHA and BHT severely interfere with the determination of TBHQ as well as PG even at 1:1 concentrations.

Table 5.4 Effect of various foreign species on the determination of 5.0×10^{-5} M TBHQ and 5.0×10^{-5} M PG

| Coexisting species | Molar Ratio | % signal change | |
|---------------------------|-------------|-----------------|------|
| | | TBHQ | PG |
| NaCl | 1:100 | 1.3 | 2.2 |
| KCl | 1:100 | 2.6 | 1.4 |
| Acetic Acid | 1:100 | 1.9 | 2.8 |
| Citric Acid | 1:100 | 1.3 | 1.9 |
| Sodium sulphite | 1:10 | 3.8 | 4.6 |
| Ascorbic acid | 1:1 | 15.2 | 2.7 |
| Butylated hydroxy anisole | 1:1 | 59.0 | 90.2 |
| Butylated hydroxy toluene | 1:1 | 60.2 | 76.1 |

5.3.6 Analytical Application

Under optimum conditions, the developed sensor was employed for the determination of TBHQ and PG in coconut oil and butter samples (with the extraction procedure as given in chapter 2, section 2.7.4). The obtained results are compared with that of standard spectrophotometric method for PG²⁵⁹ and HPLC-UV method for TBHQ.²⁵⁶ In a range of 5.0×10^{-5} M to 5.0×10^{-6} M of TBHQ in coconut oil, recovery percentage ranging from 97% to 101% was obtained from HPLC- UV method (Table 5.5).

Table 5.5 Application of the developed method for the determination of TBHQ in coconut oil and butter samples and comparison with HPLC-UV

| <i>Developed method</i> | | | | |
|------------------------------|---|---|------------------|------------------------|
| | Added (M) | Found (M) | Recovery% | RSD^a |
| Coconut oil | 1.1×10^{-5} - 7.0×10^{-7} | 9.9×10^{-6} - 6.9×10^{-7} | 102 | 3.1 |
| Butter | 1.0×10^{-5} - 8.0×10^{-7} | 9.8×10^{-6} - 7.8×10^{-7} | 100 | 2.4 |
| <i>HPLC-UV²⁵⁶</i> | | | | |
| Coconut oil | 5.0×10^{-5} - 5.0×10^{-6} | 5.0×10^{-5} - 4.9×10^{-6} | 99 | 1.9 |

^a Five replicates

For 9.0×10^{-5} M to 2.0×10^{-5} M PG in coconut oil, a recovery percentage in between 100% and 102% was obtained from spectrophotometric method. The results obtained from the standard methods

are in good agreement with the developed method (Table 5.6) which establishes the utility of present method.

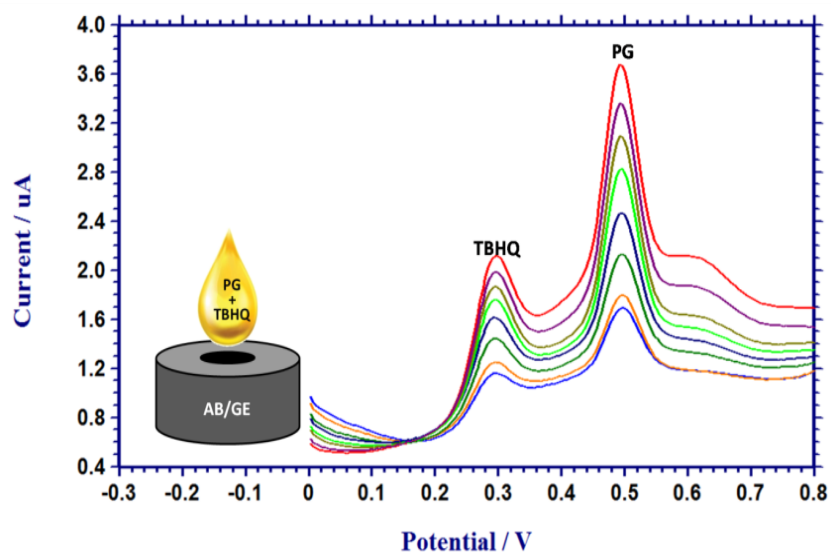
Table 5.6 Application of the developed method for the determination of PG in coconut oil and butter samples and comparison with spectrophotometric method

| <i>Developed method</i> | | | | |
|---|---|---|------------------|------------------------|
| | Added (M) | Found (M) | Recovery% | RSD^a |
| Coconut oil | 8.0×10^{-5} - 6.0×10^{-7} | 8.4×10^{-5} - 6.1×10^{-7} | 102 | 2.9 |
| Butter | 4.0×10^{-5} - 9.0×10^{-7} | 4.0×10^{-5} - 8.6×10^{-7} | 98 | 2.3 |
| <i>Spectrophotometric method</i> ²⁵⁹ | | | | |
| Coconut oil | 1.0×10^{-4} - 8.0×10^{-6} | 1.0×10^{-4} - 7.9×10^{-6} | 100 | 1.3 |

^a Five replicates

5.4 Conclusions

A sensor for individual as well as simultaneous determination of two synthetic phenolic antioxidants, TBHQ and PG has been developed. Acetylene black modified GE was fabricated and characterized by SEM imaging, surface area studies and EIS measurements. The sensor has been able to determine TBHQ/PG when these are present in a matrix as a mixture or alone. The developed sensor could be used for the determination of TBHQ and/or PG in real and commercial samples. This sensor may be considered as a cost-effective tool in food additive assay.



Scheme 5.2 Voltammetric Sensor for simultaneous determination of antioxidants – tert - butyl hydroquinone and propyl gallate

.....*OR*.....

Chapter 6

Voltammetric sensor for simultaneous determination of tryptamines – serotonin and melatonin

| | |
|--|----------------------------|
| C o n t e n t s | 6.1 Introduction |
| | 6.2 Experimental |
| | 6.3 Results and discussion |
| | 6.4 Conclusions |

This chapter details the development of a sensor for the simultaneous determination of dual analytes. An electrochemical sensor for simultaneous determination of the tryptamines, serotonin (ST) and melatonin (MT) is developed based on immobilizing acetylene black nanoparticles-chitosan (AB-C) on gold electrode. AB-C exhibited remarkable electro-catalytic activity and enabled effective resolution as well as simultaneous determination of ST and MT under optimal conditions. The electro-catalytic response of the sensor was proportional to the tryptamine concentration in the range 1.0×10^{-4} M to 5.0×10^{-7} M and 4.5×10^{-4} M to 2.0×10^{-5} M with limits of detection 1.6×10^{-7} M and 1.9×10^{-6} M for ST and MT respectively. Different kinetic parameters were also determined. The developed sensor was successfully applied for the quantification of ST and MT in biological sample.

6.1 Introduction

Serotonin (ST) or 5-hydroxytryptamine, a member of the catecholamine neurotransmitter family, which is widely distributed in central nervous system plays crucial role in the proper functioning of various processes in human body including endocrine regulation and muscle contraction.³³⁶ Deficiency of ST is associated with several states of psychological imbalance such as depression, anxiety and migraines.³³⁷ High concentration of serotonin leads to toxicity and an associated group of symptoms called serotonin syndrome (SS).³³⁸ Hence detection of serotonin is helpful in the monitoring of certain neurological and psychiatric disorders.

Melatonin (MT) or N-acetyl-5-methoxytryptamine is an essential hormone in human body synthesized from ST and secreted into blood as well as cerebrospinal fluid, mainly at night, by various parts of body mainly the parenchymal cells of pineal gland³³⁹. The best-known effect of melatonin is the regulation of circadian rhythm i.e. to reharmonise disruptions in biological clock,³⁴⁰ for which reason it is widely employed as a non-addictive, sleep-inducing drug.³⁴¹ Besides having an influence on several physiological and behavioral processes, melatonin has also been reported for being an effective antioxidant that delays the aging process due to its ability to scavenge free radicals and also as an immunomodulator in cancer treatment.³⁴² The pharmaceutical importance of melatonin makes it a 'wonder drug' or 'universal cure' among scientists.³⁴³

Various methods are reported for the simultaneous determination of serotonin and melatonin. The most often used is HPLC with different

detection methods.³⁴⁴⁻³⁴⁶ These methods are not observed to offer a cost effective, handy and simple approach for the determination of ST and MT. Whereas, voltammetry, owing to its inherent miniaturization possibilities, simplicity, fast responsiveness, cost effectiveness etc. is an outstanding technique for sensitive determination without any prior separation.^{100,324} Though there are different electrochemical sensors used for individual determination of ST or MT³⁴⁷⁻³⁵² only one voltammetric sensor for the simultaneous determination of ST and MT is known.³⁵³ The reported sensor based on carbon nanotube or graphene includes differential pulse voltammetric determination of ST and MT. Herein a sensor fabricated with acetylene black and biologically derived polymer chitosan is proposed for the simultaneous determination of ST and MT.

Acetylene black (AB) is a non-extensively used nano form of carbon. AB possesses characteristic features such as cost-effectiveness, chemical stability, electrical conductivity, catalytic property etc. The properties compatible with the electrochemical studies helps it to be widely used in electrode modification purpose and fuel cell applications.³⁵⁴⁻³⁵⁶ Chitosan, a cationic polymer prepared by deacetylation of the natural polymer chitin, is a promising functional material with different applications. Chitosan has been known to its properties such as strong adhesion capacity, excellent thin film formation ability, non-toxic nature, bio-compatibility etc.³⁵⁷⁻³⁵⁹ AB in combination with chitosan forms a brilliant modifier of the electrode surface in the development of voltammetric sensors.³⁶⁰

The proposed work illustrates the application of AB-chitosan composite modified gold electrode (AB-C/GE) for the simultaneous voltammetric determination of two well known tryptamines ST and MT. To validate the proposed procedure, the determination of tryptamines in artificial as well as real samples was performed and the obtained results were compared with reported protocols.

6.2 Experimental

Fabrication of AB-C modified gold electrode (AB-C/GE) was carried out as per the procedure detailed in chapter 2, section 2.3.5.

6.2.1 Analytical procedure

An appropriate amount of the stock solution of ST or MT (1.0×10^{-2} M) in methanol was transferred to an electrochemical cell and made up to 10 mL with supporting electrolyte (0.1M PBS, pH 7). Cyclic voltammograms and square wave voltammograms were recorded from 0 V to 0.90 V, at 0.1 Vs^{-1} , using three electrodes setup. All measurements were carried out at room temperature ($\sim 25^\circ \text{C}$).

6.3 Results and discussion

6.3.1 Electro-catalysis by AB-C

The electrochemical oxidation of a mixture of 1.0×10^{-4} M ST and MT in 0.1 M PBS, pH 7 was studied on bare GE as well as AB-C/GE using SWV at a scan rate of 0.1 Vs^{-1} . Figure 1 compares the oxidation responses of 1.0×10^{-4} M ST and MT, at bare GE and AB-C/GE when these tryptamines are present in the system simultaneously. At bare GE, ST and

MT yield irreversible oxidation peak at 0.37 V (8.9×10^{-7} A) and 0.73 V (3.4×10^{-7} A) respectively. Under the same conditions, well defined irreversible oxidation peak appears at 0.31 V (6.3×10^{-6} A) and 0.66 V (3.0×10^{-6} A) at AB-C/GE. Eight fold enhancements in the oxidation peak current at AB-C/GE is observed in comparison to bare GE, when ST and MT are oxidized simultaneously.

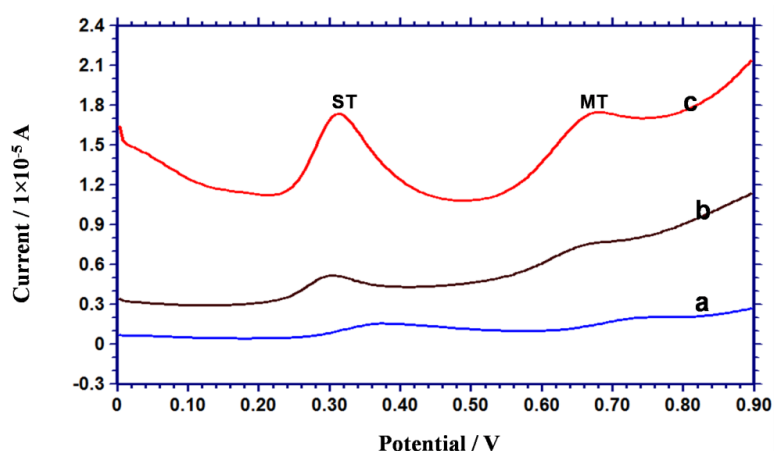


Figure 6.1 SWV of ST and MT (1.0×10^{-4} M each) at (a) bare GE (b) GE modified with 4 μ L of 1 mg/mL AB suspension and (c) GE modified with 4 μ L of 1 mg/mL AB-Chitosan suspension

To explore the synergic effect of acetylene black and chitosan on the electrochemical oxidation of ST and MT, simultaneous oxidation was performed on different electrodes, i.e. bare GE, AB/GE and AB-C/GE. SWV obtained at different electrodes are given in Figure 6.1. At bare GE, oxidation of ST and MT occurs with peak current in the order of 1.0×10^{-7} A. When simultaneous electro-oxidation of ST and MT was carried out on AB/GE, an enhancement in peak current was observed (1.4×10^{-6} A for ST and 7.1×10^{-7} A for MT). Improved electrochemical response with well

separated peaks (0.35 V) having enhanced peak current was obtained at AB-C/GE.

AB/GE enhanced the peak current for the oxidation of tryptamines by twofold compared to bare GE. The enhancement in peak current was found to be more pronounced (8fold) when AB-C composite was used to modify GE. In turn, this indicates the effective catalytic activity offered by AB as well as chitosan towards the electro-oxidation of ST and MT.

6.3.2 Performance characteristics of the sensor

6.3.2.1 Influence of various supporting electrolytes and pH of the medium

Reaction medium might offer pronounced effect on the responses of ST and MT. The oxidation of 1.0×10^{-5} M ST and 1.0×10^{-4} M MT was monitored individually in various electrolytes such as phosphate buffer solution (PBS), acetate buffer solution, citrate buffer solution, KCl, HNO₃ and NaOH. Well defined peaks with highest peak current were obtained in PBS. Therefore 0.1 M PBS was chosen as the experimental medium for voltammetric studies of ST and MT.

Electrochemical responses of 1.0×10^{-5} M ST and 1.0×10^{-4} M MT in PBS of various pH (2 to 8) were evaluated by SWV. Experimental results showed that pH has significant effect on the electro-oxidation of ST as well as MT. Increase in the anodic peak currents were observed with increase in pH. For both tryptamines maximum current was obtained at pH 7 and peak current started diminishing above pH 7. With increasing pH, a shift in over-potential to more negative values was observed. E_p (V) was plotted against

pH, which followed the linear regression equation, $E_p = -0.058 \text{ pH} + 0.71$ and $E_p = -0.038 \text{ pH} + 0.93$ for ST and MT respectively (Figure 6.2).

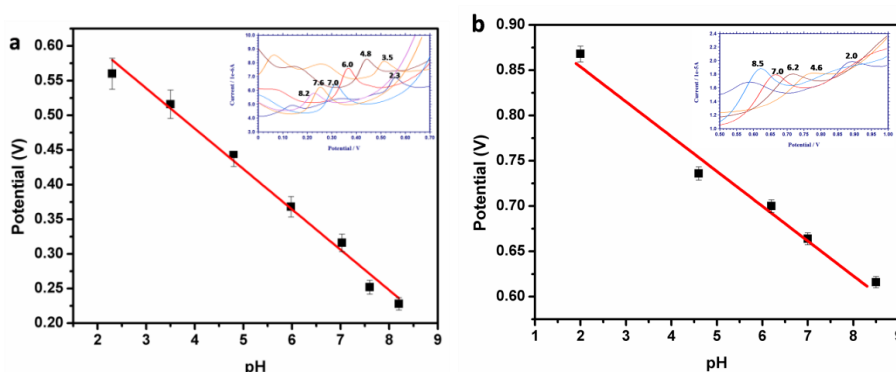


Figure 6.2 Plot of E_p vs pH for (a) 1.0×10^{-5} M ST and (b) 1.0×10^{-4} M MT, inset: voltammograms at various pH.

6.3.2.2 Effect of volume of AB-C suspension drop casted on GE and characterization of optimized AB-C/GE

The amount of modifier on GE directly determines the thickness of the AB-C film. The anodic peak current of ST was found to increase while gradually increasing the volume of AB-C solution (1 mg AB+1 mg chitosan per mL) from 2 μ L to 4 μ L and then decreases with further increase in the volume of the modifier. The enhancement of current may be attributed to the increase in number of catalytic sites per tryptamine moiety with increasing amount of modifier AB-C. The quantity of AB-C on GE reaches an optimum thickness with 4 μ L, but further increase in thickness may inhibit the flow of electrons which could have been a reason for decrease in peak current. The optimized AB-C/GE was characterized with the help of different techniques and the results are given below.

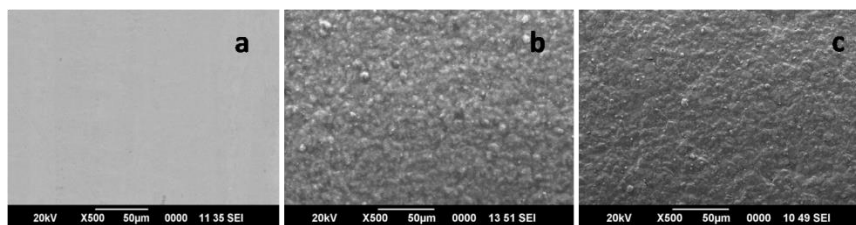


Figure 6.3 SEM images of (a) bare GE (b) GE modified with 4 μL of 1 mg/mL AB suspension and (c) GE modified with 4 μL of 1 mg/mL AB-Chitosan suspension

Figure 6.3 demonstrates the surface characteristics of bare GE, AB/GE and AB-C/GE through **SEM images**. It may be comprehended from these images that the surface of GE becomes rough when it is modified with AB or AB-C composite. It gives a clear indication of the successful modification of bare GE.

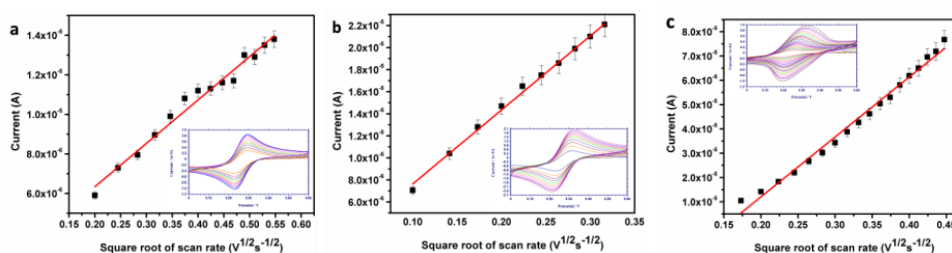


Figure 6.4 Plots of current obtained for 2mM $\text{K}_3[\text{Fe}(\text{CN})_6]$ vs. square root of scan rate at (a) bare GE (b) GE modified with 4 μL of 1mg/mL AB suspension and (c) GE modified with 4 μL of 1mg/mL AB-Chitosan suspension, inset: voltammograms obtained at various potential scan rate.

Electroactive surface area of bare GE, AB/GE and AB-C/GE was obtained with the help of the probe, 2 mM $\text{K}_3[\text{Fe}(\text{CN})_6]$. Cyclic voltammograms of the probe were recorded at different scan rates from 0.01

Vs^{-1} to 0.1 Vs^{-1} using the above mentioned electrodes (Figure 6.4). For reversible systems, Randles Sevcik equation may be utilized to correlate the scan rate and peak current;⁵

$$I = 2.69 \times 10^5 A n^{3/2} D^{1/2} C v^{1/2}$$

From slopes of the plots, electro-active surface area of different electrodes was calculated. Surface area obtained was 0.0135 cm^2 , 0.0482 cm^2 and 0.1669 cm^2 for bare GE, AB/GE and AB-C/GE respectively. Twelffold enhancement in electro-active surface area was observed when bare GE was modified with $4 \mu\text{L}$ of AB-C composite. Enhancement in surface area points to the enhancement of active catalytic surface.

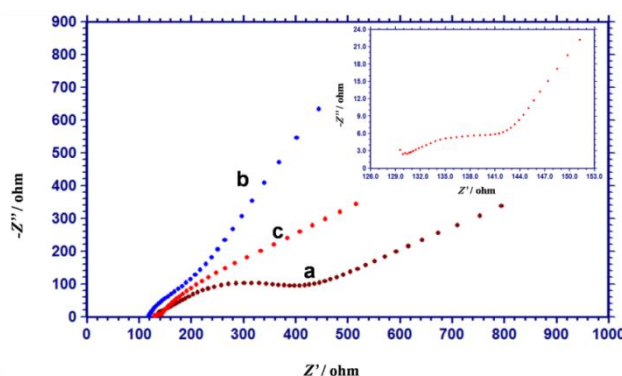


Figure 6.5 EIS obtained in 0.1 M KCl containing $5 \text{ mM } [\text{Fe}(\text{CN})_6]^{3-/4-}$ at (a) bare GE (b) GE modified with $4 \mu\text{L}$ of 1 mg/mL AB suspension (c) GE modified with $4 \mu\text{L}$ of $1 \text{ mg/mL AB-Chitosan}$ suspension and (inset) zoomed image of (c)

This was again supported by the results obtained from **electrochemical impedance spectrum (EIS) analysis**. EIS measurements of bare GE and AB-C/GE were carried out in $[\text{Fe}(\text{CN})_6]^{3-/4-}$ mixture in 0.1 M KCl . Resultant Nyquist plots are given in Figure 6.5. R_{ct} values

corresponding to each plot was obtained by fitting them with equivalent circuits. An observable decrease in R_{ct} value upon modification of the electrode points to the easiness rendered towards the electron transfer by AB-C to GE surface.³²⁹

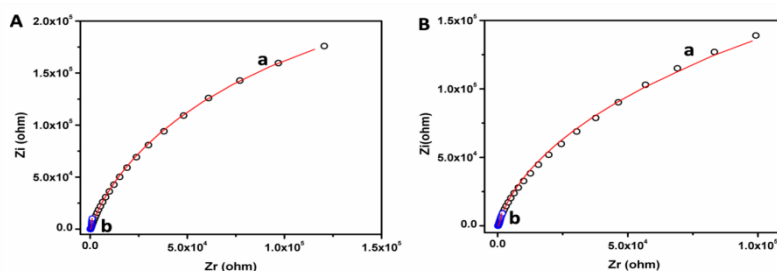


Figure 6.6 Electrochemical impedance spectrum obtained in 0.1 M PBS containing (A) 1.0×10^{-4} M ST and (B) 1.0×10^{-4} M MT at (a) bare GE and (b) GE modified with 4 μ L of 1 mg/mL AB-Chitosan suspension

Impedimetric analysis of bare and AB-C modified GE was also carried out in 0.1 M PBS containing 1.0×10^{-4} M tryptamine at a bias potential of 0.36 V and 0.74 V for ST and MT respectively (Figure 6.6). The Nyquist plots obtained for bare GE was fitted with an equivalent circuit $R_s[Q[RW]]$ whereas the same obtained for AB-C/GE was fitted with $R_s[QR][QR]$ where R_s is the solution resistance, Q the constant phase element, R the charge transfer resistance and W the Warburg impedance. The charge transfer resistance offered by bare GE towards the oxidation of 1.0×10^{-4} M ST and 1.0×10^{-4} M MT were found to be $(2.3 \pm 0.3) \times 10^5 \Omega$ and $(4.6 \pm 0.8) \times 10^5 \Omega$ respectively. Pronounced decrease in charge transfer resistance towards the oxidation of these tryptamines was observed on AB-C/GE with the values $5192 \pm 118 \Omega$ and $766 \pm 52 \Omega$ for ST and MT respectively. Very low charge transfer resistance in presence the modifier

reveals its electro-catalytic nature as well as efficient electron channelizing ability. Considerably lowered charge transfer resistance towards the electro-oxidation of ST and MT is an evidence for the effective catalytic activity shown by AB-C/GE.³²⁹

6.3.2.3 Effect of pre-concentration of ST and MT

Pre-concentration of ST/MT (1.0×10^{-4} M) at AB-C/GE and the subsequent SWV scan were performed. The accumulation was carried out for different time span in an open circuit between the potential limits 1 V to -1 V. After each accumulation step anodic current of ST/MT was recorded using SWV. It was found that as accumulation time increases, current decreases. It may be deduced that ST as well as MT does not undergo adsorptive pre-concentration at AB-C/GE.

6.3.3 Mechanistic and kinetic aspects of electrochemical oxidation of ST and MT

6.3.3.1 Diffusion controlled electro-oxidation

To ascertain the nature of electrochemical oxidation of ST (1.0×10^{-4} M) at AB-C/GE, the potential was scanned at increasing rate from 0.03 Vs^{-1} to 0.20 Vs^{-1} using LSV under the same experimental conditions (Figure 6.7a). A linear relationship was obtained between peak intensity (I_p) and square root of scan rate ($v^{1/2}$), suggesting a diffusion controlled process.²⁷³ In order to confirm the diffusion controlled mechanism, $\log I_p$ was plotted against $\log v$, which exhibited a linear relationship. The linear regression equation obtained was $\log I_p = 0.58 \log v - 0.45$; $R^2 = 0.99$. A

slope of 0.50 confirms the diffusion controlled electro-oxidation of ST at AB-C/GE.²⁷³

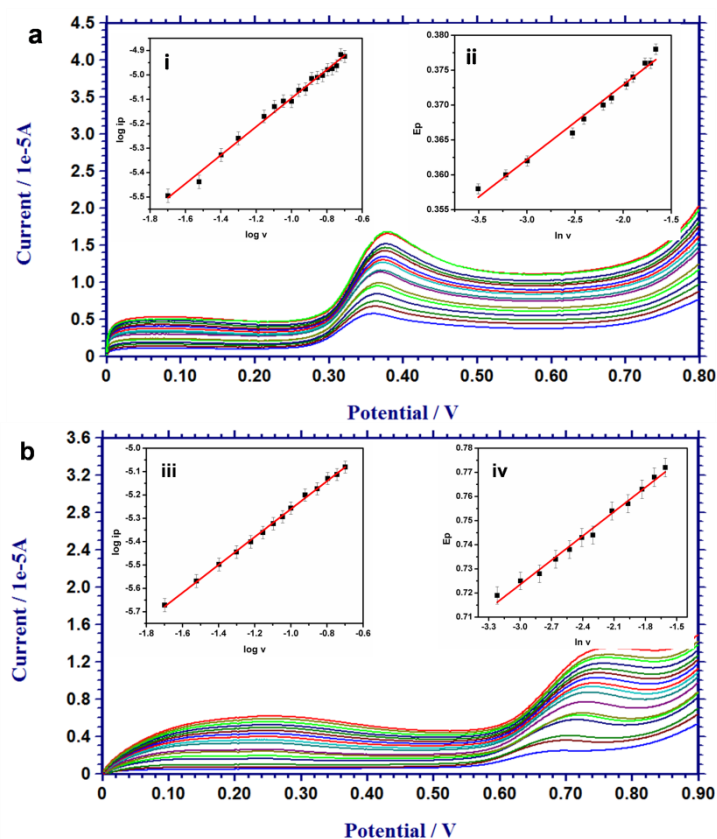


Figure 6.7 LSV response of (a) 1.0×10^{-4} M ST with varying scan rates from 0.03 Vs^{-1} to 0.1 Vs^{-1} , inset i : a plot of $\log I_p$ vs. $\log v$, inset ii: a plot of E_p vs. $\ln v$ (b) 1.0×10^{-4} M MT with varying scan rates from 0.02 Vs^{-1} to 0.20 Vs^{-1} , inset iii: a plot of $\log I_p$ vs. $\log v$, inset iv: a plot of E_p vs. $\ln v$

Influence of scan rate on the oxidation process of (1.0×10^{-4} M) MT was also investigated by LSV (Figure 6.7 b). The scan rate was varied from 0.02 Vs^{-1} to 0.20 Vs^{-1} . The peak current increases with scan rate and in addition, peak current varies linearly with square root of scan rate

demonstrating diffusion controlled process. Again it was observed that, $\log I_p$ vs. $\log \nu$ varies linearly, with a linear regression equation, $\log I_p = 0.60 \log \nu - 4.66$; $R^2 = 0.99$. Obtained slope confirms the diffusion controlled oxidation of MT.

6.3.3.2 Calculation of diffusion coefficient from chronoamperometric studies

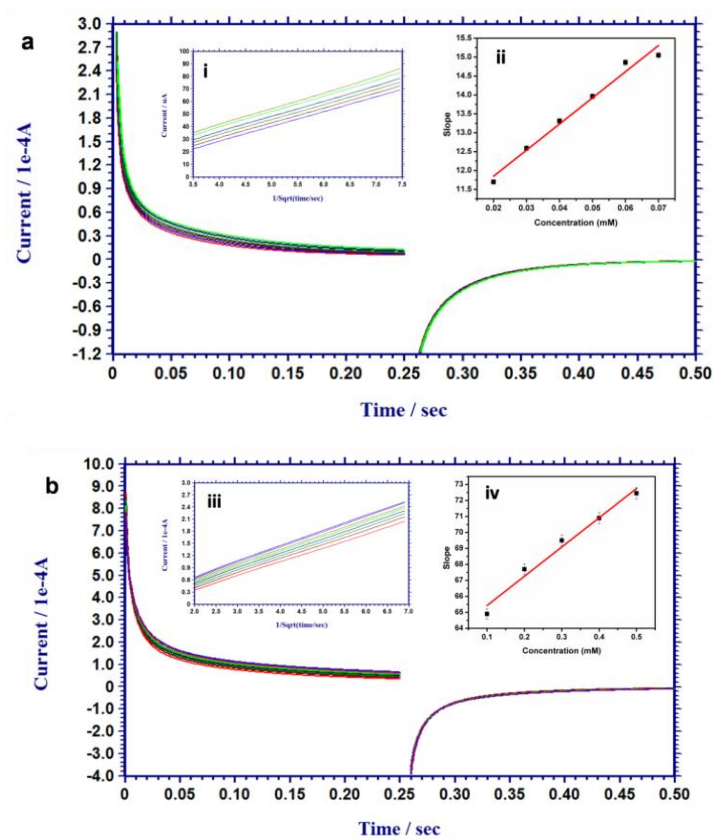


Figure 6.8 Overlay of chronoamperograms for various concentrations of (a) ST and (b) MT, inset (i) plot of current for ST vs. $t^{1/2}$ (ii) plot of slope of (I_p vs. $t^{1/2}$) vs. concentration of ST (iii) plot

of current for MT vs. $t^{1/2}$ (iv) plot of slope of (I_p vs. $t^{1/2}$) vs. concentration of MT

Chronoamperometric studies of ST and MT were carried out and the chronoamperograms are given in Figure 6.8 a and 6.8 b. Cottrellian decay of transient current was observed for the electro-oxidation of ST and MT at various concentrations. The slopes of the experimental plots of current vs. $t^{1/2}$ were plotted against their concentration. Slope obtained for the resultant plot was used to calculate D , diffusion coefficient by means of Cottrell equation.³

$$I_p = nFA D^{1/2} C \pi^{-1/2} t^{-1/2}$$

Diffusion coefficient obtained for ST and MT are $1.09 \times 10^{-5} \text{ cm}^2 \text{ s}^{-1}$ and $1.11 \times 10^{-6} \text{ cm}^2 \text{ s}^{-1}$.

6.3.3.3 Calculation of number of electrons

From Figure 6.7 a and b, it is clear that the over-potential for oxidation of ST as well as MT shows a shift towards higher value on increasing the scan rate. This gives a clear indication of irreversibility of oxidation of the tryptamines.³³⁰ Charge transfer coefficient, α was calculated as per the latest considerations of IUPAC,³⁶¹ according to which

$$\alpha = (RT/F) (d \ln|j| / dE)$$

Where $d \ln|j| / dE$ is the reciprocal of the slope of Tafel plot, j is the current density, R , T and F have their usual meaning. Values of α for the oxidation of ST and MT were calculated to be 0.48 and 0.45 which are closer to the theoretical value 0.5 (for an irreversible process).^{330,361}

Total number of electrons (n) involved in the reaction is calculated using the following equation.

$$E_p - E_{p_{1/2}} = 0.047 / (1 - \alpha)n$$

Where, E_p and $E_{p_{1/2}}$ denotes peak potential and half peak potential respectively.³ For ST and MT, $E_p - E_{p_{1/2}}$ was obtained as 0.04 V and 0.05 V respectively, from which the number of electrons involved in the oxidation of tryptamines were calculated to be 2.2 and 1.8 respectively. This evidently points to the involvement of 2 electrons in the oxidation of ST as well as MT.³⁶²⁻³⁶⁶

6.3.3.4 Variation of overpotential (E_p) with scan rate (v)

E_p and $\ln v$ shows linear relationship, with a slope of 0.01 and 0.03 for ST and MT respectively (Figure 6.7 a and 6.7 b). In accordance with Nicholson and Shain equation³⁶⁷ for an irreversible system,

$$E_p = E_p^0 + x[0.78 - \ln ksD^{-1/2} - 0.5 \ln x] + 0.5 x \ln v ;$$

$$x = RT / (1 - \alpha)nF \text{ (for oxidation)}$$

E_p vs. v graph was extrapolated to $v=0$ to get E_p^0 , the formal potential. The values obtained for diffusion coefficient (section 6.3.3.2) and slope of E_p and $\ln v$ was used to calculate electron transfer rate constant, ks for the electrochemical reaction.³⁶⁸ Heterogeneous rate constant obtained for ST and MT are $6.94 \times 10^{-3} \text{ cms}^{-1}$ and $1.44 \times 10^{-3} \text{ cms}^{-1}$ respectively. It may be inferred that electro-oxidation of ST is ~ 4.8 times faster than that of MT at AB-C/GE by which higher current is obtained for ST than MT even at the same concentration.

6.3.4 Variation of peak current with concentration of ST/MT

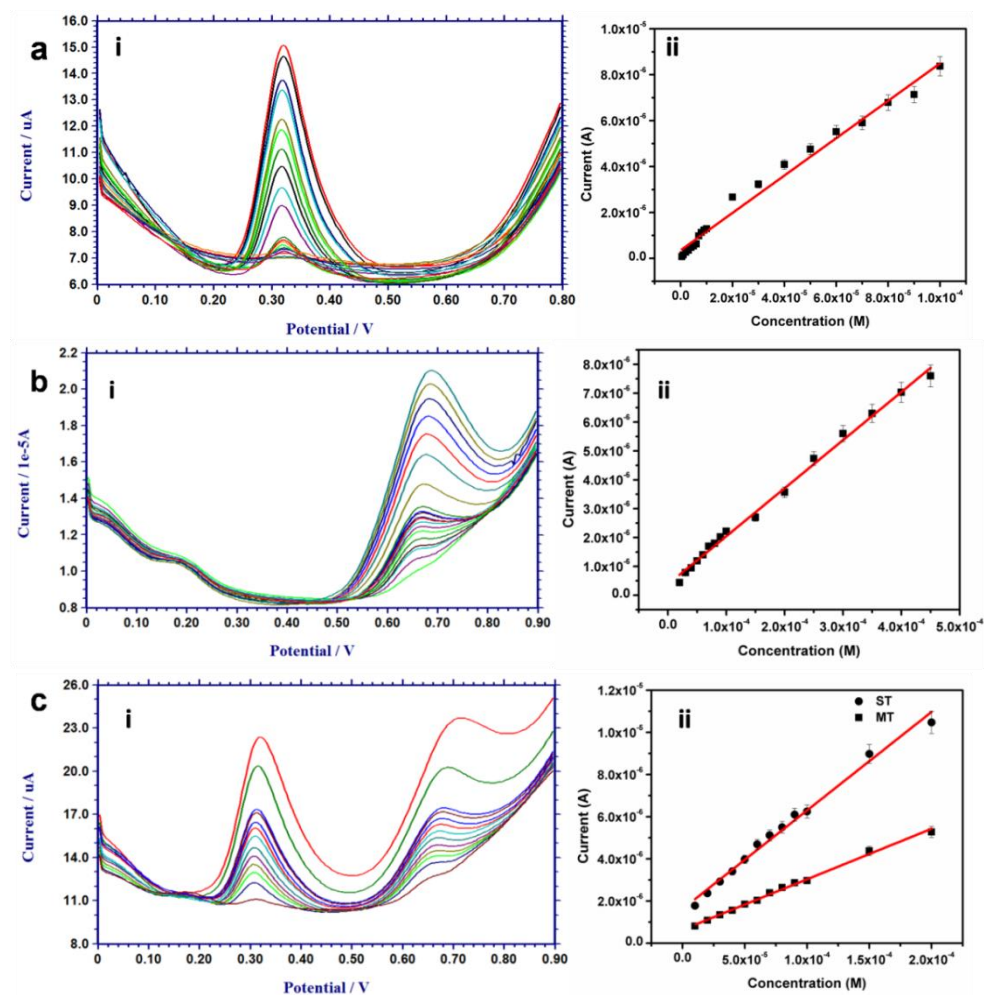


Figure 6.9 SWV response of (a.i) various concentrations of ST in the range 1.0×10^{-4} M to 5.0×10^{-7} M, (a.ii) plot of anodic peak current vs. concentration (1.0×10^{-4} M to 5.0×10^{-7} M) (b.i) various concentrations of MT in the range 4.5×10^{-4} M to 2.0×10^{-5} M, (b.ii) plot of anodic peak current vs. concentration (4.5×10^{-4} M to 2.0×10^{-5} M) (c.i) simultaneous oxidation of ST and MT in an equimolar mixture with concentration of each antioxidant ranging 2.0×10^{-4} M to

1.0×10^{-5} M, (c.ii) plot of anodic peak current for simultaneous oxidation of ST and MT vs. concentration (2.0×10^{-4} M to 1.0×10^{-5} M)

In order to evaluate the catalytic efficiency of AB-C/GE towards the oxidation of ST, the effect of varying concentration upon its oxidation peak current was examined. Concentration of ST was varied from 1.0×10^{-3} M to 5.0×10^{-7} M (Figure 6.9a). An increase in peak current with concentration was observed. But linearity between concentration and peak current was obtained in the range 1.0×10^{-4} M and 5.0×10^{-7} M. The linear regression equation is given below.

$$I_p = (8.7 \pm 0.9) \times 10^{-2} C + (2.9 \pm 0.8) \times 10^{-7}; R^2 = 0.99$$

SWV behaviour of various concentration of MT was analyzed. Figure 6.9 b shows the voltammograms of electro-oxidation of MT with concentration in the range 6.0×10^{-4} M and 2.0×10^{-5} M in phosphate buffer solution of pH 7. The anodic current showed linear relationship with increasing concentration of MT between 4.5×10^{-4} M and 2.0×10^{-5} M and linear regression equation is given as

$$I_p = (1.9 \pm 0.2) \times 10^{-2} C + (4.5 \pm 0.7) \times 10^{-7}; R^2 = 0.99$$

Limit of detection (LOD) was calculated making use of the equation $3s/m$, where 's' is the standard deviation of the response obtained for lowest concentration of ST/MT and 'm' is the slope of calibration graph. LOD was calculated to be 1.55×10^{-7} M and 1.81×10^{-6} M for ST and MT respectively.

Voltammetric behaviour of 1:1 mixture of ST and MT was analyzed on AB-C/GE (Figure 6.9 c). It is seen that the peak current of both ST and

MT increases linearly with increasing concentration in between 2.0×10^{-4} M and 1.0×10^{-5} M. Linear regression equation followed by ST and MT and LOD are given below respectively.

$$I_p = (5.0 \pm 0.3) \times 10^{-2} C + (1.2 \pm 0.4) \times 10^{-7}; R^2 = 0.99; \text{LOD} = 3.49 \times 10^{-7} \text{ M}$$

$$I_p = (2.4 \pm 0.1) \times 10^{-2} C + (4.7 \pm 0.2) \times 10^{-7}; R^2 = 0.99; \text{LOD} = 8.59 \times 10^{-7} \text{ M}$$

On comparison of the linear ranges, linear regression equations and limit of detection of the tryptamines for the individual or simultaneous determination of comparable results were obtained (Table 6.1).

Table 6.1 Comparison of results obtained for individual as well as simultaneous determination of ST and MT

| | Analyte | Linear Range (M) | Linear regression equation | LOD (M) |
|--------------|---------|---|---|-----------------------|
| Individual | ST | 1.0×10^{-4} - 5.0×10^{-7} | $I_p = 8.7 \times 10^{-2} C + 2.9 \times 10^{-7}$ | 1.55×10^{-7} |
| | MT | 4.5×10^{-4} - 2.0×10^{-5} | $I_p = 1.9 \times 10^{-2} C + 4.5 \times 10^{-7}$ | 1.81×10^{-6} |
| Simultaneous | ST | 2.0×10^{-4} - 1.0×10^{-5} | $I_p = 5.0 \times 10^{-2} C + 1.2 \times 10^{-7}$ | 3.49×10^{-7} |
| | MT | 2.0×10^{-4} - 1.0×10^{-5} | $I_p = 2.4 \times 10^{-2} C + 4.7 \times 10^{-7}$ | 8.59×10^{-7} |

6.3.4.1 Comparison of developed sensor with latest reported methods

A large number of electrochemical methods suitable for tryptamine assessment are reported. Among these, only one voltammetric sensor³⁵³ focuses on the simultaneous determination of ST and its derivative MT. To

demonstrate the performance of the presently developed sensor with the voltammetric sensors reported earlier, a comparison of linear working range and lowest limit of detection of latest reported works have been done and the results are listed in Table 6.2 and Table 6.3. Though the proposed sensor shows only comparable results, it enables the simultaneous determination of two tryptamines, ST and MT. Moreover, the developed method is fast, cost-effective and easy to handle.

Table 6.2 Comparison of the proposed sensor with latest reported sensors for serotonin

| Electrode | Linear Range (M) | LOD (M) | References |
|---|---|-----------------------|--|
| IL-graphene/GCE | 1.0×10^{-5} - 2.0×10^{-7} | 7.0×10^{-8} | Liu et al. (2015) ³⁶⁹ |
| 100 kGy GI-WO ₃ /GCE | 6.0×10^{-7} - 1.0×10^{-8} | 1.0×10^{-8} | Anitha et al. (2017) ³⁷⁰ |
| Fe ₃ O ₄ -MWCNT-poly(BCG)/GCE | 1.0×10^{-4} - 5.0×10^{-7} | 8.0×10^{-8} | Ran et al. (2017) ³⁷¹ |
| PEDOTNTs/rGO/AgNPs/GC | 5.0×10^{-4} - 1.0×10^{-9} | 1.0×10^{-10} | Sadanandhan et al. (2017) ³⁷² |
| AuAg/graphene/ITO | 5.1×10^{-6} - 3.0×10^{-9} | 2.0×10^{-9} | Thanh et al. (2017) ³⁷³ |
| AuNPs@PPyNPs/GSPEb | 2.0×10^{-5} - 1.0×10^{-7} | 3.0×10^{-8} | Tertis et al. (2017) ³⁷⁴ |
| Ag/Cu ₂ O/PPy/GCE | 3.0×10^{-4} - 1.0×10^{-8} | 1.0×10^{-8} | Selvarajan et al. (2018) ³⁷⁵ |
| MIS-coated PtNP/GCE | 8.0×10^{-5} - 5.0×10^{-8} | 2.0×10^{-8} | Yang et al. (2018) ³⁷⁶ |
| GC/(CNTs-ILC)/Crown | 1.0×10^{-6} - 5.0×10^{-9} | 2.0×10^{-10} | Atta et al. (2018) ³⁷⁷ |
| NiO/CNT/PEDOT/GCE | 4.0×10^{-5} - 3.0×10^{-7} | 6.0×10^{-8} | Sun et al. (2018) ³⁷⁸ |
| AB-C/GE | 1.0×10^{-4} - 5.0×10^{-7} | 1.5×10^{-7} | Proposed sensor |

Table 6.3 Comparison of the proposed sensor with latest reported sensors for melatonin

| Electrode | Linear Range (M) | LOD (M) | References |
|--|---|-----------------------|--|
| sdPtFe ₂ O ₃ /GCE | 1.0×10 ⁻³ - 1.0×10 ⁻⁶ | 1.0×10 ⁻¹⁰ | Manikandan etal. (2017) ³⁴⁷ |
| BDD | 4.0×10 ⁻⁴ - 4.0×10 ⁻⁶ | 6.0×10 ⁻⁷ | Alpar etal. (2017) ³⁴⁸ |
| SnO ₂ -Co ₃ O ₄ @rGO/IL/CPE | 6.0×10 ⁻⁶ - 2.0×10 ⁻⁸ | 4.0×10 ⁻⁸ | Zeinali etal. (2017) ³⁴⁹ |
| GCE | 2.0×10 ⁻⁴ - 5.0×10 ⁻⁶ | 3.0×10 ⁻⁷ | Kumar etal. (2017) ³⁵⁰ |
| CB/GCE | 1.0×10 ⁻⁵ -5.0×10 ⁻⁸ | 2.0×10 ⁻⁸ | Smajdor etal. (2017) ³⁵¹ |
| Cdots / Fe ₃ O ₄ NPs/GCE | 1.0×10 ⁻⁵ - 5.0×10 ⁻⁸ | 4.0×10 ⁻⁹ | Cincotto etal. (2018) ³⁵² |
| AB-C/GE | 5.0×10 ⁻⁴ -2.0×10 ⁻⁵ | 1.8×10 ⁻⁶ | Proposed sensor |

6.3.5 Selectivity and effect of possibly co-existing species

Variation of peak current with increasing concentration of ST in presence of MT (1.0×10⁻⁴ M) was studied. SWV obtained are given in Figure 6.10a. The anodic current showed linearity with increasing concentration of ST in the range 1.0×10⁻⁴ M to 5.0×10⁻⁶ M following the linear regression equation, $I_p = (6.1 \pm 0.4) \times 10^{-2} C + (1.3 \pm 0.6) \times 10^{-7}$; $R^2 = 0.99$. Limit of detection was calculated to be 1.30×10⁻⁷ M.

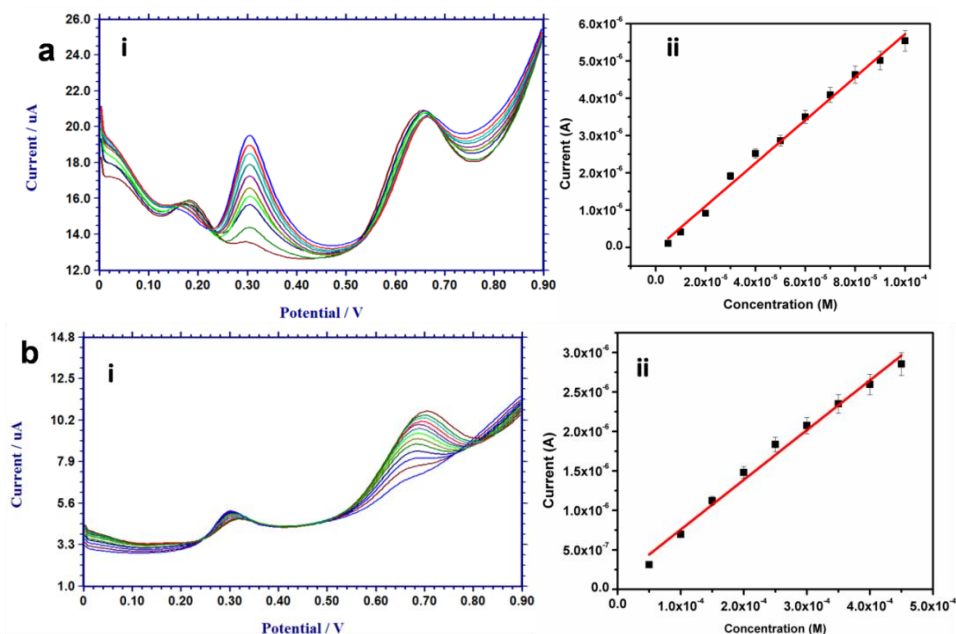


Figure 6.10 Overlay of SWV of (a.i) ST in the range 1.0×10^{-4} M to 5.0×10^{-6} M in presence of 1.0×10^{-4} M MT (a.ii) plot of anodic peak current vs. concentration of ST (b.i) MT in the range 5.0×10^{-4} M and 5.0×10^{-5} M in presence of 5.0×10^{-5} M ST (b.ii) plot of anodic peak current vs. concentration of MT

Electro-oxidation of MT in presence of ST (5.0×10^{-5} M) was also examined (Figure 6.10 b). The results show that the oxidative peak current has a linear relationship with the concentration of MT in the range 5.0×10^{-5} M and 5.0×10^{-4} M which is given in Figure 6.10b. The linear regression obtained is $I_p = (5.1 \pm 0.5) \times 10^{-3} C + (1.1 \pm 0.3) \times 10^{-8}$; $R^2 = 0.99$. LOD was calculated to be 9.39×10^{-6} M.

In order to reveal the efficacy of developed sensor towards selective determination of ST and MT, study of effects produced by co-existing species on the signal under consideration is relevant. Possibility of

interference offered by different co-existing species in blood, mainly dextrose, KCl, NaCl, glutathione, dopamine, adrenaline, creatinine, creatine, urea and ascorbic acid was explored. It was observed that even at concentrations in 100fold excess of ST as well as MT, signal change produced by species such as dextrose, KCl, NaCl, creatinine, creatine and urea was within the tolerance limit of 5% (Table 6.4). It is noteworthy that 10fold excess dopamine did not offer any interference towards ST but adrenaline interferes even at equimolar concentrations. In the case of MT determination, glutathione and adrenaline did not cause any signal change beyond 5%, at 10fold excess concentration but dopamine obeyed the tolerance limit only up to equimolar concentrations. Common interfering species ascorbic acid, at equimolar concentrations did not show interference towards ST but interferes with the determination of MT.

Table 6.4 Effect of foreign species

| Species | Molar ratio | Signal change (%) | |
|---------------|-------------|-------------------|------|
| | | ST | MT |
| Creatinine | 1:100 | 3.9 | 4.2 |
| Dextrose | 1:100 | 2.5 | 4.1 |
| KCl | 1:100 | 2.1 | 1.7 |
| Urea | 1:100 | 3.5 | 1.4 |
| Creatine | 1:100 | 4.5 | 3.8 |
| NaCl | 1:100 | 2.6 | 2.3 |
| Glutathione | 1:100 | 3.4 | - |
| Glutathione | 1:10 | - | 4.6 |
| Adrenaline | 1:10 | - | 2.9 |
| Adrenaline | 1:1 | 23.0 | - |
| Dopamine | 1:10 | - | 2.5 |
| Dopamine | 1:1 | 1.5 | - |
| Ascorbic Acid | 1:1 | 4.8 | 16.7 |

6.3.6 Application of developed sensor in synthetic blood serum

Artificial blood serum was prepared as per the earlier reports detailed in chapter 2, section 2.7.2.³²⁴ Proposed sensor was applied in the simultaneous determination of ST and MT in artificial blood serum. The results obtained are given in Table 6.5. In order to validate the developed sensor, results obtained were compared with that obtained for individual determination of ST and MT carried out by spectrophotometry²⁶⁰ described in chapter 2, section 2.8.5. (Table 6.5).

Table 6.5 Application of the sensor for the determination of ST and MT in artificial blood serum

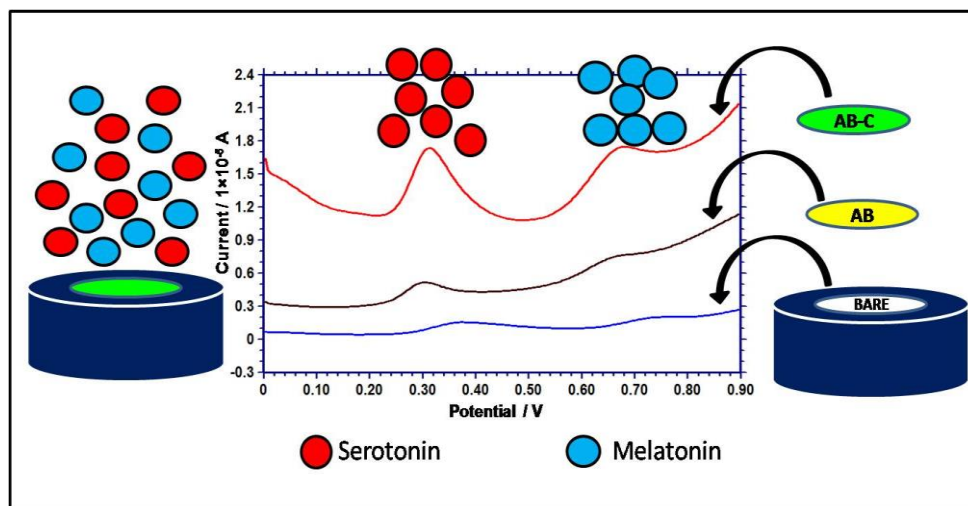
| <i>Developed method</i> | | | | |
|--|---|---|---------------------|------------------------|
| | Added (M) | Found (M) | Recovery (%) | RSD^a |
| ST | $2.0 \times 10^{-4} - 1.0 \times 10^{-5}$ | $1.9 \times 10^{-4} - 1.0 \times 10^{-5}$ | 101 | 2.6 |
| MT | $2.0 \times 10^{-4} - 1.0 \times 10^{-5}$ | $1.9 \times 10^{-4} - 1.0 \times 10^{-5}$ | 100 | 1.9 |
| <i>Spectrophotometric method²⁶⁰</i> | | | | |
| ST | $3.0 \times 10^{-4} - 1.0 \times 10^{-5}$ | $3.1 \times 10^{-4} - 1.0 \times 10^{-5}$ | 102 | 4.0 |
| MT | $6.0 \times 10^{-4} - 1.0 \times 10^{-4}$ | $5.9 \times 10^{-4} - 9.8 \times 10^{-5}$ | 101 | 3.9 |

^a Five replicates

6.4 Conclusions

In summary, a simple and sensitive sensor was developed for ST and MT. AB-C composite on GE performed very good electro catalytic activity towards the electro-oxidation of ST and MT. Different experimental

parameters which can influence the electro-oxidation of these tryptamines were optimized and various kinetic parameters were calculated. The proposed sensor shows many advantages such as simple fabrication procedure, high sensitivity, excellent catalytic activity at physiological pH values and short response time. Moreover the application of the proposed sensor is not confined to pharmaceutical quality control but extends to clinical analysis such as in artificial blood serum.



Scheme 6.1 Voltammetric sensor for simultaneous determination of tryptamines – serotonin and melatonin

.....❧.....

Fluorimetric sensor for the determination of serotonin and its metabolite 5-hydroxyindole acetic acid

| | |
|--|-----------------------------------|
| C o n t e n t s | 7.1 <i>Introduction</i> |
| | 7.2 <i>Experimental</i> |
| | 7.3 <i>Results and discussion</i> |
| | 7.4 <i>Conclusions</i> |

This chapter details the development of fluorimetric sensor based on mercapto propanoic acid capped CdTe quantum dots for the determination of the neurotransmitter serotonin (ST) and its metabolite 5-hydroxyindoleacetic acid (HIAA). The sensor is primarily based on the quenching of fluorescence induced by these molecules. Mechanism underlying the quenching has been established from lifetime analysis and it has been found that ST induces static quenching while HIAA induces quenching owing to dynamic as well as static contributions. The developed strategy enabled the effective quantification of ST within the range 1.2×10^{-6} to 1.0×10^{-7} M and HIAA in the range 1.0×10^{-5} to 1.0×10^{-6} M.

7.1 Introduction

5 - Hydroxytryptamine commonly known as serotonin (ST) is a neurotransmitter distributed mainly in central nervous system, blood platelets and intestinal mucosa. It plays crucial role in various physiological functions such as appetite, muscular contraction, cardiovascular function, aggression, depression etc.^{379,380} Under disease conditions for instance carcinoid tumors, appendicitis, schizophrenia and migraine, ST level in blood serum increases which ultimately induce toxic and fatal effects in body.^{381,382} **5-Hydroxyindoleacetic acid** (HIAA) is the major breakdown product of ST which is excreted through urine. Ageing process can induce changes in the ratio of ST to HIAA present in physiological fluids.³⁸³ ST gets released in large amounts in patients affected by carcinoid tumors grown in intestine and higher concentrations of HIAA are found in the urine of such people.³⁸⁴ ST and HIAA levels in urine act as trustworthy biomarker of swelling of appendix.³⁸⁵ Thus changes in normal functioning of the body as well as some chemicals which are prohibited by world anti doping agency can even alter the levels of ST and HIAA in human.³⁸⁶

Only a few methods are available for the determination of ST and HIAA using a single probe. Voltammetric methods³⁸⁷ and high performance liquid chromatographic (HPLC) methods have been utilized for the simultaneous determination of these compounds. These HPLC methods are coupled with diverse detection methods comprising of electrochemical,^{388,389} fluorescence³⁹⁰ and chemiluminescence detection.³⁹¹ However, a fluorescence-based sensor which relies upon a single probe for

the determination of ST and HIAA has not yet been reported. Methods based on fluorescence technique have advantages such as high sensitivity, simplicity and quick response^{43,392}, and hence form a more efficient technique for the determination of ST/HIAA.

Quantum dots (QDs), the semiconductor nanocrystals which serve as a bridge between bulk materials and nano clusters are immensely used for various applications claiming to their exceptional luminescent properties. QDs are extensively under focus of sensor technology down to the extraordinary features possessed by them chiefly photostability, longer luminescence lifetimes, high quantum yield and narrow size-tuned emission spectra in conjunction with relatively low cost of synthesis and rich as well as negotiable surface functionality.^{43,392} QDs of cadmium origin especially CdTe QDs give the best fit for the above mentioned properties⁴⁷ and used as the fluorescent probe for the present work.

The present work aims at the development of a sensing strategy for the determination of ST and its metabolite HIAA based on their efficiency in quenching the fluorescence intensity of the fluorescent probe. The strategy also depends on the effect produced by these analytes on the lifetime of the QDs. To validate the proposed work, the determination of the biomarkers in artificial blood serum as well as urine samples was performed and the obtained results were compared with reported protocols.

7.2 Experimental

7.2.1 Analytical procedure

Stock solution of ST (1.0×10^{-2} M) was prepared by dissolving 21.3 mg of ST in 10 mL water. The lower concentrations of ST were prepared by dilution of stock solution with water. For studying the effect of ST on the fluorescence intensity of MPA capped CdTe QDs, different concentrations of ST was mixed with 5 μ L of QDs and water in a cuvette keeping the total volume as 2 mL.

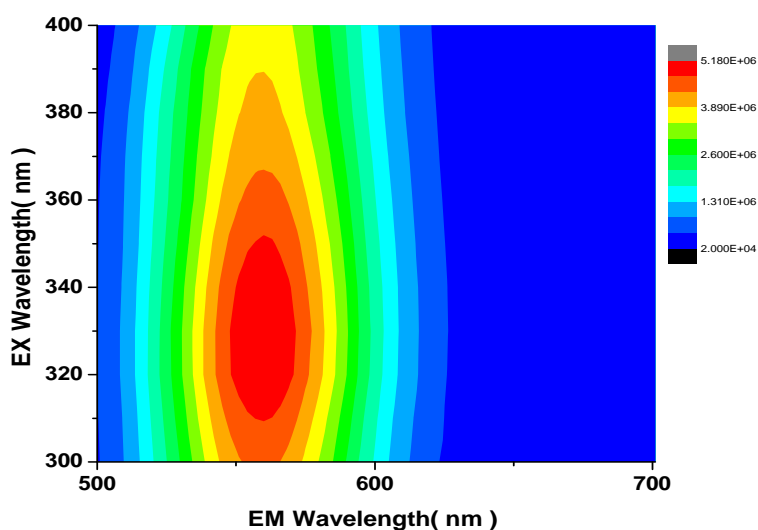


Figure 7.1 A contour map describing fluorescence intensity of QDs in a range of excitation wavelength

A contour map of fluorescence emission of QDs were plotted with excitation wavelength ranging from 300 nm to 450 nm and emission wavelength ranging from 520 nm to 750 nm. From the contour map, it is clear that the maximum emission intensity was obtained when the excitation wavelength used was in between 320 nm to 360 nm (Figure 7.1). 360 nm

was chosen as the excitation wavelength and the fluorescence emission was recorded at 560 nm.

7.2.2 HPLC-UV determination of HIAA

Aliquots (usually 20 μL) of the HIAA samples were injected into the chromatograph, and eluted with a mobile phase (acetate buffer/methanol, 95/5 v/v) pumped at 3.0 mL/min. UV detection of HIAA was done at 254 nm. Peak for HIAA was obtained after a retention time of 15 min. The peak areas obtained were plotted against the concentration of HIAA to get the calibration graph.²⁶¹

7.3 Results and Discussion

7.3.1 Characterisation and fluorescence behavior of CdTe QDs in the absence of ST or HIAA

Hydrophilic mercaptopropionic acid-capped CdTe QDs were prepared. Mercaptopropionic acid was used as the stabilizing agent of the QDs since it can generate functionalisation on the QDs surface owing to the presence of carboxylic acid moiety. Upon capping COO^- groups of MPA will be projecting out of the QDs surface. In order to understand the characteristic features of the QDs, various techniques were used as follows. Fluorescence lifetime of QDs was found to be 1.79×10^{-9} s.

UV-visible spectrum of QDs was recorded. QDs give characteristic absorption maximum at 525 nm corresponding to the transition of the electron from the highest level of valence band to the lowest level conduction band of the CdTe core.⁴⁷ A standard protocol was used to calculate the size of the QDs from the first absorption maximum and the

size obtained was 3.1 nm.³⁹³ The emission spectrum was found to be Stokes-shifted from the absorption maximum by 35 nm being centered at 560 nm. TEM images of water dispersed QDs depicts the spherical shape of the QDs. (Figure 7.2)

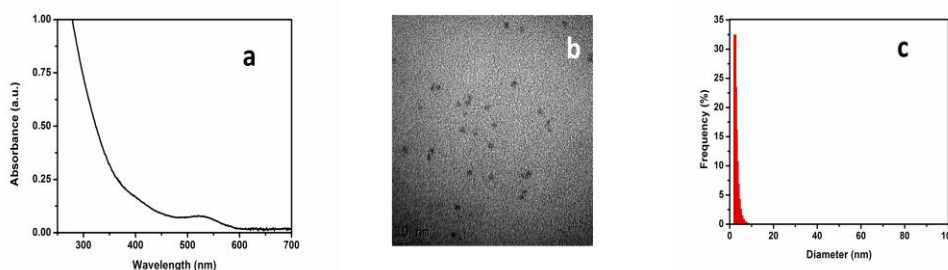


Figure 7.2 a) Absorption spectrum, b) TEM image and c) DLS spectrum of CdTe QDs

Time correlated fluorescence experiments were conducted to identify the temporal behaviour of QDs in the absence and presence of ST or HIAA. Tetra exponential behavior of the fluorescence decay was obtained upon best fitting (i.e. fit with low χ^2 value, random distributions of the weighted residuals and auto-correlation function). Previous to the addition of the analytes, shortest lifetime obtained was 0.45 ns and the longest decay time obtained was 52.68 ns. The tetra exponential decay or the complicated emission dynamics of the QDs evidently points to the surface defects that can produce the trap states which lie within the bandgap.⁵³⁻⁵⁵ The shortest decay time (fastest emission) may be ascribed to the immediately populated core-state recombination and reveal the fluorescence produced by radiative relaxation of the electrons to the ground state.^{56,57} In some cases the conduction band electrons or the excited electrons may get localized in trap states, resulting in non radiative decay.

The slowest decay may be correlated to the surface states as well as the radiative recombination of the electrons and holes^{58,59}. These different processes in combination with disparities possessed by each nano crystal in a matrix produce highly complicated multi-exponential emission dynamics.⁶⁰

7.3.2 Fluorescence behavior of CdTe-MPA QDs in the presence of ST and the mechanism behind its sensing

In presence of ST, a quenching in the fluorescence intensity of the QDs was observed. In order to recognize the mechanism underlying the quenching of QDs, different techniques were adopted which include lifetime measurements, UV-visible spectroscopy, DLS analysis, zeta potential measurement and TEM imaging.

CdTe QDs showed a high negative **zeta potential** value which reveals the high colloidal stability owned by the QDs by virtue of the presence of COO⁻ groups of the capping agent MPA. When ST was added to the QDs a decrease in the absolute value of zeta potential was observed which decreases further with increase in the concentration of ST. This in turn points to the changes produced on the surface of the QDs leading to destabilization and consequent aggregation in presence of ST. During **DLS analysis**, an enlargement in hydrodynamic volume of QDs was observed with increase in the concentration of ST. Hydrodynamic volume of CdTe QDs was 3 nm in the absence of ST and it changed to around 30 nm in presence of different concentrations of ST which points to the aggregation of QDs. From **TEM images** it is clear that the QDs have a size around 2.5 nm and the enlargement in size of the particles may be due to formation of

small aggregates in the presence of ST (Figure 7.3). TEM images also confirm the closeness of QDs in presence of ST.

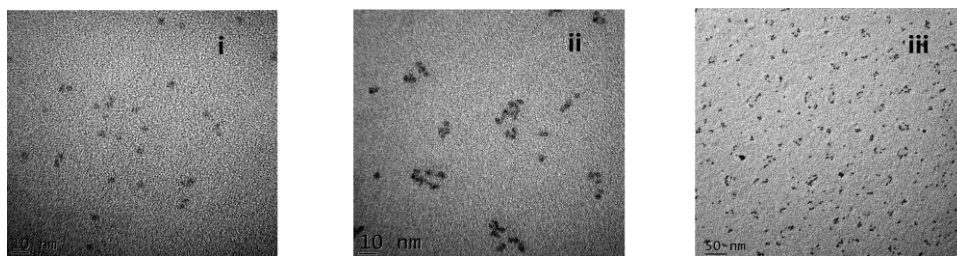


Figure 7.3 TEM image of QDs in the i) absence and ii, iii) presence of ST

Absorption spectrum of QDs in the absence and presence of ST was recorded; any shift in absorption maxima at 525 nm was not detected. But appearance of new features between the wavelength, 315 and 400 nm as well as a blue shift in the absorption maximum of ST from 287 nm was observed (Figure 7.4). These observation evidently points to the interaction between QDs and ST.

Upon addition of ST, any change in the average or the components of the lifetime of QDs was not observed. Absence of any notable change in the **lifetime** of QDs in presence of ST as well as the above mentioned results from various analyses clearly indicate the purely static quenching mechanism of QDs in presence of ST.

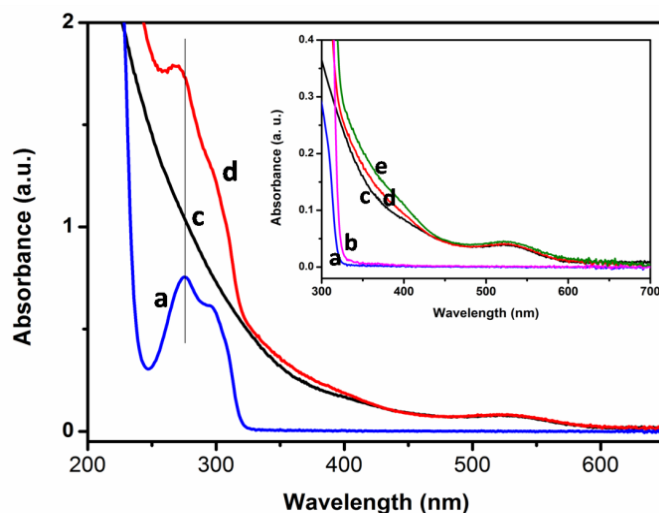


Figure 7.4 a) 5.0×10^{-5} M ST b) 1.0×10^{-4} M ST c) CdTe QDs d) 5.0×10^{-5} M ST added to QDs e) 1.0×10^{-4} M ST added to QDs; inset: zoomed image

7.3.3 Fluorescence behavior of CdTe-MPA QDs in the presence of HIAA and the mechanism behind its sensing

Fluorescence intensity of QDs was found to be quenched and red shifted in the presence of HIAA. Upon addition of HIAA to QDs, an increase in hydrodynamic volume was observed. TEM images clearly depict the more coagulated/aggregated form of QDs. Moreover, on comparing the absorption spectra of HIAA, QDs and QDs in presence of HIAA, little shift in the absorption maximum of the QDs or HIAA was observed. These may be the outcome of the non bonding interaction between the fluorophore and analyte which may induce static contribution to the quenching.³⁹⁴

A red shift in the emission spectrum of the QDs in presence of the analyte leads to two possible reasons for quenching of fluorescence. The

first possibility is the electronic coupling between adjacent QDs by hybridization of the band edge orbital leading to fluorescence quenching accompanied by red shift in the emission as well as absorption spectra.³⁹⁵ Whereas in the case of exciton energy transfer, the energy of the excited electron will be transferred from the higher band gap QDs to the smaller band gap QDs.³⁹⁶ This in turn quenches fluorescence accompanied by red shift of the emission peak. In such cases the absorption spectrum of the donor (QDs) will not show any change. In the present work, absorption spectrum of the QDs as well as HIAA did not show any variations in the presence of the other, which rules out the first possibility.

Besides the changes in the steady-state fluorescence, the fluorescence decay traces of QDs showed variations in presence of the analyte. In presence of HIAA, a profound decrease in the lifetime of QDs from 17.89 ns to 7.10 ns was noted. Different components of lifetime and thereby the average lifetime of QDs showed gradual changes upon addition of HIAA which may be produced via electron or hole transfer mechanism between the QDs and HIAA. After the addition of the analyte, fluorescence decay followed a tetra-exponential function as before. The slowest decay may be attributed to the charge transfer quenching.⁶⁰ It obviously points to the role of dynamic quenching of QDs by HIAA. Hence it may be concluded that the interaction between the QDs and HIAA can evoke H-bonding between them which brings them more closely. This facilitates the transfer of excited electrons from the QDs to the quencher inducing dynamic quenching of fluorescence.

7.3.4 Optimisation of experimental conditions

The efficiency of the ST and its metabolite HIAA in quenching the fluorescence intensity of the QDs was studied in various media such as water, 0.01 M solutions of phosphate buffer, Dulbeccos phosphate buffer, acetate buffer, citrate buffer, HCl, NaOH and NaCl. Highest quenching efficiency was obtained in water for both the analytes and hence it was chosen for further studies.

7.3.4.1 Effect of time

In order to understand achievement of the probe-quencher interaction and thereby quenching of the fluorescence intensity, intensity of CdTe QDs was monitored in the absence and presence of ST and HIAA for 30 minutes. It was observed that in the presence of analytes, quenching of fluorescence became stable in 5 minutes and hence the fluorescence spectra were obtained after an incubation period of 5 min. (Figure 7.5)

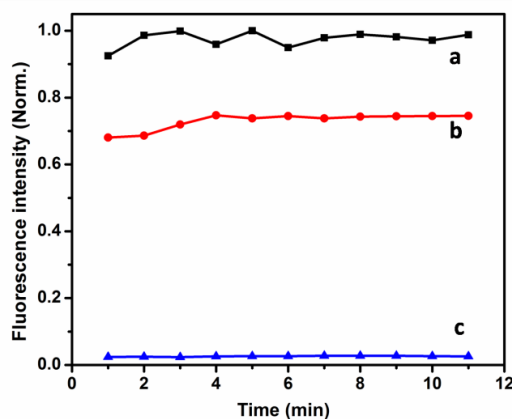


Figure 7.5 Change in fluorescence intensity of a) QDs b) 1.0×10^{-6} M ST and c) 5.0×10^{-6} M ST with time

7.3.4.2 Calibration graphs and estimation of the quenching constants

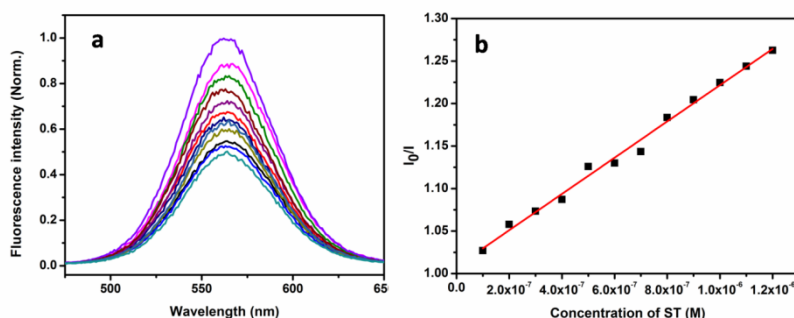


Figure 7.6 a) Fluorescence spectra of QDs in presence of varying concentration of ST and b) linear plot of $\frac{I_0}{I}$ with concentration of ST

Under optimized conditions, ST and HIAA quenched the fluorescence of the QDs effectively and the dependence of $\frac{I_0}{I}$ towards their concentration was investigated (Figure 7.6). Stern-Volmer equation was used to analyze the fluorescence quenching of CdTe-MPA QDs by ST⁴². $\frac{I_0}{I}$ showed linearity towards the concentration of ST in the range 1.2×10^{-6} M to 1.0×10^{-7} M ST following the linear regression equation $\frac{I_0}{I} = 1.09 \times 10^6 Q + 0.96$ ($R^2=0.99$). The limit of detection obtained was 7.60×10^{-8} M.

It is known that, $K_{sv} = K_q \tau_0$ and hence K_q , the bimolecular quenching constant was calculated from the Stern – Volmer constant ($K_{sv} = 1.09 \times 10^6 \text{ M}^{-1}$) and lifetime of the probe ($\tau_0 = 17.89 \text{ ns}$). The value obtained for K_q is $6.13 \times 10^{13} \text{ M}^{-1}\text{s}^{-1}$. The larger value for K_q implies the presence of a binding interaction between the QD and ST which confirms the aforementioned mechanism.

In order to understand the dependence of I_0/I towards various concentrations of HIAA, $\frac{I_0}{I}$ vs. concentration was plotted (Figure 7.7). As expected, non-linearity or positive deviation from the concentration axis was observed which strongly evidences the combined effect of both dynamic and static quenching components in the quenching process. Hence, in order to get the calibration graph, $\log(\frac{I_0}{I})$ vs. concentration was plotted. It obeyed linearity in the range 1.0×10^{-5} M to 1.0×10^{-6} M with a limit of detection 4.43×10^{-8} M.

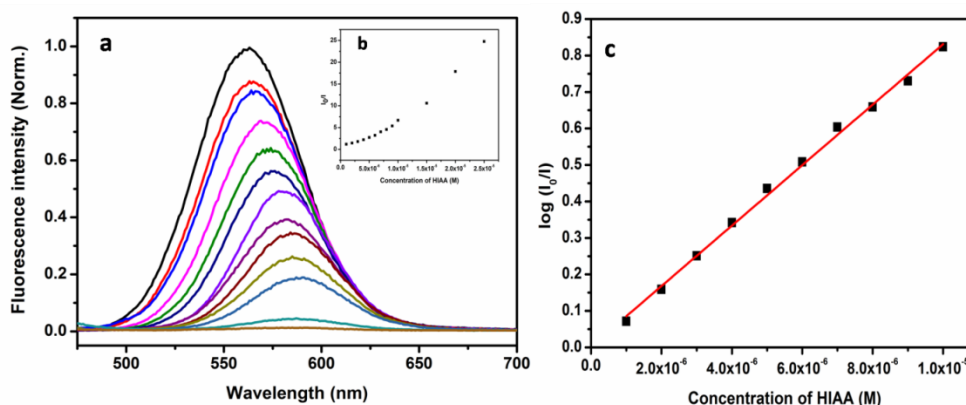


Figure 7.7 a) Fluorescence spectra of QDs in presence of various concentrations of HIAA b) plot of $\frac{I_0}{I}$ vs. concentration of HIAA and c) plot of $\log(\frac{I_0}{I})$ vs. concentration of HIAA.

When both dynamic and static contributions are present, $\frac{I_0}{I}$ behave as per the following second order quadratic equation,⁴²

$$\frac{I_0}{I} = 1 + (K_s + K_d)[Q] + K_s K_d [Q]^2$$

$\left[\frac{I_0}{I} - 1\right] \frac{1}{[Q]}$ vs $[Q]$ was plotted to quantify the static and dynamic quenching constants as the slope of the plot gives $K_s K_d$.

It was observed that the lifetime of the probe changes in presence of HIAA (Figure 7.8). $\frac{\tau_0}{\tau}$ varied linearly with concentration of HIAA in the range 3.0×10^{-5} to 5.0×10^{-7} M ($R^2=0.99$). The slope of the plot is $3.99 \times 10^4 \text{ M}^{-1} \text{ s}^{-1}$ which gives the dynamic quenching constant (K_d) since the dynamic component of the quenching action follows the equation, $\frac{\tau_0}{\tau} = 1 + K_d [Q]$. Thus from $K_s K_d$ and K_d value obtained, K_s value has been calculated which is of the order of 10^5 . This clearly confirms the contribution of static mechanism in the quenching process.

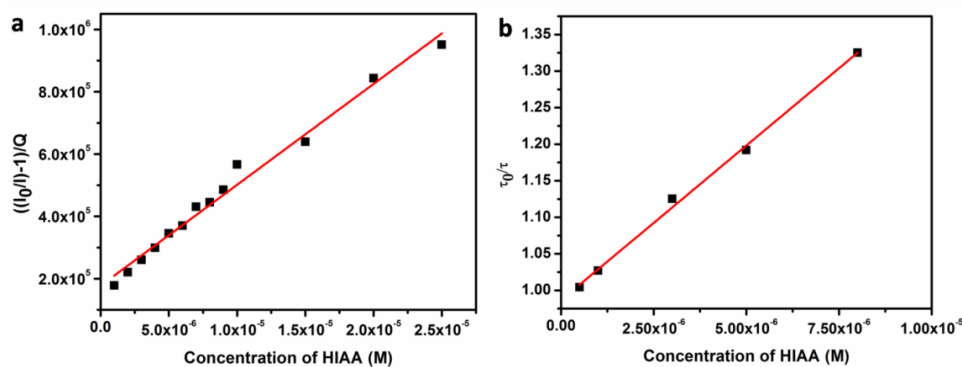


Figure 7.8 a) Plot of $\left[\frac{I_0}{I} - 1\right] \frac{1}{[Q]}$ vs concentration of HIAA b) plot of $\frac{\tau_0}{\tau}$ vs concentration of HIAA

7.3.4.3 Selectivity

The excellence of a chemical sensor is mainly revealed by the selectivity offered by its recognition element towards the analyte. So as to

identify the response of CdTe-MPA QDs towards different neurotransmitters, structurally similar species and possibly co-existing species I_0/I was determined in presence of different species including ST, dopamine, epinephrine, norepinephrine, glycine, melatonin, HIAA, urea, ascorbic acid, creatine, creatinine, glucose, NaCl and KCl. It was found that any of these species other than ST and HIAA did not produce any quenching in the intensity of the QDs even at 1.0×10^{-3} M concentration. This in turn depicts the efficacy of the probe for the sensing of ST as well as HIAA. (Figure 7.9)

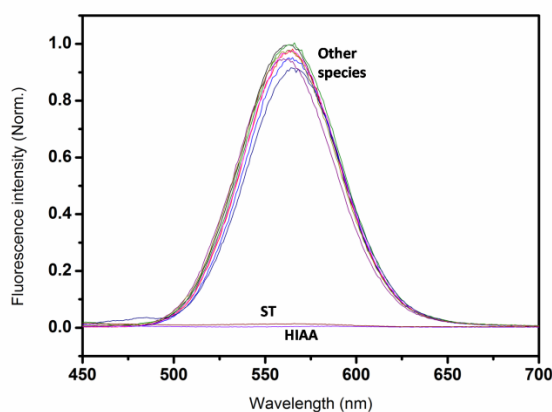


Figure 7.9 Fluorescence spectra of QDs in presence of various species at 1.0×10^{-3} M concentration

7.3.4.4 Effect of foreign species on the determination of ST and HIAA

Effect of different species on the determination of ST as well as HIAA was studied. The various species under focus were the structurally similar species such as melatonin, dopamine, epinephrine, norepinephrine and the species which may be possibly co-existing in the real matrix such as ascorbic acid, glucose, NaCl, KCl, adrenaline, and urea (Table 7.1).

Table 7.1 Effect of foreign species

| Coexisting species | Molar Ratio | % signal change | |
|--------------------|-------------|-----------------|------|
| | | ST | HIAA |
| NaCl | 1 :100 | 1.6 | 2.1 |
| KCl | 1 :100 | 2.6 | 1.9 |
| Dextrose | 1 :100 | 1.2 | 3.1 |
| Creatinine | 1 :100 | 2.4 | 3.2 |
| Creatine | 1 :100 | 1.8 | 1.6 |
| Urea | 1 :100 | 3.4 | 2.4 |
| Dopamine | 1 :100 | 2.1 | 4.2 |
| Adrenaline | 1 :100 | 4.6 | 3.8 |
| Melatonin | 1 :10 | 2.1 | - |
| Melatonin | 1 :1 | - | 3.9 |
| HIAA | 1 :1 | 15.5 | - |
| ST | 1:1 | - | 23.2 |

The interference offered by hundred fold excess concentrations of NaCl, KCl, dextrose, creatinine, creatine, urea, dopamine and epinephrine towards the determination of 5.0×10^{-7} M ST was within the tolerance limit of 5%. Melatonin did not produce any interference up to 10fold excess concentration and the metabolite of ST, HIAA induced interference even at equimolar concentrations. On the other hand, NaCl, KCl, dextrose, creatinine, creatine, urea, dopamine and epinephrine did not offer any interference towards the determination of 5.0×10^{-6} M HIAA. Melatonin did not produce any interference at equimolar concentration whereas ST interfered even at equimolar concentrations.

7.3.4.5 Application study

The performance of the sensor was evaluated by determining ST and HIAA in spiked samples of artificial blood serum and urine with the help of the calibration graph. The results were compared with those obtained from spectroscopic method²⁶⁰ (Table 7.2) and HPLC- UV²⁶¹. Comparable RSD values of the results prove the validity of the sensor.

Table 7.2 Application of the sensor for the determination of ST and HIAA in artificial blood serum

| <i>Developed method</i> | | | | |
|--|---|---|-------------------|------------------------|
| | Added (M) | Found (M) | Recovery % | RSD^a |
| ST | 1.2×10^{-6} - 1.0×10^{-7} | 1.2×10^{-6} - 1.0×10^{-7} | 102 | 2.6 |
| HIAA | 1.0×10^{-5} - 5.0×10^{-7} | 1.0×10^{-5} - 5.0×10^{-7} | 100 | 1.3 |
| <i>Spectrophotometric method²⁶⁰</i> | | | | |
| ST | 3.0×10^{-4} - 1.0×10^{-5} | 3.1×10^{-4} - 1.0×10^{-5} | 102 | 4.0 |
| <i>HPLC- UV²⁶¹</i> | | | | |
| HIAA | 1.0×10^{-3} - 8.0×10^{-5} | 1.0×10^{-3} - 8.0×10^{-5} | 103 | 3.5 |

7.4 Conclusions

The changes in the fluorescence behavior of CdTe QDs induced by ST and its metabolite HIAA have been developed in to a strategy for their determination. In presence of both the analytes, quenching in the fluorescence intensity of QDs has been observed. But interestingly, the fluorescence decay traces of QDs did not show any variations in presence of ST whereas it changed remarkably in presence of HIAA. Spectrophotometric studies and many other techniques were used to confirm the mechanism. The developed strategy enabled the effective quantification of ST within the range 1.2×10^{-6} to 1.0×10^{-7} M and HIAA in the range 1.0×10^{-5} to 1.0×10^{-6} M. The developed sensor was successfully applied for the determination of ST in artificial blood serum and HIAA in artificial urine samples.

.....❧.....

Chapter 8

Summary

Contents

- 8.1 *Developed sensors*
8.2 *Future outlook*
-

Sensitive determination of antioxidants and biomarkers with simple, cost effective and reliable methods is significant in current scenario. The present investigations mainly focused at the development of such sensors based on voltammetric and optical methodologies.

Individual determination of dopamine (DA), individual as well as simultaneous determination of propyl gallate (PG) & tert-butyl hydroquinone (TBHQ) as well as serotonin (ST) & melatonin (MT) were accomplished with voltammetric sensors developed. Determination of dual analytes- cysteamine (Cyste) and glutathione (GSH) was achieved by the colorimetric sensors based on silver nanoparticles. Determination of the dual analytes- ST and its metabolite 5-hydroxyindoleacetic acid (HIAA) was furnished with fluorescent sensors based on CdTe QDs.

The performance characteristics of all the developed sensors were optimized and applied for the determination of target molecules in real or artificial matrices.

8.1 Developed sensors

8.1.1 Voltammetric sensor for the determination of single analyte-DA

| | |
|-------------------------------|--|
| Probe | pAHNSA/CoNP/GCE |
| Analyte | Dopamine |
| Supporting electrolyte | 0.1 M Phosphate buffer solution (pH=7) |
| Linear range | 5.0×10^{-5} M to 5.0×10^{-7} M |
| Limit of detection | 1.8×10^{-8} M |
| Utility in real time analysis | Artificial samples of blood serum, urine and cerebrospinal fluid |

8.1.2 Colorimetric sensor for the determination of dual analytes- Cyste and GSH

| | |
|-------------------------------|---|
| Probe | AgNP-Tyr |
| Analyte | Cysteamine and Glutathione |
| Medium of study | 0.1 M Phosphate buffer solution (pH=7.4) |
| Linear range | GSH- 1.0×10^{-5} M to 5.0×10^{-7} M Cyste - 1.1×10^{-6} M to 5.0×10^{-8} M |
| Limit of detection | GSH - 3.7×10^{-7} M Cyste- 1.8×10^{-8} M |
| Utility in real time analysis | Artificial blood serum |

8.1.3 Voltammetric sensor for individual and simultaneous determination of dual analytes – TBHQ and PG

| | |
|-------------------------------|--|
| Probe | AB/GE |
| Analyte | tert-butyl hydroquinone and propyl gallate |
| Supporting electrolyte | 0.1 M Phosphate buffer solution (pH=2) |
| Linear range | TBHQ - 1.0×10^{-4} M to 3.0×10^{-7} M PG - 1.0×10^{-4} M to 7.0×10^{-8} M |
| Limit of detection | TBHQ - 2.8×10^{-8} M PG - 4.3×10^{-8} M |
| Utility in real time analysis | Spiked samples of coconut oil and butter |

8.1.4 Voltammetric sensor for individual and simultaneous determination of dual analytes – ST and MT

| | |
|-------------------------------|--|
| Probe | AB-C/GE |
| Analyte | Serotonin and melatonin |
| Supporting electrolyte | 0.1 M Phosphate buffer solution (pH=7) |
| Linear range | ST - 1.0×10^{-4} M to 5.0×10^{-7} M MT - 4.5×10^{-4} M to 2.0×10^{-5} M |
| Limit of detection | ST - 1.6×10^{-7} M MT - 1.9×10^{-6} M |
| Utility in real time analysis | Artificial blood serum |

8.1.5 Fluorescence sensor for the determination of dual analytes - ST and HIAA

| | |
|-------------------------------|--|
| Probe | CdTe-MPA |
| Analyte | Serotonin and 5-Hydroxyindole acetic acid |
| Medium of study | Water |
| Linear range | ST - 1.2×10^{-6} M to 1.0×10^{-7} M HIAA - 1.0×10^{-5} M to 1.0×10^{-6} M |
| Limit of detection | ST - 7.6×10^{-8} M HIAA - 4.4×10^{-8} M |
| Utility in real time analysis | Artificial blood serum and urine |

8.2 Future outlook

World of sensors has unveiled numerous applications for monitoring almost everything around us. Future research in sensor technology will be focussed to innovate and improvise sensor devices for *in-vivo* use. Significant progress in this regard can be achieved only by a team of multi-disciplinary researchers from chemistry, physics, biology, materials science, electronics and other related fields. Commercial mass production of portable hand-held, cheap and reliable sensing devices will help to address emerging concerns in medical diagnostics, food quality control, environmental monitoring, defense and industrial manufacturing process. Thus, rapid advancements in field of sensors will improve safety and quality of life.

.....❧.....

References

- 1 G. G. Cammann, E. A. Guilbault, H. Hal, R. Kellner and O. S. Wolfbeis, *The Cambridge Definition of Chemical Sensors, Cambridge Workshop on Chemical Sensors and Biosensors*, Cambridge University Press, New York (1996)
- 2 I. R. Sinclair, *Sensors and Transducers*, Newnes, Boston (2001)
- 3 A. J. Bard and L. R. Faulkner, *Electrochemical Methods: Fundamentals and Applications*, John Wiley & Sons, New York (2001)
- 4 C. M. A. Brett and A. M. O. Brett, *Electrochemistry: Principles, Methods, and Applications*, Oxford University Press, Oxford (1993)
- 5 J. E. B. Randles, *Trans. Far. Soc.*, **44**, 327 (1948)
- 6 R. Holze, *Experimental Electrochemistry: A Laboratory Textbook*, Wiley-VCH, Weinheim (2009)
- 7 L. R. Faulkner, *J. Chem. Educ.*, **60**, 262 (1983)
- 8 D. T. Sawyer, A. Sobkowiak and J. L. Roberts, *Electrochemistry for Chemists*, John Wiley & Sons, New York (1995)
- 9 Z. Galus, *Fundamentals of Electrochemical Analysis*, Ellis Horwood, New York (1994)
- 10 P. T. Kissinger and W. R. Heineman, *Laboratory Techniques in Electroanalytical Chemistry*, Marcel Dekker, New York (1996)
- 11 C. G. Zoski, *Handbook of Electrochemistry*, Elsevier, Amsterdam (2007)
- 12 H. H. Girault, *Analytical and Physical Electrochemistry*, EPFL Press, Lausanne (2004)

References

- 13 X. H. Lin, Y. F. Zhang, W. Chen and P. Wu, *Sens. Actuators B*, **122**, 309 (2007)
- 14 A. J. Bard, *J. Chem. Edu.*, **60**, 302 (1983)
- 15 R. W. Murray, *Acc. Chem. Res.*, **13**, 135 (1980)
- 16 R. W. Murray, A. G. Ewing and R. A. Durst, *Anal. Chem.*, **59**, 379A (1987)
- 17 J. M. Zen, A. S. Kumar and D. M. Tsai, *Electroanal.*, **15**, 1073 (2003)
- 18 A. Salimi, R. Hallaj, S. Soltanian, and H. Mamkhezri, *Anal. Chim. Acta*, **594**, 24 (2007)
- 19 N. J. Wittenberg and C. L. Haynes, *Nanomed. Nanobiotechnol.*, **1**, 237 (2009)
- 20 D. Thomas, Z. Rasheed, J. S. Jagan and K. Girish Kumar, *J. Food Sci. Technol.*, **52**, 719 (2015)
- 21 U. Sivasankaran, A. Thomas, A. R. Jose and K. Girish Kumar, *J. Electrochem. Soc.*, **164**, B292 (2017)
- 22 W. R. Seitz, *Optical Ion Sensing; In: Fiber Optic Chemical Sensors and Biosensors II*, CRC press, Boca Raton, Florida (1991)
- 23 P. Gründler, *Chemical Sensors: An Introduction for Scientists and Engineers*, Springer-Verlag, Berlin, Heidelberg (2007)
- 24 P. C. A. Jerónimo, A. N. Araujo, M. Conceicao and B. S. M. Montenegro, *Talanta*, **72**, 13 (2007)
- 25 W. L. Barnes, A. Dereux and T. W. Ebbesen, *Nature*, **424**, 824 (2003)
- 26 P. K. Jain and M. A. El-Sayed, *Nano Lett.*, **7**, 2854 (2007)
- 27 J. Wilcoxon, *J. Phys. Chem. B*, **113**, 2647 (2009)

-
- 28 P. K. Jain, K. S. Lee, I. H. El-Sayed and M. A. El-Sayed, *J. Phys. Chem. B*, **110**, 7238 (2006)
- 29 L. M. Liz-Marzán, *Langmuir*, **22**, 32 (2006)
- 30 M. Wang, K. Su, J. Cao, Y. She, A. M. A. El-Aty, A. Hacımüftüoğlu, J. Wang, M. Yan, S. Hong, S. Lao, Y. Wang, *Talanta*, **192**, 295 (2019)
- 31 A. Henglein and M. Giersig, *J. Phys. Chem. B*, **103**, 9533 (1999)
- 32 Z. S. Pillai and P. V. Kamat, *J. Phys. Chem. B*, **108**, 945 (2004)
- 33 Q. Yuan and X. Wang, *Nanoscale*, **2**, 2328 (2010)
- 34 T. K. Sau and A.L. Rogach, *Adv. Mater.*, **22**, 1781 (2010)
- 35 C. J. Murphy, T. K. Sau, A. M. Gole, C. J. Orendorff, J. Gao, L. Gou, S. E. Hunyadi and T. Li, *J. Phys. Chem. B*, **109**, 13857 (2005)
- 36 R. Subbiah, M. Veerapandian and K.S. Yun, *Curr. Med. Chem.*, **17**, 4559 (2010)
- 37 J. P. Wilcoxon and B. L. Abrams, *Chem. Soc. Rev.*, **35**, 1162 (2006)
- 38 G. Doria, J. Conde, B. Veigas, L. Giestas, C. Almeida, M. Assunção, J. Rosa and P. V. Baptista, *Sensors*, **12**, 1657 (2012)
- 39 A. P. Demchenko, *Introduction to Fluorescence Sensing*, 2nd Edn., Springer, Switzerland, 1 (2015)
- 40 G. Weber and D. M. Hercules, *Fluorescence and Phosphorescence Analysis. Principles and Applications*, Interscience Publishers, John Wiley & Sons, New York, 217 (1966)
- 41 N. B. D. Lima, S. M. C. Gonçalves, S. A. Júnior and A. M. Simas, *Sci. Rep.*, **3**, 2395 (2013)

References

- 42 J. R. Lakowicz, *Principles of Fluorescence Spectroscopy*, Kluwer Academic and Plenum Publishers, New York (2000)
- 43 A. E. Vikraman, A. R. Jose, M. Jacob and K. Girish Kumar, *Anal. Methods*, **7**, 6791 (2015)
- 44 U. R. Genger, M. Grabolle, S. C. Jaricot, R. Nitschke, T. Nann, *Nat. methods*, **5**, 763 (2008)
- 45 G. G. Guilbault, *Practical Fluorescence*, 2ndEdn., Marcel Dekker, New York (1990)
- 46 https://en.wikipedia.org/wiki/Stokes_shift
- 47 A. R. Jose, A. E. Vikraman and K. Girish Kumar, *New J. Chem.*, **41**, 10828 (2017)
- 48 Quantum Dots and their Applications, <http://www.understandingnano.com/quantum-dots-applications.html>, accessed on 3rd Feb 2019
- 49 U. Resch-Genger, M. Grabolle, S. Cavaliere-Jaricot, R. Nitschke and T. Nann, *Nat. Methods*, **5**, 763 (2008)
- 50 N. Hildebrandt, C. M. Spillmann, W. R. Algar, T. Pons, M. H. Stewart, E. Oh, K. Susumu, S. A. Díaz, J. B. Delehanty and I. L. Medintz, *Chem. Rev.*, **117**, 536 (2017)
- 51 M. Green, *Semiconductor Quantum Dots: Organometallic and Inorganic Synthesis*, RSC nanoscience and nanotechnology, RSC publication, UK (2014)
- 52 L. E. Brus, *J. Chem. Phys.*, **80**, 4403 (1984)
- 53 M. G. Bawendi, P. J. Carroll, W. L. Wilson and L. E. Brus, *J. Chem. Phys.*, **96**, 946 (1992)
- 54 J. A. Kloepfer, S. E. Bradforth and J. L. Nadeau, *J. Phys. Chem. B*, **109**, 9996 (2005)

- 55 I. S. Liu, H. H. Lo, C. T. Chien, Y. Y. Lin, C. W. Chen, Y. F. Chen, W. F. Su and S. C. Liou, *J. Mater. Chem.*, **18**, 675 (2008)
- 56 J. Y. Zhang, X. Y. Wang and M. Xiao, *Opt. Lett.*, **27**, 1253 (2002)
- 57 X. Y. Wang, J. Y. Zhang, A. Nazzal, M. Darragh and M. Xiao, *Appl. Phys. Lett.*, **81**, 4829 (2002)
- 58 M. J. Ruedas-Rama, A. Orte, E. A. H. Hall, J. M. Alvarez-Pez and E. M. Talavera, *Chem. Phys. Chem.*, **12**, 919 (2011)
- 59 M. J. Ruedas-Rama, A. Orte, E. A. H. Hall, J. M. Alvarez-Pez and E. M. Talavera, *Chem. Commun.*, **47**, 2898 (2011)
- 60 M. J. Ruedas-Rama, A. Orte, E. A. H. Hall, J. M. Alvarez-Pez and E. M. Talavera, *Analyst*, **137**, 1500 (2012)
- 61 T. Rajh, O. I. Micic' and A. J. Nozik', *J. Phys. Chem.*, **97**, 11999 (1993)
- 62 J. M. Asha, R. Arunkumar, R. Rajalingam and E. M. Sayed, *Nanosci. Nanotechnol. Lett.*, **3**, 125 (2011)
- 63 X. Ding, L. Qu, R. Yang, Y. Zhou and J. Li, *Luminescence*, **30**, 465 (2015)
- 64 S. Gallaqher, S. Comby, M. Wojdyla, T. Gunnlaugsson, J. M. Kelly, Y. K. Gun'ko, I. P. Clark, G. M. Greetham, M. Towrie and S. J. Quinn, *Inorg. Chem.*, **52**, 4133 (2013)
- 65 P. Kumar, P. Kumar, L. M. Bharadwaj, A. K. Paul, S. C. Sharma, P. Kush and A. Deep, *Bio. Nano. Sci.*, **3**, 95 (2013)
- 66 G. A. Ozin, A. C. Arsenault and L. Cademartiri, *Nanochemistry: A Chemical Approach to Nanomaterials*, RSC Publ., Cambridge. (2009)
- 67 L. Cademartiri and G. A. Ozin, *Concepts of Nanochemistry*, Wiley-VCH, Weinheim (2009)

References

- 68 T. Asefa, C. T. Duncan and K. K. Sharma, *Analyst*, **134**, 1980 (2009)
- 69 D. T. Pierce and J. X. Zhao, *Trace Analysis with Nanomaterials*, Wiley-VCH, Weinheim (2010)
- 70 A. Merkoçi, *Biosensing Using Nanomaterials*, John Wiley & Sons, New York (2009)
- 71 J. Motonaka and L. R. Faulkner, *Anal. Chem.*, **65**, 3258 (1993)
- 72 H. Zhang, C. Hu, W. Lan and S. Hu, *Anal Bioanal. Chem.*, **380**, 303 (2004)
- 73 X. Dang, C. Hu, Y. Wei, W. Chen and S. Hu, *Electroanal.*, **23**, 1949 (2004)
- 74 P. Xie, X. Chen, F. Wang, C. Hu and S. Hu, *Colloids and Surf. B*, **48**, 17 (2006)
- 75 G. Li, Z. Ji and K. Wu, *Anal. Chim. Acta*, **577**, 178 (2006)
- 76 P. Deng, J. Fei, J. Zhang and Y. Feng, *Food Chem.*, **124**, 1231 (2011)
- 77 G. Wang, Y. Dong, X. Zhu, W. Zhang, C. Wang and H. Jiao, *Analyst*, **136**, 5256 (2011)
- 78 X. Wei, Q. Zhao, W. Wu, T. Zhou, S. Jiang, Y. Tong and Q. Lu, *Sensors*, **16**, 1539 (2016)
- 79 X. Yang, F. Wang and S. Hu, *Colloids Surf. B*, **54**, 60 (2007)
- 80 P. Deng, J. Fei and Y. Feng, *J. Electroanal. Chem.*, **648**, 85 (2010)
- 81 P. Deng, Z. Xu, Y. Feng and J. Li, *Sens. Actuators B*, **168**, 381 (2012)

- 82 L. Athouel, P. Arcidiacono, C. Ramirez-Castro, O. Crosnier, C. Hamel, Y. Dandeville, P. Guillemet, Y. Scudeller, D. Guay, D. Belanger and T. Brousse, *Electrochim. Acta*, **86**, 268 (2012)
- 83 Y. Zhang, W. You, Z. Gao and T. Yang, *Croat. Chem. Acta*, **86** (3), 309 (2013)
- 84 P. Deng, Z. Xu and Y. Kuang, *J. Electroanal. Chem.*, **707**, 7 (2013)
- 85 P. Deng, Z. Xu, J. Li and Y. Kuang, *Microchim. Acta*, **180**, 861 (2013)
- 86 P. Deng, Z. Xu, R. Zeng and C. Ding, *Food Chem.*, **180**, 156 (2015)
- 87 C. Guo, C. Chen, Z. Luo and L. Chen, *Anal. Method.*, **4**, 1377 (2012)
- 88 Y. Huang, H. Yan and Y. Tong, *J. Electroanal. Chem.*, **743**, 25 (2015)
- 89 D. Sun and H. Zhang, *Anal. Chim. Acta*, **557**, 64 (2006)
- 90 D. Sun and H. Zhang, *Water Res.*, **40**, 3069 (2006)
- 91 H. Zhang, *Bioelectrochem.*, **68**, 197 (2006)
- 92 X. Yang, M. Gao, H. Hu and H. Zhang, *Phytochem. Anal.*, **22**, 291 (2011)
- 93 H. Zhang, M. Gao and X. Yang, *Colloids Surf. B*, **87**, 378 (2011)
- 94 J. Song, J. Yang, J. Zeng and J. Tan, L. Zhang, *Microchim. Acta*, **171**, 283 (2010)
- 95 P. Deng, Y. Feng and J. Fei, *Microchim. Acta*, **175**, 233 (2011)
- 96 X. Yang, H. Qin, M. Gao and H. Zhang, *J. Sci. Food Agric.*, **91**, 2821 (2011)
- 97 L. Lin, J. Yang, R. Lin, L. Yu, H. Gao, S. Yang and X. Li, *J. Pharm. and Biomed. Anal.*, **72**, 74 (2013)

References

- 98 R. Wang, K. Wu and C. Wu, *Anal. Method.*, **7**, 8069 (2015)
- 99 A. E. Vikraman, Z. Rasheed, L. Rajith, L. A. Lonappan and K. Girish Kumar, *Food Anal. Methods*, **6**, 775 (2013)
- 100 A. Thomas, A. E. Vikraman, D. Thomas and K. Girish Kumar, *Food Anal. Methods*, **8**, 2028 (2015)
- 101 N. Xu, Y. Ding, H. Ai and J. Fei, *Microchim. Acta*, **170**, 165 (2010)
- 102 T. Zhou, Y. Tao, H. Jin, B. Song, T. Jing, D. Luo, Y. Zhou, Y. Zhou, Y. Lee and S. Mei, *Plos One*, 1 (2016)
- 103 H. Shuai, K. Huang and Y. Chen, *J. Mat. Chem.*, **4**, 1185 (2016)
- 104 A. A.Lahcen, S. A.Errayess and A. Amine, *Microchim. Acta*, **183**, 2169 (2016)
- 105 D. Lee, Y. H. Kim and S. Park, *Electrochem. Soc.*, **168 (8)**, G93 (2016)
- 106 W. Yazhen, Q. Hongxin, H. Siqian and X. Junhui, *Sens. Actuators B*, **147**, 587 (2010)
- 107 W. Yazhen, *Bioelectrochem.*, **81**, 86 (2011)
- 108 Y. Huang, M. Chen, X. Li and C. Zhang, *Electroanal.*, **29**, 1141 (2017)
- 109 H. Ibrahim, Y. Temerk and N. Farhan, *Talanta*, **179**, 75 (2018)
- 110 P. Deng, Z. Xu and Y. Feng, *J. Electroanal. Chem.*, **683**, 47 (2012)
- 111 P. Deng, Z. Xu and J. Li, *Microchim. Acta*, **181**, 1077 (2014)
- 112 A. Balamurugan and S. M. Chen, *Anal. Chim. Acta*, **596**, 92 (2007)
- 113 L. J. Murphy, *Anal. Chem.*, **70**, 2928 (1998)
- 114 B. W. Zewde and S. Admassie, *J. Power Sources*, **216**, 502 (2012)

-
- 115 A. Meneguzzi, M. C. Pham, J. C. Lacroix, B. Piro, A. Adenier, C. A. Ferreira and P.C. Lacaze, *J. Electrochem. Soc.*, **148**, B121 (2001)
- 116 H. Bhandari, V. Bansal, V. Choudhary, and S. K. Dhawan, *Polym. Int.*, **58**, 489 (2009)
- 117 A. Geto and C. M. A. Brett, *J. Solid State Electrochem.*, **20**, 2969 (2016)
- 118 M. Amare, W. Lakew and S. Admassie, *Anal. Bioanal. Chem.*, **3**, 4 (2011)
- 119 M. Amare and S. Admassie, *Talanta*, **93**, 122 (2012)
- 120 M. Amare and S. Admassie, *Bull. Chem. Soc. Ethiop.*, **26**, 73 (2012)
- 121 A. Geto, M. Amare, M. Tessema and S. Admassie, *Anal. Bioanal. Chem.*, **404**, 525 (2012)
- 122 A. Geto, M. Amare, M. Tessema and S. Admassie, *Electroanal.*, **24**, 659 (2012)
- 123 M. Amare, S. Abicho and S. Admassie, *J. of AOAC Int.*, **97**, 2 (2014)
- 124 P. Gupta and R. N. Goyal, *Electrochim. Acta.*, **151**, 1 (2015)
- 125 M. Tefera, A. Geto, M. Tessema and S. Admassie, *Food Chem.*, **210**, 156 (2016)
- 126 S. Jesny and K. Girish Kumar, *J. Electroanal. Chem.*, **801**, 153 (2017)
- 127 M. Amare and G. Menkir, *Heliyon*, **3**, 1 (2017)
- 128 S. K. Yadav, B. Agrawal, P. Chandra and R. N. Goyal, *Biosens. Bioelectron.*, **55**, 337 (2014)
- 129 A. Geto, M. Tessema and S. Admassie, *Synth. Met.*, **191**, 135 (2014)
- 130 Rosy, M. Raj and R. N. Goyal, *Sens. Actuators B*, **233**, 445 (2016)

References

- 131 M. Raj, P. Gupta, R. N. Goyal and Y-B.Shim, *Sens. Actuators B*, **239**, 993 (2016)
- 132 P. Gupta and R. N. Goyal, *RSC Adv.*, **5**, 40444 (2015)
- 133 A. J.Haes, D. A. Stuart, S. Nie and R. P. V. Duyne, *J. Fluoresc.*, **14**, 355 (2004)
- 134 J. S. Lee, A. K. R. Lytton-Jean, S. J.Hurst and C. A. Mirkin, *Nano. Lett*, **7**, 2112 (2007)
- 135 Y. Chen, J. Aveyard and R. Wilson, *Chem. Commun.*, 2804 (2004)
- 136 S. H.Liu, Z. H. Zhang andM. Y. Han, *Anal. Chem.*, **77**, 2595 (2005)
- 137 K. Yoosaf, B. I. Ipe,C. H. Suresh and K. G. Thomas, *J. Phys. Chem. C*, **111**, 12839 (2007)
- 138 C. L. Schofield, A. H. Haines, R. A. Field and D. A. Russell, *Langmuir*, **22**, 6707 (2006)
- 139 D. Xiong, M. Chen and H. Li, *Chem. Commun.*, 880 (2008)
- 140 D. R. Bae, W. S. Han, J. M. Lim, S. Kang, J. Y. Lee, D. Kang and J. H. Jung, *Langmuir*, **26**, 2181 (2009)
- 141 J. D. Swartz, C. P. Gulka, F. R. Haselton and D. W. Wright, *Langmuir*, **27**, 15330 (2011)
- 142 S.T. Dubas and V. Pimpan, *Talanta*, **76**, 29 (2008)
- 143 H. Wei, C. Chen, B. Han and E. Wang, *Anal. Chem.*, **80**, 7051 (2008)
- 144 H. Li and Y. Bian, *Nanotechnology*, **20**, 1 (2009)
- 145 H. Li, Z. Cui and C. Han, *Sens. Actuators B*, **143**, 87 (2009)
- 146 M. Nidya, M. Umadevi and B. J. M. Rajkumar, *Spectrochim. Acta Part A*, **133**, 265 (2014)

- 147 H. K. Sung, S. Y. Oh, C. Park and Y. Kim, *Langmuir*, **29**, 8978 (2013)
- 148 Y. Yao, D. Tian and H. Li, *ACS Applied Mat. & Int.*, **2**, 684 (2010)
- 149 G. Wang, Y. Dong, X. Zhu, W. Zhang, C. Wang and H. Jiao, *Analyst*, **136**, 5256 (2011)
- 150 M. Özyürek, N. Güngör, S. Baki, K. Güçlü and R. Apak, *Anal. Chem.*, **84**, 8052 (2012)
- 151 M. Elavarasi, A. Rajeshwari, S. A. Alex, D. N. Kumar, N. Chandrasekaran and A. Mukherjee, *Anal. Methods*, **6**, 5161 (2014)
- 152 G. Wang, X. Xu, L. Cao, C. He, Z. Lia and C. Zhang, *RSC Adv.*, **4**, 5867 (2014)
- 153 S. K. Vaishnav, K. Patel, K. Chandraker, J. Korram, R. Nagwanshi, K. K. Ghosh and M. L. Satnami, *Spectrochim. Acta Part A*, **179**, 155 (2017)
- 154 S. Ma, J. He, M. Guo, X. Sun, M. Zheng and Y. Wang, *Colloids Surf. A*, **538**, 343 (2018)
- 155 Z. Chen, X. Zhang, H. Caoa and Y. Huang, *Analyst*, **138**, 2343 (2013)
- 156 Y. Ma, H. Niu, X. Zhang and Y. Cai, *Chem. Commun.*, **47**, 12643 (2011)
- 157 J. V. Rohit, J. N. Solanki and S. K. Kailasa, *Sens. Actuators B*, **200**, 219 (2014)
- 158 V. V. Kumar and S. P. Anthony, *Anal. Chim. Acta*, **842**, 57 (2014)
- 159 D. Su, X. Yang, Q. Xia, Q. Zhang, F. Chai, C. Wang and F. Qu, *Nanotechnology*, **25**, 1 (2014)

References

- 160 J. Duan, H. Yin, R. Wei and W. Wang, *Biosens. Bioelec.*, **57**, 139 (2014)
- 161 A. Nayal, A. Kumar, R. K. Chhatra and P. S. Pandey, *RSC Adv.*, **4**, 39866 (2014)
- 162 Z. Cheng, G. Li, N. Zhang and H. Liu, *Dalton Trans.*, **43**, 4762 (2014)
- 163 K. B. A. Ahmed, R. Senthilnathan, S. Megarajan and V. Anbazhagan, *J. Photochem. Photobio.*, **151**, 39 (2015)
- 164 P. P. Kumar, L. Kathuria and V. Haridas, *New J. Chem.*, **40**, 8382 (2016)
- 165 D. K. Ban and S. Paul, *Applied Surf. Sci.*, **458**, 245 (2018)
- 166 Y. Bhattacharjee, D. Chatterjee and A. Chakraborty, *Sens. Actuators B*, **255**, 210 (2018)
- 167 R. Rajamanikandan M. Ilanchelian, *Mat. Today Commun.*, **15**, 61 (2018)
- 168 P. Jarujamrus, M. Amatatongchai, A. Thima, T. Khongrangdee and C. Mongkontong, *Spectrochim. Acta Part A*, **142**, 86 (2015)
- 169 R. P. Modi, V. N. Mehta and S. K. Kailasa, *Sens. Actuators B*, **195**, 562 (2014)
- 170 K. Patel, J. R. Bhamore, T. J. Park and S. K. Kailasa, *Chem. Select*, **3**, 10182 (2018)
- 171 P. Joshi, S. Sarkar, S. K. Soni and D. Kumar, *Polyhedron*, **120**, 142 (2016)
- 172 N. Yang, Y. Gao, Y. Zhang, Z. Shen and A. Wu, *Talanta*, **122**, 272 (2014)

- 173 P. Joshi, R. Painuli and D. Kumar, *ACS Sust. Chem. Engg.*, **5**, 4552 (2017)
- 174 R. Painuli, P. Joshi and D. Kumar, *Sens. Actuators B*, **272**, 79 (2018)
- 175 R. Hu, L. Zhang and H. Li, *New J. Chem.*, **38**, 2237 (2014)
- 176 L. Chen, Y. Ye, H. Tan and Y. Wang, *Colloids Surf. A*, **478**, 1 (2015)
- 177 G. Wu, C. Dong, Y. Li, Z. Wang, Y. Gao and Z. Shen, A. Wu, *RSC Adv.*, **5**, 20595 (2015)
- 178 Y. Qi, Z. Qu, Q. Wang, M. Zhang and G. Shi, *Anal. Chim. Acta*, **980**, 65 (2017)
- 179 Y. Ye, Y. Guo, Y. Yue, H. Huang, L. Zhao, Y. Gao and Y. Zhang, *Anal. Methods*, **7**, 566 (2015)
- 180 A. Contino, G. Maccarrone, M. Zimbone, R. Reitano, P. Musumeci, L. Calcagno and I.P. Oliveri, *J. Colloid Interface Sci.*, **462**, 216 (2016)
- 181 J. Peng, G. Liu, D. Yuan, S. Feng and T. Zhou, *Talanta*, **167**, 310 (2017)
- 182 X. Gao, Y. Lu, S. He, X. Li and W. Chen, *Anal. Chim. Acta*, **879**, 118 (2015)
- 183 M. Ihsan, A. Niaz, A. Rahim, M. I. Zaman, M. B. Arain, Sirajuddin, T. Sharif and M. Najeeb, *RSC Adv.*, **5**, 91158 (2015)
- 184 S. Lee, Y. Nam, H. Lee, Y. Lee and K. Lee, *Sens. Actuators B*, **237**, 643 (2016)
- 185 K. Noh, Y. Nam, H. Lee and K. Lee, *Analyst*, **140**, 8209 (2015)
- 186 V. Balakumar, P. Prakash, K. Muthupandi and A. Rajan, *Sens. Actuators B*, **241**, 814 (2017)

References

- 187 R. Choudhury and T. K. Misra, *Colloids Surf. A*, **545**, 179 (2018)
- 188 K. Phoonsawat, N. Ratnarathorn, C. S. Henry and W. Dungchai, *Analyst*, **143**, 3867 (2018)
- 189 H. Wang, D. Chen, L. Yu, M. Chang and L. Ci, *Spectrochim. Acta Part A*, **137**, 281 (2015)
- 190 K. B. A. Ahmed, M. Mariappan and A. Veerappan, *Sens. Actuators B*, **244**, 831 (2017)
- 191 H. Hassanvand and P. Hashemi, *Anal. Sci.*, **34**, 568 (2018)
- 192 S. S. J. Xavier, C. Karthikeyan, G. G. Kumar, A. R. Kim and D. J. Yoo, *Anal. Methods*, **6**, 8165 (2014)
- 193 Q. Ma, J. Song, S. Zhang, M. Wang, Y. Guo and C. Dong, *Colloids Surf. B*, **148**, 66 (2016)
- 194 D. C. M. Ferreira, G. F. Giordano, C. C. D. S. P. Soares, J. F. A. D. Oliveira, R. K. Mendes, M. H. Piazzetta, A. L. Gobbi and M. B. Cardoso, *Talanta*, **141**, 188 (2015)
- 195 J. Peng, J. Ling, X. Zhang, L. Zhang, Q. Cao and Z. Ding, *Sens. Actuators B*, **221**, 708 (2015)
- 196 S. L. D'souza, R. Pati and S. K. Kailasa, *Appl. Nanosci.*, **5**, 747 (2015)
- 197 A. K. Parmar, N. N. Valand, K. B. Solanki and S. K. Menon, *Analyst*, **141**, 1488 (2016)
- 198 L. Hu, S. Hu, L. Guo, T. Tang and M. Yang, *Anal. Methods*, **8**, 4903 (2016)
- 199 S. Menon, A. R. Jose, S. Jesny and K. G. Kumar, *Anal. Methods*, **8**, 5801 (2016)
- 200 E. Detsri and P. Seehara, *Colloids Surf. A*, **533**, 125 (2017)

-
- 201 Y. Gao, Y. Wu and J. Di, *Spectrochim. Acta Part A*, **173**, 207 (2017)
- 202 S. Mohammadi and G. Khayatian, *Spectrochim. Acta Part A*, **185**, 27 (2017)
- 203 P. J. Rivero, E. Ibañez, J. Goicoechea, A. Urrutia, I. R. Matias and F. J. Arregui, *Sens. Actuators B*, **251**, 624 (2017)
- 204 K. Rajar, Sirajuddin, A. Balouch, M.I.Bhanger, M. T. Shah, T. Shaikh and S. Siddiqu, *Applied Surf. Sci.*, **435**, 1080 (2018)
- 205 E. Zor, *Talanta*, **184**, 149 (2018)
- 206 S. Rostami, A. Mehdinia, A. Jabbari, E. Kowsari, R. Niroumand and T. J. Booth, *Sens. Actuators B*, **271**, 64 (2018)
- 207 A. Amirjani and D. H. Fatmehsari, *Talanta*, **176**, 242 (2018)
- 208 M. T. Alula, L. Karamchand, N. R. Hendricks and J. M. Blackburn, *Anal. Chim. Acta*, **1007**, 40 (2018)
- 209 M. Jafari, J. Tashkhourian and G. Absalan, *Talanta*, **178**, 870 (2018)
- 210 F. Li, J. Liu, Y. Hu, N. Deng and J. He, *Talanta*, **186**, 330 (2018)
- 211 S. Basiri, A. Mehdinia and A. Jabbari, *Colloids Surf. A*, **545**, 138 (2018)
- 212 A. Arshad, H. Wang, X. Bai, R. Jiang, S. Xu and L. Wang, *Spectrochim. Acta Part A*, **206**, 16 (2019)
- 213 J. H. Wang, H. Q. Wang, H. L. Zhang, X. Q. Li, X. F. Hua, Y. C. Cao, Z. L. Huang and Y. D. Zhao, *Anal. Bioanal. Chem.*, **388**, 969 (2007)
- 214 X. L. Diao, Y. S. Xia, T. L. Zhang, Y. Li and C. Q. Zhu, *Anal. Bioanal. Chem.*, **388**, 1191 (2007)

References

- 215 J. H. Wang, H. Q. Wang, H. L. Zhang, X. Q. Hua, X. F. Hua, Z. L. Huang and Y. D. Zhao, *Colloids Surf. A*, **305**, 48 (2007)
- 216 Y. Yu, Y. Lai, X. Zheng, J. Wu, Z. Long and C. Liang, *Spectrochim. Acta Part A Mol. Biomol. Spectrosc.*, **68**, 1356 (2007)
- 217 H. Li and F. Qu, *Chem. Mater.*, **19**, 4148 (2007)
- 218 Y.S. Xia and C.Q. Zhu, *Talanta*, **75**, 215 (2008)
- 219 J. F. Sun, C.L. Ren, L. H. Liu and X. G. Chen, *Chin. Chem. Lett.*, **19**, 855 (2008)
- 220 J. Yuan, W. Guo and E. Wang, *Anal. Chem.*, **80**, 1141 (2008)
- 221 Y.Q. Wang, C. Ye, Z.H. Zhu and Y.Z. Hu, *Anal. Chim. Acta*, **610**, 50 (2008)
- 222 J. Du, Y. Wu, X. Hao and X. Zhao, *J. Mol. Struct.*, **1006**, 650 (2011)
- 223 E. J. L. Martinez, L. M. Garcia, M.L. F. de Cordova, J.L.M. Santos, S.S.M. Rodrigues and A. R. Medina, *Food Addit. Contam. Part A-Chem.*, **30**, 1485 (2013)
- 224 R. Q. Aucelio, A. I. P. Cordoves, J. L. X. Lima, A. B. B. Ferreira, A. M. E. Guas, and A. R. da Silva, *Spectrochim. Acta*, **100**, 155 (2013)
- 225 L. M. García, E. J. L. Martínez, M. L. F. de Córdoba, J. L. M. Santos, S. S. M. Rodrigues and A. R. Medina, *J. Pharm. Biomed. Anal.*, **80**, 147 (2013)
- 226 L. M. Garcia, J. L. M. Santos, A. R. Medina and E. J. L. Martinez, *J. Food Drug Anal.*, **21**, 426 (2013)
- 227 A. R. Medina, L. M. Garcia, E.J. L. Martinez, J. L. M. Santos and M. L. F. de Cordova, *Curr. Pharm. Anal.*, **9**, 237 (2013)
- 228 P. Wu, Y. Li and X. P. Yan, *Anal. Chem.*, **81**, 6252 (2009)

- 229 L. Zhang, C. Xu and B. Li, *Microchim. Acta.*, **166**, 61 (2009)
- 230 L. Shang, L. Zhang and S. Dong, *Analyst*, **134**, 107 (2009)
- 231 S. Ge, C. Zhang, Y. Zhu, J. Yu and S. Zhang, *Analyst*, **135**, 111 (2010)
- 232 X. Wang, Y. Lv and X. Hou, *Talanta*, **84**, 382 (2011)
- 233 F. Yang, Q. Ma, W. Yu and X. Su, *Talanta*, **84**, 411(2011)
- 234 W. Zhong, C. Zhang, Q. Gao and H. Li, *Microchim. Acta*, **176**, 101(2012)
- 235 O. Adegoke, E. Hosten, C. McClelland and T. Nyokong, *Anal. Chim. Acta*, **721**, 154 (2012)
- 236 S. S .M. Rodrigues, A. S. Lima, L. S. G. Teixeira, M. G. A. Korn and J. L. M. Santos, *Fuel*, **117**, 520 (2014)
- 237 M. Cao, C. Cao, M. Liu, P. Wang and C. Zhu, *Microchim. Acta*, **165**, 341 (2009)
- 238 P. Wu and X.P. Yan, *Biosens. Bioelectron.*, **26**, 485 (2010)
- 239 J. Yuan, W. Guo, J. Yin and E. Wang, *Talanta*, **77**, 1858 (2009)
- 240 X. Li, Y. Zhou, Z. Zheng, X. Yue, Z. Dai, S. Liu and Z. Tang, *Langmuir*, **25**, 6580 (2009)
- 241 F. Qu, X. Zhou, J. Xu, H. Li and G. Xie, *Talanta*, **78**, 1359 (2009)
- 242 Z. Zheng, X. Li, Z. Dai, S. Liu and Z. Tang, *J. Mater. Chem.*, **21**, 16955(2011)
- 243 R. Kuang, X. Kuang, S. Pan, X. Zheng, J. Duan and Y. Duan, *Microchim. Acta*, **169**, 109 (2010)
- 244 Y. Chen, Z. Chen, Y. He, H. Lin, P. Sheng, C. Liu, S. Luo and Q. Cai, *Nanotechnology*, **21**,1 (2010)

References

- 245 M. Zhang, X. Cao, H. Li, F. Guan, J. Guo, F. Shen, Y. Luo, C. Sun and L. Zhang, *Food Chem.*, **135**, 1894 (2012)
- 246 S. Li, Z. Ga and N. Shao, *Talanta*, **129**, 86 (2014)
- 247 Z. Liu, S. Liu, X. Wang, P. Li and Y. He, *Sens. Actuators B*, **176**, 1147 (2013)
- 248 S. Huang, F. Zhu, H. Qiu, Q. Xiao, Q. Zhou, W. Su and B. Hu, *Colloids Surf. B*, **117**, 240 (2014)
- 249 Y. Shen, S. Liu, J. Yang, L. Wang, X. Tan and Y. He, *Sens. Actuators B*, **199**, 389 (2014)
- 250 L. Ding, B. Zhang, C. Xu, J. Huang and Z. Xia, *Anal. Methods*, **8**, 2967 (2016)
- 251 G. Jin, Y. Zhang and W. Cheng, *Sens. Actuators B*, **107**, 528 (2005)
- 252 L. Zou, Z. Gu, N. Zhang, Y. Zhang, Z. Fang, W. Zhu and X. Zhong, *J. Mater. Chem.*, **18**, 2807 (2008)
- 253 R. M. Kark, J. R. Lawrence, V. E. Pollack, C. L. Pirani, R. C. Muehrcke, H. Silva, A primer of urinalysis, second ed., Hoeber Medical Division, Harper & Row, New York (1964)
- 254 Ringer's solution (pH 7.3-7.4), Cold Spring Harb. Protoc. (2008). doi:10.1101/pdb.rec11273
- 255 Artificial cerebrospinal fluid (ACSF), Cold Spring Harb. Protoc. (2011), doi:10.1101/pdb.rec065730
- 256 X. Lin, Y. Ni and S. Kokot, *Anal. Chim. Acta*, **765**, 54 (2013)
- 257 J. Sedllak and R.H. Lindsay, *Anal. Biochem.*, **25**, 192 (1968)
- 258 A. K. Mishra, A. Mishra and P. Chattopadyay, *Arch. Appl. Sci. Res.*, **2**, 251 (2010)

- 259 AOAC, Official Methods of Analysis of the Association of Official Analytical Chemists, p. 1140 (15thed.) Virginia: Arlington (1990)
- 260 Q. Jin, L. Shan, J. Yue and X. Wang, *Food Chem.*, **108**, 779 (2008)
- 261 P. S. Draganac, S. J. Steindei and W. G. Trawick, *Clin. Chem.*, **26**, 910 (1980)
- 262 H. R. Zare, N. Rajabzadeh, N. Nasirizadeh and M. M. Ardakani, *J. Electroanal. Chem.*, **589**, 60 (2006)
- 263 C. Missale, S. R. Nash, S. W. Robinson, M. Jaber and M. G. Caron, *Physiol. Rev.*, **78**, 189(1998)
- 264 M. Wightman, L. J. May and A.C. Michael, *Anal. Chem.*, **60**, 769A(1988)
- 265 J. Chen, Y. P. Shi and J.Y. Liu, *J. Chromatogr. A*, **1003**, 127(2003)
- 266 G. H. Ragab, H. Nohta and K. Zaitso, *Anal. Chim. Acta*, **403**, 155 (2000)
- 267 J. J. B. Nevado, J. M. L. Gallego and P. B. Lauguna, *J. Pharm. Biomed. Anal.*, **14**, 571 (1996)
- 268 Y. S. Zhao, S. L. Zhao, J. M. Huang and F. G. Ye, *Talanta*, **85**, 2650 (2011)
- 269 J. Kim, M. Jeon, K. J. Paeng and I. R. Paeng, *Anal. Chim. Acta*, **619**, 87 (2008)
- 270 Y. Li, H. Song, L. Zhang, P. Zuo, J. Yao and W. Chen, *Biosens. Bioelectron.*, **78**, 308 (2016)
- 272 T. Gan, J. Sun, Q. Wu, Q. Jing and S. Yu, *Electroanal.*, **25**, 1505 (2013)
- 273 A. M. Bond (1980) *Modern Polarographic Methods in Analytical Chemistry*. Marcel Dekker, New York

References

- 274 F. Wang, C. Chi, B. Yu and B. Ye, *Sens. Actuators B*, **221**, 1586 (2015)
- 275 X. Zhuang, H. Wang, T. He and L. Chen, *Microchim. Acta*, **183**, 3177 (2016)
- 276 V. Mani, M. Govindasamy, S. Chen, R. Karthik and S. Huang, *Microchim. Acta*, **183**, 2267 (2016)
- 277 S. F. Rahman, K. Min, S. Park, J. Park, J. C. Yoo and D. Park, *Biotechnol. Bioprocess Eng.*, **21**, 627 (2016)
- 278 G. V. R. Reddy, T. M. Reddy, P. V. Narayana, P. Gopal and K. Reddaiah, *Indian J. Adv. Chem. Sci.*, **4(3)**, 250 (2016)
- 279 D. Uzun, A.B. Gunduzalp and E. Hasdemir, *J. Electrochem. Soc.*, **747**, 68 (2015)
- 280 Y. Liu and S. Zhao, *Asian J. Chem.*, **26(3)**, 677 (2014)
- 281 A. J. S. Ahammed, N. C. D. Nath, G. Xu, S. Kim and J. Lee, *J. Electrochem. Soc.*, **158(6)**, F106 (2011)
- 282 M. Pivato, M. F. Prats and A. Masi, *Arch. Biochem. Biophys.*, **560**, 83 (2014)
- 283 A. Safavi, N. Maleki, E. Farjami and F. A. Mahyari, *Anal. Chem.*, **81**, 7538 (2009)
- 284 R. N. Appala, S. Chigurupati, R. V. V. S. S. Appala, K. K. Selvarajan and J.I. Mohammad, *Scientifica*, **2016**, 1 (2016)
- 285 I. Rahman, A. Kode and S. K. Biswas, *Nat. Protoc.*, **1**, 3159 (2006)
- 286 T. E. Tipple and L. K. Rogers, *Methods Mol. Biol.*, **889**, 315 (2012)
- 287 H. Kataoka, Y. Imamura, H. Tanaka and M. Makita, *J. Pharm. Biomed. Anal.*, **11**, 963 (1993)

- 288 A. R. Sarkar, C. H. Heo, E. Kim, H.W. Lee, H. Singh, J. J. Kim, H. Kang, C. Kang and H. M. Kim, *Chem. Commun.*, **51**, 2407 (2015)
- 289 A. Bishayee, D.V. Rao and R.W. Howell, *Acta Oncol.*, **39**, 713 (2000)
- 290 M. Stachowicz, B. Lehmann, A. Tibi, P. Prognon, V. Daurat and D. Pradeau, *J. Pharm. Biomed. Anal.*, **17**, 767 (1998)
- 291 M.B. Pagès, J.M. Canals, F.P. Cordelières, J.A. Parker, J.R. Pineda, G. Grange, E.A. Bryson, M. Guillermier, E. Hirsch, P. Hantraye, M.E. Cheetham, C. Néri, J. Alberch, E. Brouillet, F. Saudou and S. Humbert, *J. Clin. Invest.*, **116**, 1410 (2006)
- 292 G. Liu, Z. Wang, D. Wu, A. Zhou and G. Liu, *Livest. Sci.*, **122**, 86 (2009)
- 293 P. Zhu, T. Oe and I. A. Blair, *Rapid Commun. Mass Spectrom.*, **22**, 432 (2008)
- 294 L. P. Yap, H. Sancheti, M. D. Ybanez, J. Garcia, E. Cadenasand D. Han, *Methods Enzymol.*, **473**,137 (2010)
- 295 U. Sivasankaran, S. Jesny, A. R. Jose and K.Girish Kumar, *Anal. Sci.*, **33**, 281 (2017)
- 296 M. Hsiung, Y.Y. Yeo, K. Itiaba and J.C. Crawhall, *Biochem. Med.*, **19**, 305 (1978)
- 297 A. J. Jonas and J. A. Schneider, *Anal. Biochem.*, **114**, 429 (1981)
- 298 R. A. Garcia, L. L. Hirschberger and M. H. Stipanuk, *Anal. Biochem.*, **170**, 432 (1988)
- 299 L.A. Smolin and J.A. Schneider, *Anal. Biochem.*, **168**, 374 (1988)
- 300 B. Rezaei, H. Khosropour and A.A. Ensafi, *Ionics*, **20**, 1335 (2014)

References

- 301 T. B. Wei, J. F. Chen, X. B. Cheng, H. Li, B. B. Han, Y. M. Zhang, H. Yao and Q. Lin, *Org. Chem. Front.*, **4**, 210 (2017)
- 302 Q. Lin, T. T. Lu, X. Zhu, T. B. Wei, H. Li and Y. M. Zhang, *Chem. Sci.*, **7**, 5341 (2016)
- 303 S. Jesny, S. Menon and K. Girish Kumar, *RSC Adv.*, **6**, 75741 (2016)
- 304 L. Li and B. Li, *Analyst*, **134**, 1361 (2009)
- 305 K. B. Walters and D. Zhang, *J. Phys. Chem. C*, **117**, 27146 (2013)
- 306 X. Li, J. J. Lenhart and H. W. Walker, *Langmuir*, **26**, 16690 (2010)
- 307 K. Siriwardana, A. Wang, M. Gadogbe, W. E. Collier, N. C. Fitzkee and D. Zhang, *J. Phys. Chem. C Nanomater. Interfaces*, **119**, 2910 (2015)
- 308 B. O. Leung, F. Jalilehv, V. Mah, M. Parvez and Q. Wu, *Inorg. Chem.*, **52**, 4593 (2013)
- 309 F. Shahidi, Handbook of Antioxidants for Food Preservation, p.53, Woodhead Publishing Series in Food Science, Technology and Nutrition (2015)
- 310 S. N. Robledo, M. A Zón, C. D. Ceballos and H. Fernández, *Food Chem.*, **127**, 1361 (2011)
- 311 Y. Guan, Q. Chu, L. Fu, T. Wu and J. Ye, *Food Chem.*, **94**, 157 (2006)
- 312 W. Liu, K. Zhang, J. Yu and Y. A. Bi, *Food Anal. Methods.*, doi:10.1007/s12161-017-0891-5 (2017)
- 313 L. F. Capitan-Vallvey, M. C. Valencia and E. A. Nicolas, *Anal. Chim. Acta*, **503**, 179 (2004)

- 314 X. Yue, W. Zhu, S. Ma, S. Yu, Y. Zhang, J. Wang, Y. Wang, D. Zhang and J. Wang, *J. Agric. Food Chem.*, **64**, 706 (2016)
- 315 T. O. Monteiro, S. Y. Neto, F. S. Damos and R. C. S. Luz, *J. Electroanal. Chem.*, **774**, 36 (2016)
- 316 S. T. Cyriac, D. Thomas, A. E. Vikraman and K. Girish Kumar, *J. Electrochem. Soc.*, **163**, B683 (2016)
- 317 K. Robards and S. Dilli, *Analyst*, **112**, 933 (1987)
- 318 T. G. Diaz, A. G. Cabanillas, M. F. A. Franco, F. Salinas and J. C. Vire, *Electroanalysis*, **10**, 497 (1998)
- 319 G. Ziyatdinova, K. Os'kina, E. Ziganshina and H. Budnikov, *Anal. Methods*, **7**, 8344 (2015)
- 320 Y. Ni, L. Wang and S. Kokot, *Anal. Chim. Acta*, **412**, 185 (2000)
- 321 A. A. H. Rocha, M. Casagrande, L. S. Schaumlöffel, Y. P. Silva and C. M. S. Piatnicki, *Energy Fuels*, DOI: 10.1021/acs.energyfuels.7b00204 (2017)
- 322 M. Li, Y. Qi, Y. Ding, Q. Zhao, J. Fei and J. Zhou, *Sens. Actuators B*, **168**, 329 (2012)
- 323 R. Wang, K. Wu and C. Wu, *Anal. Methods*, **7**, 8069 (2015)
- 324 A. Thomas, U. Sivasankaran and K. Girish Kumar, *Spectrochim. Acta Part A*, **188**, 113 (2018)
- 325 U. Sivasankaran, A. E. Vikraman, D. Thomas and K. Girish Kumar, *Food Anal. Methods*, **9**, 2115 (2016)
- 326 Z. Rasheed, A. E. Vikraman, D. Thomas, J. S. Jagan and K. Girish Kumar, *Food Anal. Methods*, **8**, 213 (2015)
- 327 S. Ghoreishi and N. Behpour, *Food Chem.*, **132**, 637 (2012)
- 328 D. C. Fuente, J. A. Acuna, M. D. Vazquez, L. M. Tascon and P. S. Batanero, *Talanta*, 441 (1999)

References

- 329 R. Pauliukaite, M. E. Ghica, O. F. Filho and C. M. A. Brett, *Electrochim. Acta*, **55**, 6239 (2010)
- 330 F. Anson, W. Z. Huang and X. X. Gao, *Electrochemistry and electroanalytical chemistry*, Beijing University Press, Beijing (1983)
- 331 T. Marketa, C. Jaromira, N. Tomas and S. Renata, *Energy Fuels*, **28**, 4731 (2014)
- 332 Z. Wang, F. Yang, H. Zheng, X. Quin, J. Luo, Y. Li and D. Xiao, *Analyst*, **139**, 316 (2014)
- 333 A. T. Araujo, J. A. M. Barbosa, H. L. Viana and V. S. Ferreira, *Fuel*, **90**, 707 (2011)
- 334 L. Augi, L. M. A. Huertaz, Y. P. Seden and J. M. Pingarron, *Electroanal. Chem.*, **414**, 141 (1996)
- 335 Y. Dai, L. Xueyan, L. Fan, X. Lu and X. Kan, *Biosens. Bioelec.*, **86**, 741 (2016)
- 336 T. N. Wise, L. M. Arnold and V. Maletic, *CNS Spectr.*, **10**, 1 (2005)
- 337 M. T. Lin, H. J. Tsay, W. H. Su and H. Y. Cheuh, *Am. J. Physiol.*, **274**, 1260 (1998)
- 338 G. K. Isbister, S. J. Bowe, A. Dawson and I. M. Whyte, *Clin. Toxicol.*, **42**, 277 (2004)
- 339 R. J. Reiter, *News Physiol. Sci.*, **1**, 202 (1986)
- 340 C. A. Medeiros, P. F. C. Bruin, L. A. Lopes, M. C. Magalhaes, M. L. Seabra and V. D. Bruin, *J. Neurol.*, **254**, 459 (2007)
- 341 K. Petrie, A.G. Dawson, L. Thompson and R. Brook, *Biol. Psychiatry*, **33**, 526 (1993)
- 342 R. J. Reiter et al., *J. Pineal Res.*, **18**, 1 (1995)

- 343 C. Ruzsas and B. Mess, *NeuroendocrinolLett.*, **21**, 17 (2000)
- 344 M. C. Ortega, J. J. Laserna, A. Reyes and M. Morell, *Anal. Lett.*, **19**, 1097 (1986)
- 345 T. Harumi, H. Akutsu and S. Matsushima, *J.Chromatogr. B Biomed Appl.*, **675**, 152 (1996)
- 346 J. Cao, S. J. Murch, R. O'Brien and P. K. Saxena, *J.Chromatogr. A*, **1134**, 333 (2006)
- 347 P. N. Manikandan and V. Dharuman, *Electroanal.*, **29**, 1524 (2017)
- 348 N. Alpar, P. T. Pinar, Y. Yardım and Z. Senturk, *Electroanal.*, **29**, 1691 (2017)
- 349 H. Zeinali, H. Bagheri, Z. M. Khoshhesab, H. Khoshsafar and A. Hajian, *Mater. Sci. Eng. C*, **71**, 386 (2017)
- 350 N. Kumar and R. N. Goyal, *Current Pharm. Anal.*, **13**, 85 (2017)
- 351 J. Smajdor, R. Piech, M. Pięk and B. P. Bator, *J. Electroanal. Chem.*, **799**, 278 (2017)
- 352 F. H. Cincotto, D. A. S. Carvalho, T. C. Canevari, H. E. Toma, O. F. Filho and F. C. Moraes, *RSC Adv.*, **8**, 14040 (2018)
- 353 F. J. V. Gomez, A. Martín, M. F. Silva and A. Escarpa, *Microchim. Acta*, **182**, 1925 (2015)
- 354 A. Thomas and K. Girish Kumar, *J. Electrochem. Soc.*, **165**, B351 (2018)
- 355 G. Jin, Z. Mingang, Y. Shijian, Y. Xiaoyan and W. Shiwei, *Ionics*, doi:10.1007/s11581-017-2351-z (2017)
- 356 X. Zhu, T. N. L. Doan, Y. Yu, Y. Tian, K. E. K. Sun, H. Zhao and P. Chen, *Ionics*, **22**, 71 (2016)

References

- 357 J. Kalaiselvi, M. Sundararajan and M. R.Prabhu, *Ionics*, doi: 10.1007/s11581-018-2485-7(2018)
- 358 M. Rinaudo, *Prog.Polym. Sci.*, **31**, 603 (2006)
- 359 Q. Xiao, M. Feng, Y. Liu, S. Lu, Y.He and S. Huang, *Ionics*, **24**, 845 (2018)
- 360 W. Yazhen, Q. Hongxin, H. Siqian and X. Junhui, *Sens. Actuat. B*, **147**, 587 (2010)
- 361 R. Guidelli, R. G. Compton, J. M. Feliu, E. Gileadi, J. Lipkowski, W. Schmickler and S. Trasatti, *Pure Appl. Chem.*, **86**, 245 (2014)
- 362 W. X. Ping, Z. Lan, L. W. Rong, D. J. Ping, C. H. Qing and C. G. Nan, *Electroanal.*, **14**, 1654 (2002)
- 363 J. Li and X. Lin, *Sens. Actuators B*, **124**, 486 (2007)
- 364 A. Radi and G. E. Bekhiet, *Bioelectrochem. Bioenerg.*, **45**, 275 (1998)
- 365 Y. Sun, J. Fei, J. Hou, Q. Zhang, Y. Liu and B. Hu, *Microchim. Acta*, **165**, 373 (2009)
- 366 M. Z.Wrona and G. Dryhurst, *J. Org. Chem.*, **52**, 2817 (1987)
- 367 R. S. Nicholson and I. Shain, *Anal. Chem.*, **36**, 706 (1964)
- 368 M. Najafi, M. A.Khalilzadeh and H. A. Karimi-Maleh, *Food. Chem.*, **158**, 125 (2014)
- 369 P. Liu, M. Dong, J. Lu, H.Guo, X. Lu and X. Liu, *Ionics*, **21**, 1111 (2015)
- 370 G. Ran, X.Chen and Y. Xia, *RSC Adv.*, **7**, 1847 (2017)
- 371 A. C. Anithaa, K. Asoka and C. Sekar, *Sens. Actuat. B*, **238**, 667 (2017)

- 372 N. K.Sadanandhan, M.Cheriyathuchenaaramvalli, S. J. Devaki and A. R. R.Menon, *J. Electroanal. Chem.*, **794**, 244 (2017)
- 373 T. D. Thanh, J. Balamurugan, H. V. Hien, N. H. Kim and J. H. Lee, *Biosens. Bioelectron.*, **96**, 186 (2017)
- 374 M. Tertiş, A. Cernat, D. Lacatiş, A. Florea, D. Bogdan, M. Suciuc, R. Săndulescu and C. Cristea, *Electrochem. Commun.*, **75**, 43 (2017)
- 375 S. Selvarajan, A. Suganthi and M. A. Rajarajan, *Ultrasonics – Sonochemistry*, **44**, 319 (2018)
- 376 Y. Yang, Y. Zeng, C. Tang, X. Zhu, X. Lu, L. Liu, Z. Chen and L. Li, *Microchim. Acta*, **185**, 219 (2018)
- 377 N. F. Atta, Y. M. Ahmed and A. Galal, *Electroanal.*, **30**, 1 (2018)
- 378 D. F. Sun, H. J. Li, M. J. Li, C. P. Li, H. L. Dai, D. Z.Sun and B. H. Yang, *Sens. Actuators B*, **259**, 433 (2018)
- 379 L. A. Houghton, W. Atkinson, R. P. Whitaker, P. J. Whorwell and M. J. Rimmer, *Gut*, **52**, 663 (2003)
- 380 M. Some and A. Helander, *Life Sci.*, **71**, 2341 (2002)
- 381 P. C. Emson, R. F. T. Gilbert, H. Martensson and A. Nobin, *Cancer*, **54**, 715 (1984)
- 382 D. L. Garver and J. M. Davis, *Life Sci.*, **24**, 383 (1979)
- 383 S. M. Dursun, R. P. Whitaker, H. Andrews and M. A. Reveley, *Hum. Psychopharm.*, **12**, 365 (1997)
- 384 S. Banik and T. Lahiri, *Biomed. Res.*, **21**, 255 (2000)
- 385 S. Bolandparvaz, M. Vasei, A. A. Owji, N. Ataee, A. Amin, Y. Daneshbod and V. Hosseini, *Clin. Biochem.*, **37**, 985 (2004)

References

- 386 A. Uzan, M. Kabouche, F. Imbault and G. Le Fur, *Headache*, **19**, 267 (1979)
- 387 R. N. Goyal, M. Oyama, V. K. Gupta, S. P. Singh and R. A. Sharma, *Sens. Actuators B*, **134**, 816 (2008)
- 388 K. Thorre, M. Parvda, S. Sarre, G. Ebinger and Y. Michotte, *J. Chromatogr. B*, **694**, 297 (1997)
- 389 J. S. Kang, M. S. Mun, H. S. Shin and S. C. Lee, *Anal. Sci. Technol.*, **8**, 215 (1995)
- 390 T. Yoshitake, R. Iizuka, K. Fujino, O. Inoue, K. Yamagata, H. Nohta and M. Yamaguchi, *Anal. Sci.*, **20**, 1687 (2004)
- 391 L. Zhang, Y. Zhao, J. Huang and S. Zhao, *J. Chrom.*, **967**, 190 (2014)
- 392 D. Thomas, L. Lonappan, L. Rajith, S. T. Cyriac and K. Girish Kumar, *J. Fluoresc.*, **23**, 473 (2013)
- 393 W. W. Yu, L. H. Qu, W. Z. Guo and X. G. Peng, *Chem. Mater.*, **15**, 2854 (2003)
- 394 R. Koole, P. Liljeroth, C. de Mello Donegá, D. L. Vanmaekelbergh and A. Meijerink, *J. Am. Chem. Soc.*, **128**, 10436 (2006)
- 395 S. A. Crooker, J. A. Hollingsworth, S. Tretiak and V. I. Klimov, *Phys. Rev. Lett.*, **89**, 186802 (2002)
- 396 M. T. Kumara, B. C. Tripp and S. Muralidharan, *J. Phys. Chem. C*, **111**, 5276 (2007)

..........

List of Publications and Presentations

Publications

1. **Ambily Thomas**, K. Girish Kumar, Electro-oxidation of Dopamine at CoNP-pAHNSA modified electrode: A sensitive approach to its determination, *J. Electrochem. Soc.*, 165 (10), B466 (2018).
2. **Ambily Thomas**, K. Girish Kumar, Acetylene black-chitosan mediated electro-oxidation of serotonin and melatonin: An efficient platform for simultaneous voltammetric sensing, *Ionics*, doi:10.1007/s11581-018-2652-x, (2018). (In press)
3. **Ambily Thomas**, K. Girish Kumar, Electro-catalytic resolution and simultaneous determination of two phenolic antioxidants, *J. Electrochem. Soc.*, 165, B351 (2018).
4. **Ambily Thomas**, U. Sivasankaran, K. Girish Kumar, Biothiol induced colour change of silver nanoparticles: A colorimetric sensing strategy, *Spectrochim. Acta Mol. Biomol. Spectrosc.*, 188, 113 (2018)
5. **Ambily Thomas**, A. E. Vikraman, D. Thomas, K. Girish Kumar, Voltammetric Sensor for the Determination of TBHQ in Coconut Oil, *Food Anal. Methods*, 8, 2028 (2015).
6. U. Sivasankaran, **Ambily Thomas**, A. R. Jose, K. Girish Kumar, Poly (Bromophenol Blue)-Gold Nanoparticle Composite: An Efficient Electrochemical Sensing Platform for Uric Acid, *J. Electrochem. Soc.*, 164, B292 (2017).

Presentations

1. An electrochemical sensor for the wonder drug-melatonin (**Ambily Thomas** and K. Girish Kumar, MatCon2019, CUSAT , Kochi, March 2019)
2. The first example of a structurally authenticated neutral zero-valent cadmium complex (Lincy Tom, **Ambily Thomas**, M. R. P. Kurup, MatCon2019, CUSAT , Kochi, March 2019)
3. A voltammetric sensor for propyl gallate (**Ambily Thomas** and K. Girish Kumar, workshop on Nano Bio-Sensors : present status and future perspectives (NANOSE 2018), Department of Bioelectronics and Biosensors, Alagappa University, Karaikudy, March 2018).
4. An Eco-friendly voltammetric sensor for serotonin (**Ambily Thomas** and K. Girish Kumar, A National Seminar on Current Trends in Chemistry CTriC 2018, Cochin University of Science and Technology, Kochi, January 2018).
5. Colorimetric sensing of Cysteine and Cysteamine (**Ambily Thomas** and K. Girish Kumar, Prof. K.V. Thomas Endowment International Symposium on NEW TRENDS IN APPLIED CHEMISTRY (NTAC-2017); Sacred Heart College, Thevara)
6. Biothiol induced color change of Ag NPs: Colorimetric Sensing Strategy. (**Ambily Thomas** and K. Girish Kumar, A National Seminar on Current Trends in Chemistry CTriC 2017; Cochin University of Science and Technology, Kochi)
7. Determination of cysteamine: A colorimetric approach (**Ambily Thomas** and K. Girish Kumar, 26th Swadeshi Science Congress,

A National Seminar; Central Marine Fisheries Research Institute, Kochi, 2016)

8. MWCNT - Modified Gold Electrode Sensor for the Determination of TBHQ (**Ambily Thomas** and K. Girish Kumar, MatCon2016, CUSAT , Kochi, January 2016)

.....❧.....